COLD-FORMING EFFECT ON STAINLESS STEEL SECTIONS

Author: Milon Kanti Howlader

Supervisor: Ing. Michal Jandera, Ph.D

University: Czech Technical University in Prague

Czech Technical University in Prague
Date: 05.01.2015

CZECH TECHNICAL UNIVERSITY IN PRAGUE
Faculty of Civil Engineering
Thákurova 7, 166 29 Prague 6, Czech Republic

MASTER'S THESIS PROPOSAL

study programme:
study branch: SUSCOS
academic year: 2014/15

Student's name and surname: MILON KANTI HOWLADER
Department: DEPARTMENT OF STEEL AND TIMBER STR.
Thesis supervisor: MICHAL JANDERA
Thesis title: COLD-FORMING EFFECT ON STAINLESS STEEL SECTIONS
Thesis title in English

Framework content: ANALYTICAL AND NUMERICAL MODELLING OF STAINLESS STEEL SECTION COLD FORMING PROCESS USING EXPETIMENTAL DATA FOR MATERIAL STRENGTH INCREASE, DEVELOPMENT OF SIMPLE PREDICTIVE FORMULA.

Assignment date: 24. 9. 2014 Submission date: 19. 12. 2014

If the student fails to submit the Master's thesis on time, they are obliged to justify this fact in advance in writing, if this request (submitted through the Student Registrar) is granted by the Dean, the Dean will assign the student a substitute date for holding the final graduation examination (2 attempts for FGE remain). If this fact is not appropriately excused or if the request is not granted by the Dean, the Dean will assign the student a date for retaking the final graduation examination, FGE can be retaken only once. (Study and Examination Code, Art 22, Par 3, 4.)

The student takes notice of the obligation of working out the Master's thesis on their own, without any outside help, except for consultation. The list of references, other sources and names of consultants must be included in the Master's thesis.

M. Jandera
Master's thesis supervisor

p. ?
Head of department

Date of Master's thesis proposal take over: 24.9.2014

Student

This form must be completed in 3 copies – 1x department, 1x student, 1x Student Registrar (sent by department)

No later than by the end of the 2nd week of instruction in the semester, the department shall send one copy of BT Proposal to the Student Registrar and enter data into the faculty information system KOS. (Dean's Instruction for Implementation of Study Programmes and FGE at FCE CTU Art. 5, Par. 7)

AUTHOR'S DECLARATION

I, Milon Kanti Howlader declare that this thesis work presented here are my own and has been generated by me as the result of my own original research.

Prague, 05 January, 2015

.....
Milon Kanti Howlader

ACKNOWLEDGEMENTS

I would like to express my deepest appreciation and thanks to my thesis supervisor Ing. Michal Jandera, Ph.D, Department of Steel and Timber Structure, Faculty of Civil Engineering, Czech Technical University in Pragure, he has been a tremendous mentor for me. I would like to thank him for his affectionate and unfailing guidance, constant supervision, energetic encouragement, constructive and helpful criticism and suggestions at every stage throughout the course of this dissertation works. His friendly advice on both research as well as on my career have been priceless and truly speaking without his supervision and constant help this dissertation would not have been possible.

I am tremendous indebted to Prof. Ing. František Wald, CSc, who is the coordinator of SUSCOS_M Master program for organizing this interesting programs and also for his valuable comments and suggestions about selecting this thesis topics and way of writing the thesis.

I am thankful to all of my colleagues in SUSCOS_M program for their encouragement and company which really help me to live in Europe, away from home.

I wish to express my special thanks to my parents, my beloved wife Sharmili Sarker, and my sister for their love, patience, understanding, sacrifice and encouragement during the pursuit of my academic work. Your prayer for me was what sustained me thus far.

Finally, I would also like to thank the Erasmus Mundus scholarship agency for giving me the financial support to come in Europe and to pursue this Masters program.

To My Parents

ABSTRACT

Stainless steel exhibits a greater extent of strain hardening than carbon steel, which leads to a significant change in the mechanical properties (increase in the yield strength and decrease in ductility) of the stainless steel material due to cold forming process. These changes of mechanical properties depend mainly on the magnitude of the residual stresses and equivalent plastic strain induced by the cold working. In this study, an analytical model is developed for determining the residual stresses and corresponding plastic strain from the analytical solution of Quach, W. M. (2005) by using Maple for different stage of cold forming process. The Maple model is validated from the previous numerical and experimental data for each step of cold working such as coiling, uncoiling including flattening of sheet and cold bending of sheet including springback. Here the increased material properties are determined after cold bending for corner and flat faces considering the residual stresses and plastic strain and validated with the Grander, L (2002) test results. For the prediction of the increased yield strength, new material properties with respect to induced plastic strain are set after cold bending process in the Maple from the test result of Marik, J. and Jandera, M. (2014). The analysis for increased yield strength is done for four stainless steel grades, i.e., austenitic (1.4404), ferritic (1.4003), lean-duplex (1.4162) and duplex (1.4462) and the result is compared with the previous predicted model of strength increase.

Keywords: *stainless steel, analytical modelling, cold forming, residual stresses, plastic strain, yield strength enhancement.*

TABLE OF CONTENTS

Page no.

Author's Declaration i
Acknowledgements ii
Abstract iv
Table of contents v-vii
List of figures viii-x
List of tables xi-xiii

1 State of art 1
1.1 Stainless steel 1
1.1.1 Chemical composition 1
1.1.2 Types of stainless steel 2
1.1.2.1 Austenitic stainless steels 2
1.1.2.2 Ferritic stainless steels 3
1.1.2.3 Martensitic stainless steels 3
1.1.2.4 Duplex stainless steels 4
1.1.2.5 Precipitation hardening steels 4
1.1.3 Mechanical Properties 4
1.2 Cold-forming 10
1.2.1 Forming process 10
1.2.2 Forms of sections 11
1.2.3 Specific problems in cold formed section 12
1.2.3.1 Local buckling 12
1.2.3.2 Web crippling 12
1.2.3.3 Flange curling 13
1.3 Plasticity 13
1.3.1 Plasticity and material response 13
1.3.2 Corner region of increased strength 14
1.4 Previous works on cold formed materials 15
1.4.1 Carbon steel 15

1.4.2 Stainless steel 17
1.4.2.1 Strength enhancement at corner 17
1.4.2.2 Strength increase in the flat faces 21
1.4.2.3 Strength enhancement in the whole section 22
1.4.3 Residual stresses 23
1.4.3.1 Experimental works 23
1.4.3.2 Theoretical approach 26
2 Objectives 28
3 Analytical modelling 29
3.1 Axial expression 29
3.2 Analytic solution for coiling and uncoiling 30
3.2.1 Assumptions 30
3.2.2 Geometric properties 30
3.2.3 Material modelling 30
3.2.4 For coiling 35
3.2.5 For uncoiling including flattening 39
3.2.6 Verification of model 42
3.3 Analytical solution due to cold bending 51
3.3.1 Material modelling 52
3.3.2 Theory of cold bending of sheet 53
3.3.3 Cold bending of stainless steel 55
3.3.4 Validation of analytical solution due to cold bending 60
3.3.5 Validation of analytical solution for complete press-breaking (including springback) 63
3.3.6 Increase of strength due to cold forming 66
3.3.6.1 For corner 68
3.3.6.2 For flat face 69
4 Test data analysis 71
4.1 Previous tensile test 71
4.2 Increased strength at corner and flat faces 72
4.2.1 Austenitic steel 72
4.2.2 Ferritic steel 89

4.2.3 Lean-duplex steel 91
4.2.4 Duplex steel 93
4.3 Compilation of data 95
4.3.1 For increased corner strength 95
4.3.2 For increased flat faces strength 101
4.3.3 Proposed modification of Rossi, B. et, al. (2013) model 103
4.3.4 Comparison of corner strength with the ultimate strength of annealed material 111
4.4 Increased yield strength for the whole section 112
5 Summary and conclusions 114
6 Future Works 116
References 117
Annex A: Material properties at corner due to cold bending (austenitic steel) **121**
Annex B: Variation of material properties with respect to induced plastic strain **132**

LIST OF FIGURES

Number	Name	Page
Figure 1.1	Classification of stainless steels according to nickel and chromium content [SCI (2003)].	2
Figure 1.2	Effect of the parameter *n* on the non-linearity of the stress-strain curve [SCI (2003)].	5
Figure 1.3	Typical stress-strain curves for stainless steel and carbon steel in the annealed condition (longitudinal tension) [SCI (2006)].	6
Figure 1.4	Relationship between the tensile and compressive 0.2% proof stress [Rossi, B. et, al. (2013)].	9
Figure 1.5	General forming process of Cold-formed steel sections [Cruise, R.B., and Gardner, L. (2008)].	11
Figure 1.6	Typical forms of sections for cold-formed members [CEN(1996), EN 1993-1-3]	12
Figure 1.7	Proposed 0.2% proof stress distributions for press-braked sections and cold-rolled boxes [Gardner, L. (2000)].	14
Figure 3.1	Direction of sheet axis.	29
Figure 3.2	Stress-strain curves of the austenitic stainless steel (tensile coupon test).	34
Figure 3.3	Stress path of a surface point of a strain-hardening steel strip during the coiling-uncoiling process [Quach, W. M.(2005)].	43
Figure 3.4	Comparison of residual stresses and equivalent plastic strain between Quach analytical solution and analytical solution using Maple due to coiling of Austenitic sheet.	45-46
Figure 3.5	Comparison of residual stresses and equivalent plastic strain between Quach analytical solution and analytical solution using Maple due to uncoiling including flattening of Austenitic sheet.	49-50
Figure 3.6	Manufacturing process of press-braked sections.	52
Figure 3.7	Schematic diagram of a sheet under pure bending with a large curvature.	52

Figure 3.8	Comparison of residual stresses and equivalent plastic strain due to cold bending by using nominal and true stress-strain relationship of austenitic steel.	59-60
Figure 3.9	Comparison of residual stresses and equivalent plastic strain between Quach analytical solution and analytical solution using Maple due to cold bending of Duplex sheet.	61-62
Figure 3.10	Press-braking operation and springback due to unloading.	63
Figure 3.11	Loading, unloading and residual stresses in cold bent section.	63
Figure 3.12	Comparison of residual stresses due to press-braking.	65
Figure 3.13	Comparison of Maple analysis and Test data of material behaviour due to cold bending at corner.	68
Figure 3.14	Formation of square hollow section (SHS) by cold-rolling.	69
Figure 3.15	Comparison of Maple analysis and Test data of material behaviour due to cold bending at flat face.	70
Figure 4.1	Detail drawing of tested coupons of stainless steel sheet.	71-72
Figure 4.2	Variation of material properties with respect to induced plastic strain.	74-77
Figure 4.3	Stress strain diagram at corner of the specimen.	78-79
Figure 4.4	Stress strain diagram at flat face of the specimen.	79-80
Figure 4.5	Variation of material properties for different r_i/t ratio at corner (austenitic steel).	81
Figure 4.6	Variation of increased corner strength against r_i/t ratio due to cold bending (austenitic steel).	82
Figure 4.7	Van den Berg, G.J. and Van der Merwe, P. (1992) model.	83
Figure 4.8	Ashraf, M. et al. (2005) model.	84
Figure 4.9	Cruise, R.B. and Gardner, L (2008) model.	85
Figure 4.10	Rossi, B. et, al. (2013) model.	85
Figure 4.11	Comparison of models for predicting the corner strength increase (austenitic steel).	86
Figure 4.12	Variation of material properties for different R_i/t ratio at flat face (austenitic steel).	87

Figure 4.13	Variation of increased strength at flat faces against R_i/t ratio due to cold bending (austenitic steel).	88
Figure 4.14	Comparison of predicted model for the strength increase at flat faces due to cold rolling (austenitic steel).	89
Figure 4.15	Variation of increased corner strength against r_i/t ratio due to cold bending (ferritic steel).	90
Figure 4.16	Variation of increased strength at flat faces against R_i/t ratio due to cold bending (ferritic steel).	91
Figure 4.17	Variation of increased corner strength against r_i/t ratio due to cold bending (lean duplex).	92
Figure 4.18	Variation of increased strength at flat faces against R_i/t ratio due to cold bending (lean-duplex steel).	93
Figure 4.19	Variation of increased corner strength against r_i/t ratio due to cold bending (duplex steel).	94
Figure 4.20	Variation of increased strength at flat faces against R_i/t ratio due to cold bending (duplex steel).	95
Figure 4.21	Relationship between the $\sigma_{u,a}$ and $\sigma_{0.2,c}$ for commonly used r_i/t ratio 1.5.	111

LIST OF TABLES

Number	Name	Page
Table 3.1	Residual stresses and equivalent plastic strain through thickness at the end of coiling.	44
Table 3.2	Residual stress and equivalent plastic strain through thickness at the end of uncoiling including flattening.	48
Table 3.3	Residual stress and equivalent plastic strain through thickness due to cold bending of sheet.	58
Table 3.4	Mechanical properties of duplex stainless steel of grade UNS31803 alloy tested by Rasmussen, K. J. R. et, al. (2003).	60
Table 3.5	Material properties for HY-80 steel [Weng, C. C. and White, R. N. (1990)].	64
Table 3.6	Measured material Properties for SHS 80×80×4 [Gardner, L (2002)].	66
Table 3.7	Geometric properties of the cold bend section [Grander, L. (2002)].	67
Table 4.1	Summary of tensile material properties for austenitic steel sheet.	72
Table 4.2	1.4404 grade tensile material properties for the coupons with induced plastic deformation.	73
Table 4.3	Summary of tensile material properties for ferritic steel sheet.	89
Table 4.4	1.4003 grade tensile material properties for the coupons with induced plastic deformation.	90
Table 4.5	Summary of tensile material properties for lean-duplex steel sheet.	91
Table 4.6	1.4162 grade tensile material properties for the coupons with induced plastic deformation.	92
Table 4.7	Summary of tensile material properties for duplex steel sheet.	93
Table 4.8	1.4462 grade tensile material properties for the coupons with induced plastic deformation.	94

Table 4.9	Comparison of obtained analytical results with the previous proposed models for austenitic steel.	97
Table 4.10	Comparison of obtained analytical results with the previous proposed models for ferritic steel.	98
Table 4.11	Comparison of obtained analytical results with the previous proposed models for lean-duplex steel.	99
Table 4.12	Comparison of obtained analytical results with the previous proposed models for duplex steel.	100
Table 4.13	Comparison of obtained analytical results with the previous proposed models for austenitic steel.	101
Table 4.14	Comparison of obtained analytical results with the previous proposed models for ferritic steel.	102
Table 4.15	Comparison of obtained analytical results with the previous proposed methods for lean-duplex steel.	102
Table 4.16	Comparison of obtained analytical results with the previous proposed models for duplex steel.	103
Table 4.17	Comparison of obtained analytical results with the previous and new proposed models for austenitic steel.	105
Table 4.18	Comparison of obtained analytical results with the previous and new proposed models for ferritic steel.	106
Table 4.19	Comparison of obtained analytical results with the previous and new proposed models for lean-duplex steel.	107
Table 4.20	Comparison of obtained analytical results with the previous and new proposed models for duplex steel.	108
Table 4.21	Comparison of obtained analytical results with the previous and new proposed models for austenitic steel.	109
Table 4.22	Comparison of obtained analytical results with the previous and new proposed models for ferritic steel.	109
Table 4.23	Comparison of obtained analytical results with the previous and new proposed models for lean-duplex steel.	110
Table 4.24	Comparison of obtained analytical results with the previous and new proposed models for duplex steel.	110

Table 4.25 Calculation of strength increase for whole section due to cold rolling. 113

Table 4.26 Calculation of strength increase for whole section due to cold rolling using expression used for carbon steel. 113

1. STATE OF ART

1.1. STAINLESS STEEL

Stainless steels have not been widely used as traditional structural materials in building and civil engineering. It has been used for the purpose where there has been some other very important issues driving the design, generally for resistance of corrosion, sanitary qualities or architectural requirements rather than the inherent structural properties of the steel. The primary reason for this diminutive use in structural applications is usually the alleged and actual cost of stainless steel as a material. Due to the development over the last few years, both in availability of materials and attitudes to durability, are now offering a new prospect for stainless steels to be considered as primary structural materials.

1.1.1. Chemical Composition

In metallurgy, stainless steel, also known as inox steel or inox come from French "*inoxydable*", is a alloy of iron which contain chromium, nickel and small amount of carbon content and sometimes containing other elements, such as molybdenum, titanium and nitrogen which are resistant to corrosion or rusting associated with exposure to bulk environment (water and moist air). It differs from carbon steel by the presence of chromium content. Unprotected carbon steel readily rusts when exposed to air and moisture. The rust (iron oxide film, $Fe_2O_3 \cdot nH_2O$) is active and accelerates corrosion by forming more iron oxide, and due to the larger volume of the iron oxide tends to flake and fall away. The presence of sufficient chromium in stainless steels forms a passive film of chromium oxide on the surface of the steel. The film is strongly adherent due to the similar size of the steel and oxide ions, usually self repairing and highly resistant to chemical attack, which prevents additional surface corrosion by resisting oxygen diffusion to the steel surface and prevent the corrosion to spread into the metal's internal structure. In strongly acid or alkaline environments the layer may be broken down which are not repaired, and finally corrosion occurs.

1.1.2. Types of Stainless Steel

Stainless steel can be classified into five basic groups according to their metallurgical structure showing different properties, predominantly in respect of strength, corrosion resistance and ease of fabrication. The percent amount of nickel (Ni) and chromium (Cr) content varies for different types of stainless steel which is shown in Fig. 1.1.

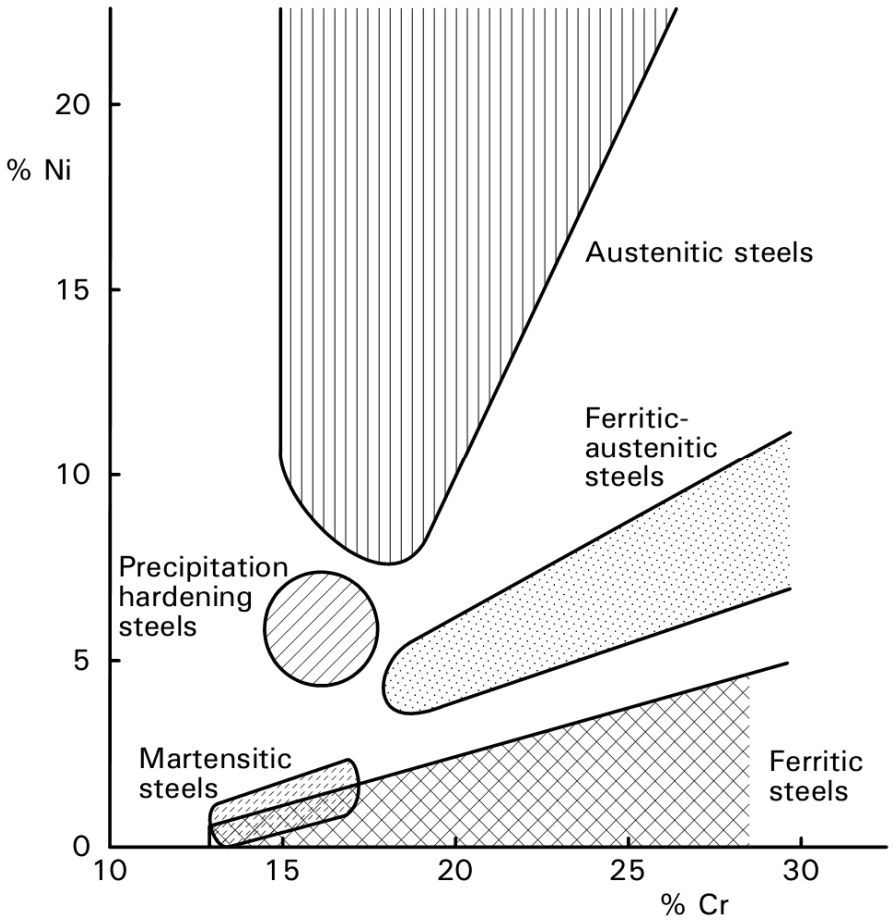

Figure 1.1: Classification of stainless steels according to nickel and chromium content [SCI (2003)].

The five groups are summarised below

1.1.2.1. Austenitic Stainless Steels

Austenitic grades are commonly in use for stainless structural applications accounting for up to 80% of all stainless steel production. They are non magnetic and the most general austenitic alloys are iron-chromium-nickel steels which are widely known as the 300

series. At room temperature it has austenitic microstructure and contains comparatively soaring amounts of nickel. The presence of high chromium and nickel, are the most corrosion resistant affording unusually fine mechanical properties of the stainless group. It has high ductility, formability, are readily weldable and offer good corrosion resistance, but prone to stress corrosion cracking. It can be successfully used from cryogenic temperature to the red-hot temperature of furnace and jet engines. Their strengths are reasonable and they cannot be hardened by heat treatment, but can be hardened (i.e. made stronger) significantly by cold-working.

1.1.2.2. Ferritic Stainless Steels

Ferritic stainless steel consists of iron-chromium alloys (relatively little nickel alloy) with body-centered cubic crystal structures, widely known as 400 series. They can have good ductility, strength, formability and fabrication property but at high temperature the strengths are relatively poor as compared to austenitic grades. They are generally not as corrosion resistant as the austenitic grades, while being highly defiant to stress corrosion cracking. Ferritic stainless steels are magnetic but cannot be hardened or strengthened by heat treatment because they contain less than 0.10% carbon. They can only be hardened by cooling as like of the austenitic grades.

The specific use of ferritic stainless steel largely depends on their level of chromium content. Lower-chromium grades are generally used in automotive-exhaust systems. Intermediate-chromium grades (approx.17% chromium) are expansively used in domestic appliances. High-chromium grades are used in applications ensuing higher corrosion or oxidation resistance. Now a days, ferritic stainless steels account up to 25-30 % of world stainless production.

1.1.2.3 Martensitic Stainless Steels

Martensitic stainless steels are similar to low alloy or carbon steels, boasting a structure similar to the ferritic steels with body-centered tetragonal (bct) crystal structure and they are classed as a "hard" ferro-magnetic group. They are magnetic and have higher strength, higher wear and fatigue resistance than the austenitic and ferritic grades but decreases ductility and toughness. However, due the addition of carbon, they can be tempered and

hardened by heat treatment and thus extensively used in a situation where strength is more important than the corrosion resistance. The main alloying element is chromium, typically 12 to 15%, molybdenum (0.2-1%), no nickel, except for two grades, and 0.1-1.2% carbon. The carbon content affects forming and welding of these hardenable steels. To prevent cracking and gaining useful properties and, they usually require preheating and post weld heat treatment.

1.1.2.4 Duplex Stainless Steels

Duplex stainless steels are called "duplex" because they have a mixed two-phase microstructure consisting of particles of austenitic and ferritic stainless steel. When this stainless steel is melted, it hardens from the liquid phase to a completely ferritic structure. About half of the ferritic grains transform to austenitic grains as the material cools to room temperature so outcome is a microstructure of roughly 50% austenite and 50% ferrite. The higher the annealing temperature indicates larger percentage of the ferrite content. As of the mixture of two grains, they have higher mechanical strengths, equivalent weldability, lesser formability and similar or higher corrosion resistance remarkably with respect to stress corrosion cracking resistance to chloride compared to the austenitic group.

1.1.2.5 Precipitation Hardening Steels

Precipitation hardening stainless steels provide a most favourable combination of the properties of martensitic and austenitic grades. As martensitic grades, they have ability to gain high strength through heat treatment and they also have the equivalent corrosion resistance to that of austenitic stainless steel. They can be supplied in a solution treated condition, which is readily workable. After machining or another fabrication method, to enhance the strength of the steel, a single, low temperature heat treatment can be applied. The component undergoes no distortion, as it is carried out at low temperature.

1.1.3. Mechanical Properties

The stress-strain characteristics of stainless steels differ from that of carbon steels, basically in the shape of the stress-strain curve. Carbon steel normally shows linear elastic performance up to its yield limit and a plateau before strain hardening is encountered, whereas, stainless steel has a more rounded response (non-linearity) with no well-defined yield stress. For that reason, the yield strength of stainless steel are generally determined

in terms of a proof strength defined for a particular offset permanent strain (conventionally the 0.2% strain), as specified in the Fig. 1.3. It can absorb significant impact without fracturing due to its outstanding ductile property (especially the austenitic grades) and their strain hardening characteristics.

The nonlinearity of the stress-strain behaviour of stainless steel alloys is commonly described by the Ramberg-Osgood with the relationship between the initial Young's modulus E_0, the 0.2% proof stress $\sigma_{0.2}$ and the strain-hardening exponent n given by:

$$\varepsilon = \frac{\sigma}{E_0} + 0.002\left(\frac{\sigma}{\sigma_{0.2}}\right)^n \tag{1.1}$$

The degree of non-linearity of the stress-strain curve is characterised by the strain-hardening exponent n which is called Ramberg-Osgood coefficient where lower n values represent a greater degree of non-linearity shown in Fig. 1.2.

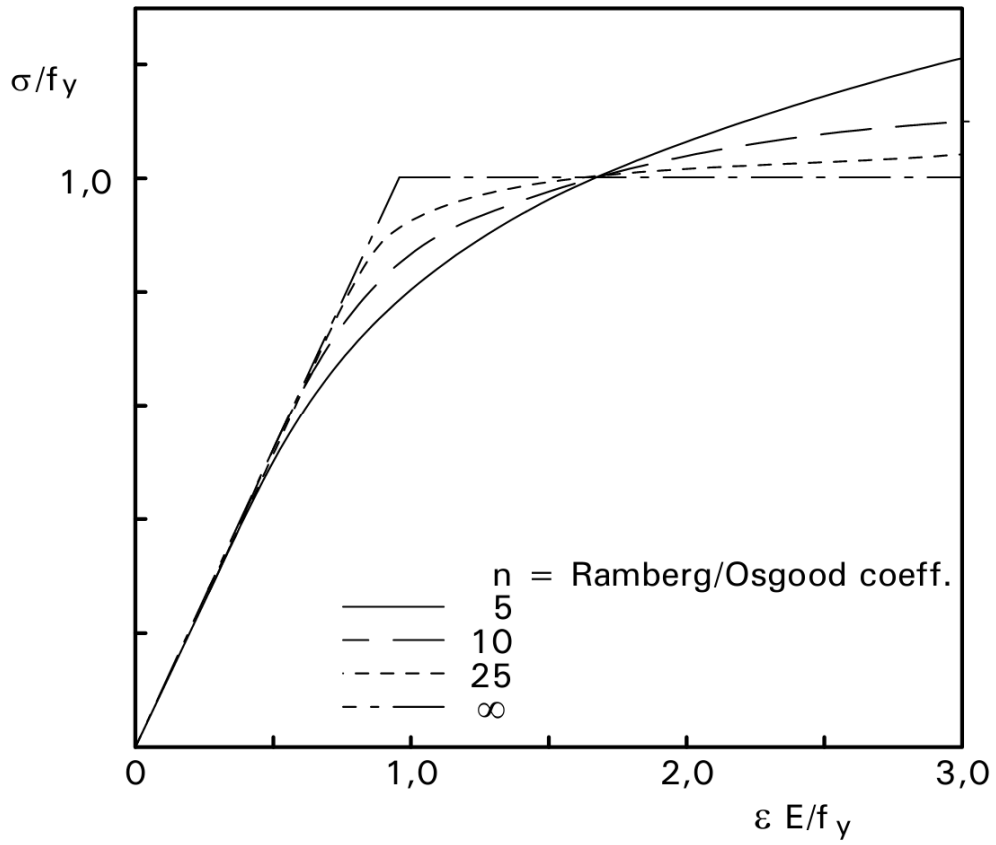

Figure 1.2: Effect of the parameter n on the non-linearity of the stress-strain curve [SCI (2003)].

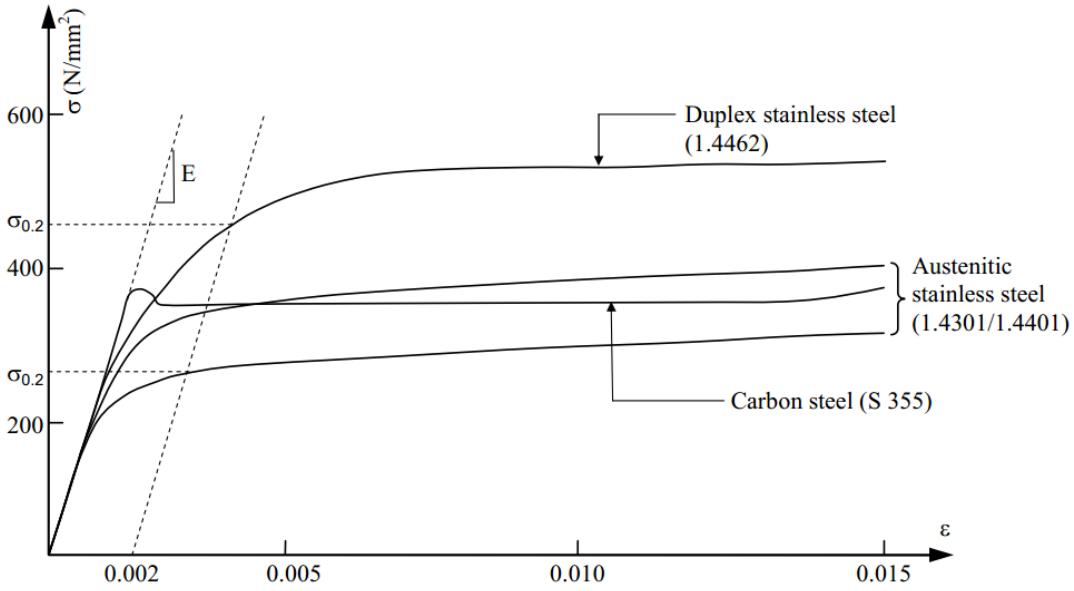

Figure 1.3: Typical stress-strain curves for stainless steel and carbon steel in the annealed condition (longitudinal tension) [SCI (2006)].

The value of n is defined from the ratio of the stress at the limit of proportionality (conventionally the 0.01% proof strength, $\sigma_{0.01}$) to the 0.2% proof strength, $\sigma_{0.2}$ are given as follows.

$$n = \frac{\ln(20)}{\ln(\sigma_{0.2}/\sigma_{0.01})} \tag{1.2}$$

As for determining the strain-hardening exponent n, it requires to match the measured stress-strain curve exactly at the 0.01% proof stress $\sigma_{0.01}$ and the 0.2% proof stress $\sigma_{0.2}$, so the Ramberg-Osgood expression can closely approximate the measured stress-strain curve up to the point of 0.2% proof stress. Therefore, the use of Ramberg-Osgood expression for the higher strain, say as greater than 0.2%, it can escort to overestimate the stresses with a great inaccuracy which was pointed out by subsequent previous researches.

Recently a number of researches have been conducted [Macdonald, M. et, al. (2000), Mirambell, E. and Real, E. (2000), Olsson, A. (2001), Rasmussen, K. J. R. (2003), Gardner, L. and Nethercot, D. A. (2004)] to model the stress-strain behaviour of stainless steel for higher strains and a number of stress-strain relationships have got from these studies. But each of them has the capability to accurately predict a limited strain range or

for the tensile stress-strain behaviour only. The limitations of these recent proposals are examined in detail below.

Macdonald M. et, al. (2000) recognized that for higher value of strain, it can be modified the existing expression of Ramberg-Osgood in such manner that the exponent *n* becomes a function of stress. The accurate function of stress was obtained by fitting the curve from the overall measured stress-strain curve for each individual coupon test, but its relevance is limited for the specimen for which *n* has been determined.

Olsson, A. (2001) observed that if the measured stress-strain curve is converted to the true stress-nominal strain curve, then it approaches a straight line at high strains, and proposed that the true stress-nominal strain curve can be approximated by the Ramberg-Osgood expression for strains up to the total strain $\varepsilon_{2.0}$ at the 2% proof stress (or the so called the 2% total strain) and a straight line from this point onwards as an average fit to the stress-strain curve. However, in his proposed curve, he used the strain hardening exponent *n*, which is determined by using the 0.2% and 1% proof stresses, and an inaccuracy may lead to arise in the important strain below $\varepsilon_{0.2}$ (where $\varepsilon_{0.2}$ is the total strain corresponding to the 0.2% proof stress $\sigma_{0.2}$).

Mirambell, E. and Real, E. (2000), have modelled the nominal stress-strain behaviour at high strains by the use of the basic Ramberg-Osgood relationship (Eq. 1.1) up to the 0.2% proof stress ($\sigma_{0.2}$) and a modified Ramberg-Osgood expression for the stress, between the 0.2% proof stress ($\sigma_{0.2}$) and the ultimate stress (σ_u) given by:

$$\varepsilon = \frac{\sigma - \sigma_{0.2}}{E_{0.2}} + \varepsilon_{pu}\left(\frac{\sigma - \sigma_{0.2}}{\sigma_u - \sigma_{0.2}}\right)^{n'_{0.2,u}} + \varepsilon_{0.2}, \qquad \sigma > \sigma_{0.2} \tag{1.3}$$

where,

$E_{0.2}$ is the tangent modulus at the 0.2% proof stress,

σ_u and ε_{pu} are the ultimate strength and the plastic strain at ultimate strength respectively,

$n'_{0.2,u}$ is the strain-hardening exponent that can be determined from the ultimate strength and an intermediate stress. For determining the value of σ_u, ε_{pu} and $n'_{0.2,u}$, experimental stress-strain curves are needed.

Rasmussen, K. J. R. (2003) proposed a full-range stress-strain expression, in which the Ramberg-Osgood expression (Eq. (1.1)) is valid for the stress range up to the 0.2% proof stress and a new expression for the stress higher than $\sigma_{0.2}$ given by:

$$\varepsilon = \frac{\sigma - \sigma_{0.2}}{E_{0.2}} + \varepsilon_u \left(\frac{\sigma - \sigma_{0.2}}{\sigma_u - \sigma_{0.2}} \right)^m + \varepsilon_{0.2}, \qquad \sigma > \sigma_{0.2} \tag{1.4}$$

in which,

$$e = \frac{\sigma_{0.2}}{E_0} \tag{1.5}$$

$$\varepsilon_{0.2} = \frac{\sigma_{0.2}}{E_0} + 0.002 \tag{1.6}$$

$$E_{0.2} = \frac{E_0}{1 + 0.002n/e} \tag{1.7}$$

$$\frac{\sigma_u}{\sigma_{0.2}} = \frac{1}{0.2 + 185e} \quad ; \text{for austenitic and duplex alloys} \tag{1.8}$$

$$\frac{\sigma_u}{\sigma_{0.2}} = \frac{1 - 0.0375(n-5)}{0.2 + 185e} \quad ; \text{ for all alloys} \tag{1.9}$$

$$\varepsilon_u = 1 - \frac{\sigma_{0.2}}{\sigma_u} \tag{1.10}$$

$$m = 1 + 3.5 \left(\frac{\sigma_{0.2}}{\sigma_u} \right) \tag{1.11}$$

Where, e is the non-dimensional 0.2% proof stress, σ_u and ε_u are the ultimate stress and the total strain at ultimate stress respectively. In the above full-range stress-strain curve, Eq. 1.9 is less accurate than Eq. 1.8 for austenitic and duplex alloys, but is more generally applicable for all alloys as Eq. 1.9, which has the influence of n.

Gardner, L. and Nethercot, D. A. (2004) noticed that the expressions of Mirambell, E. and Real, E.'s (2000) and Rasmussen, K. J. R.'s (2003) do not give the excellent results for compressive stress-strain behaviour as the ultimate stress in compression cannot be obtained from the compression tests of flat coupons. So, they have proposed to use the 1.0% proof stress $\sigma_{1.0}$ instead of ultimate strength σ_u in the expression of Mirambell, E. and Real, E's (2000) and Ramberg-Osgood analogy for the stress up to $\sigma_{0.2}$.

$$\varepsilon = \frac{\sigma - \sigma_{0.2}}{E_{0.2}} + \left(0.008 - \frac{\sigma_{1.0} - \sigma_{0.2}}{E_{0.2}}\right)\left(\frac{\sigma - \sigma_{0.2}}{\sigma_{1.0} - \sigma_{0.2}}\right)^{n'_{0.2,1.0}} + \varepsilon_{0.2}, \qquad \sigma > \sigma_{0.2} \tag{1.12}$$

where, $n'_{0.2,1.0}$ is a strain-hardening exponent representing a curve that passes through $\sigma_{0.2}$ and $\sigma_{1.0}$ which can be determined from measured stress-strain curves.

Recently, Rossi B. et, al. (2013) analysed the existing data from the previous research papers on tensile and compressive coupon tests and it was shown that the compressive 0.2% proof strength is on average 5% lower than that for tension which is shown in Fig. 1.4. Also, tests on both cold-rolled and hot-rolled material prove that higher strengths are achieved in transverse to the rolling direction than in the direction parallel of rolling.

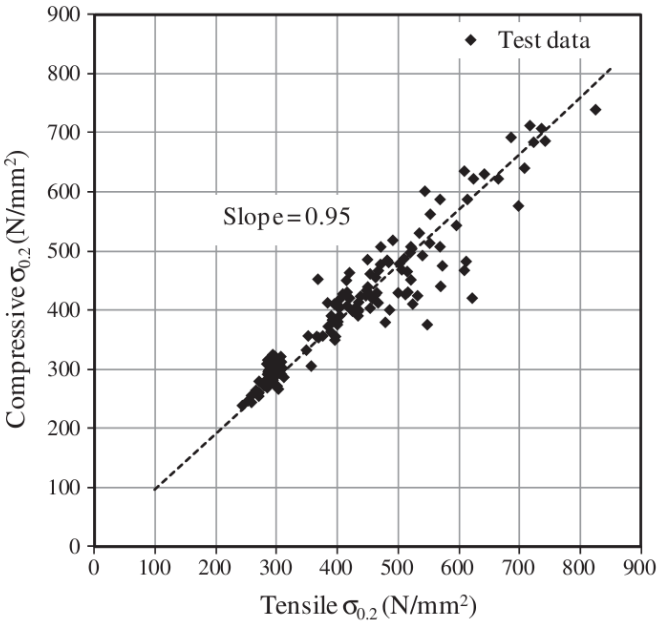

Figure 1.4: Relationship between the tensile and compressive 0.2% proof stress [Rossi, B. et, al. (2013)].

From a structural point of view, anisotropy and non-symmetry of annealed materials are not as important as the non-linearity. The rounded shape stress-strain curve influences the strength and stiffness of a member, depending on the stress level in the member. For example, buckling failure in a compression member is associated with the value of tangent modulus, as a result, for failure stresses below the proof strength, a stainless steel column will tend to be feebler than a similar carbon steel column of the same proof strength. On the other hand, for failure stresses above the proof strength, a stainless steel column will be stronger than the corresponding carbon steel one [SCI (2003)].

1.2. COLD-FORMING

In steel construction, there are two main categories of steel section fabrication named hot-rolling steel and cold-forming. Hot-rolled steel sections have been used in the building and construction industries for more than one hundred years. As compared to thick hot-rolled sections, cold-formed light members can be manufactured for relatively light loads and/or short spans. Presently, cold-formed steel is being used widely in residential and light commercial building constructions because unusual sectional configurations can be produced economically by cold-forming operations, and consequently favourable strength-to-weight ratios can be achieved. Cold-formed steel sections are economical, light weight, non-combustible, recyclable and has superior corrosion resistance, attractive manifestation and ease of prevention and maintenance.

1.2.1. Forming Process

Cold-formed steel structural members are formed from either hot-rolled or mostly formed from cold-rolled steel sheets or strips by cold-forming in roll formation machines or by press brake operations. Roll forming is widely used for better production capacity. In this process, the roll forming machine forms the steel strip as required shape of the section by supplying the strips from the coil incessantly through successive pair of roller acting as male and female die. Then the element is cut as required lengths by automatic cut-off tools. However, for sections made by press braking operation, flat sheets or short lengths of strips cutting from the coil are fed into a press break and the required fold is made through the full length of the section. This process is used for simple configuration of

section and production is limited. Generally, press breaking operation requires to be repeated several times to complete the forming process of a section. It is a semi-automated process used to make open profile, such as angles and channels, in limited quantities. In air press-braking method, the elastic spring back is allowed by over-bending the sheet, which is more usually used than coin press-braking, in where the die and the tool are fit into one another. The typical thickness of cold-formed thin walled steel products ranges from 0.4mm to about 6.4mm, although plates as thick as 25mm can also be cold-formed successfully into structural shapes by some manufacturers. The formation of an angle section by press-braking and a square box section by cold rolling is represented in Fig. 1.5.

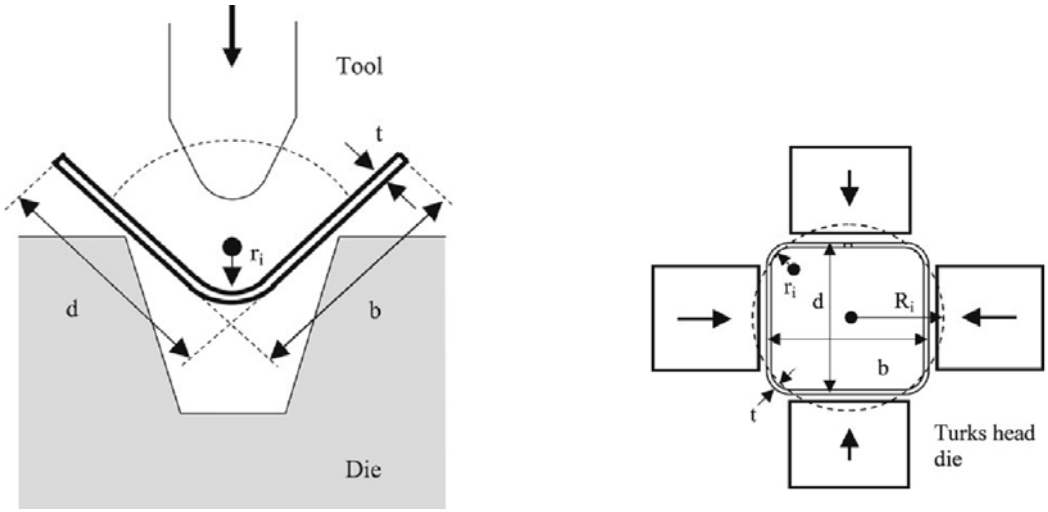

(a) Press-braking of an angle *(b) Cold rolling of a box section*

Figure 1.5: General forming process of Cold-formed steel sections [Cruise, R.B., and Gardner, L. (2008)].

1.2.2. Forms of Sections

Structural elements which are commonly used in buildings are in a range of section shapes: tubular sections, including the well-known square, rectangular, circular and elliptical hollow sections, and open sections such as angles, channels and lipped channels. Typical forms of sections for cold-formed members are shown in Fig. 1.6 below.

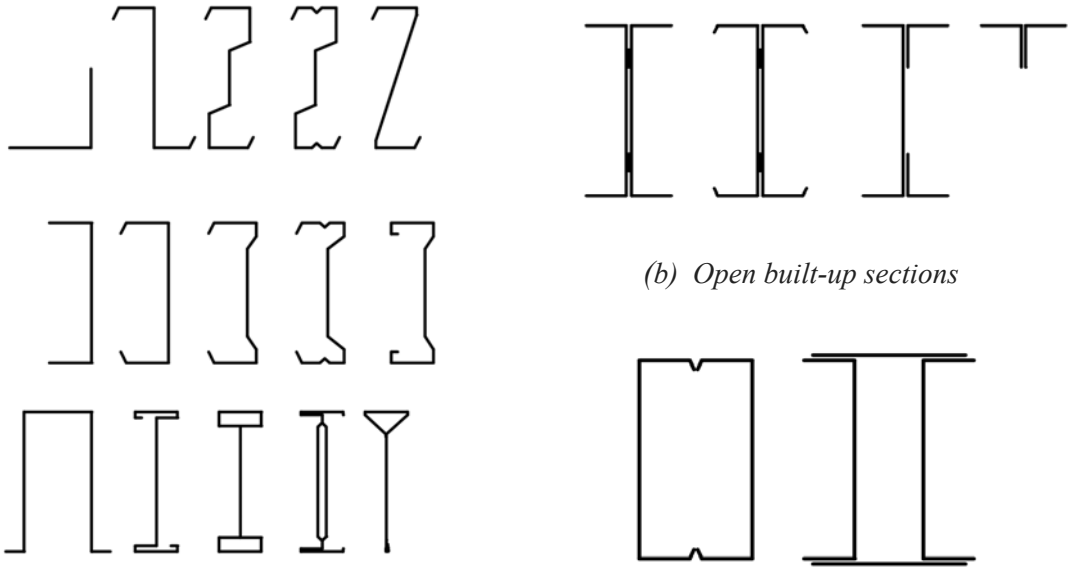

(a) Single open sections

(b) Open built-up sections

(c) Closed built-up sections

Figure 1.6: Typical forms of sections for cold-formed members [CEN (1996), EN 1993-1-3]

1.2.3. Specific Problems in Cold Formed Section

1.2.3.1. Local Buckling

In cold-formed steel design, it is often necessary not practical to provide load bearing and end bearing stiffeners. This is always the case in continuous sheeting and decking spanning several support points. The depth to thickness ratios of the webs of cold-formed steel sections are comparatively larger than hot-rolled structural members. This property causes local buckling of the cold-formed sections at stress levels lower than the actual yield stress of the steel. However, the member can carry loads after local buckling has occurred due to the redistribution of the stresses called post-buckling behaviour.

1.2.3.2. Web Crippling

Crippling of the web is one of the failure means that must be taken into consideration in cold-formed steel design due to the high local intensity of loads and/or reactions. Web crippling causes deformation in the web of the section. Due to the interaction of the web with the flange, as the web element deform, deformation also occurs in the flange elements. If the flanges are restrained against deformation, this restraint will also provide

some resistance against web deformation. This allows the section to resist higher loads before web crippling can occur [Avci, O. (2002)].

1.2.3.3. Flange Curling

The non-linear curling of flange in cold formed section is the tendency of willowy flanges to buckle towards the neutral axis for increasing flexural curvature. The load bearing resistance of curling should be taken into account of a very wide flange in a profile subjected to flexure. The load bearing resistance is reduced if the curling is larger than the 5% of the depth of the profile cross-section. In this case, the decrease in the length of the lever arm for parts of the wide flanges, and to the possible effect of the bending of the webs should be taken into account. [CEN (1996) EN 1993-1-3)]

1.3. PLASTICITY

Prior to the cold-forming process is applied to the flat strip, it has already experienced the coiling, uncoiling and flattening process for both cold rolling and press breaking, which is denoted as simply as the coiling-uncoiling process. In the coiling-uncoiling process, first for the compact storage and transportation of cold-rolled strips, they are coiled into rolls and subsequently uncoiled from the roll and required to turn into flat shape before cold-forming forces are applied. The coiling-uncoiling processes of the sheet material and the cold forming process due to the formation of the cross-section are occurred at ambient temperature ensuing the plastic deformations through the material thickness.

1.3.1. Plasticity and Material Response

Depending on the cross section formation process, say as, in press-braking method, where the sheet material is formed into the required profile by creating individual bows along its span, or cold-rolling, where gradual deformation through a series of successive rollers of the uncoiled metal sheet fabricates the final cross-section profile; generate different intensity of plastic deformation. The plastic deformations induced during the formation of cold formed section has great influence on the material response following a new loading path, such as increase in yield and ultimate strength, hardness and fragility; reduction of its malleability, ductility and resistance to corrosion as well as induce residual

stresses. So the structural behaviour of the formed section is greatly affected and cannot be predicted on the basis of the mechanical properties of the virgin materials.

The materials with a conspicuously defined yield point, such as carbon steels, due to the cold-forming process, the stress-strain behaviour turn into rounded shape. The varying level of plastic strain experienced, with the corner regions being the most prejudiced, the material properties also exhibit non-uniformities around the cold formed section. Stainless steel with round shape stress-strain behaviour, due to cold-working, a significant strain hardening show a more prominent response.

1.3.2. Corner Region of Increased Strength

The increased strength due to cold forming is, however, confined to a small area at the position of bending and this increase dependent on the method of manufacture. For instance, Cruise, R. B. and Gardner, L. (2008) establish that sections fabricated from annealed material by first forming the flat sheet into a circular hollow section, and then turned it into a rectangular hollow section (shown in Fig. 1.5(b)) exhibit large increase of strength in the corners zone and moderate strength increase in the flat regions. If the section is fabricated from a flat sheet by direct bending then there is no increase of strength in the flat zone of the section, with a large enhancement at the corner zone, which is larger than the increase of strength at the corner due to indirect fabrication. The proof strength enhancement due to the corner forming extend beyond the corner radius of two times the thickness for cold-rolled box sections, while for press breaking it exist within the corner radius which are shown in Fig. 1.7 below.

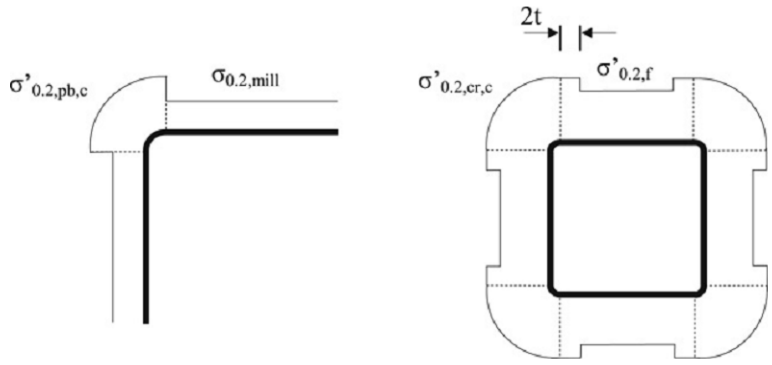

Figure 1.7: Proposed 0.2% proof stress distributions for press-braked sections and cold-rolled boxes [Cruise, R. B. and Gardner, L. (2008)].

1.4. PREVIOUS WORKS ON COLD FORMED MATERIALS

1.4.1. Carbon Steel

The experimental work of strength enhancement due to cold-forming at the corners of carbon steel sections was first studied by Karren, K.W (1967). For this reason, a series of coupon tests on the virgin materials and the corners of the section were performed. From the coupon tests, he concluded that the cold forming could significantly increase the yield strength, but the effect in the increase of ultimate strength was considerably less, and the method of cold forming had only little effect on the material properties of corners. His test specimens were formed using all three processes of cold forming i.e. roll-forming, air press-braking and coin press-braking.

Based on the substantial amount of test data, he identified that significant effect of the r_i/t on the corner properties of the section, with a decrease in r_i/t ratio causing an increase in the corner strength. The ratio of ultimate and yield stress ($f_{u,v}/f_{y,v}$) of the virgin material was also identified as an important parameter.

A semi-empirical equation was derived to define the yield strength ($f_{y,c}$) of the corner .

$$f_{y,c} = \frac{B_c f_{y,v}}{\left(\frac{r_i}{t}\right)^m} \tag{1.13}$$

in which

$$B_c = 3.289\left(\frac{f_{u,v}}{f_{y,v}}\right) - 0.861\left(\frac{f_{u,v}}{f_{y,v}}\right)^2 - 1.34 \tag{1.14}$$

$$m = 0.06\left(\frac{f_{u,v}}{f_{y,v}}\right) + 0.031 \tag{1.15}$$

Where, $f_{y,v}$ and $f_{u,v}$ are the yield strength and ultimate strength of the virgin material respectively, r_i is the inside bend radius and t is the thickness of the sheet.

Afterwards, Karren, K.W. and Winter, G. (1967) observed the influence of cold-forming methods on the mechanical properties of flat portions of open sections. From the observation, they have found that the large increase in the yield strength of the flat part of the roll forming method due to the rolling pressure on the flat portions and the strain hardening and aging of carbon steel sheets. In case of press-braking method, only the strain hardening and aging of carbon steel sheets are responsible to the enhancement of the yield strength in the flat face as there is no effect on the flat face due to the press-breaking process and they have suggested of taking the yield strength of the virgin materials in the flat faces of the press-breaking formation. They also proposed an equation to calculate the full-section tensile yield strength ($f_{y,a}$) for both press-braking and roll-formed sections:

$$f_{y,a} = Cf_{y,c} + (1-C) f_{y,f} \tag{1.16}$$

Where C is the ratio of corner area to the total cross-sectional area, $f_{y,c}$ and $f_{y,f}$ are the average tensile yield strength of the corners and the flat faces respectively.

CEN1996, EN 1993-1-3 and BSI1998, BS5950 accounts the increased strength of the corner due to cold working of the carbon steel sections and allow it in the increase of strength in the whole section by the following expression.

$$f_{y,a} = f_{y,v} + (f_{u,v} - f_{y,v}) \frac{knt^2}{A_g} \tag{1.17 a}$$

but,

$$f_{y,a} \leq \frac{(f_{u,v} + f_{y,v})}{2} \tag{1.17 b}$$

Where,

A_g is the gross cross-sectional area

k is a numerical coefficient that depends on the type of forming as follows:

$k = 7$ for cold-rolling

$k = 5$ for other methods of forming (BS5950 use $k = 5$ for both forming process)

n is the number of 90^0 bends in the cross- section with an internal radius $r \leq 5$ t (fractions of 90^0 bends should be counted as fractions of n)

t is the design core thickness of the steel material before cold-forming, exclusive of metal and organic coatings.

According to the provisions of both EN and BS design standards, the use of Eq. 1.17 in design is limited only to fully effective sections.

1.4.2. Stainless Steel

1.4.2.1. Strength Enhancement at Corner

The great extent of strain hardening property of stainless steel alloys, increase the interest of the researchers to investigate the strength enhancement of the corners of cold-formed stainless steel sections. Coetsee, J. S. et, al. (1990) were the first to investigate the effect of cold work on the strength of cold-formed stainless steel sections by studying three different grades of stainless steel lipped channel sections formed by press-braking. Comparing the stress-strain curve of the virgin sheet to the weighted average stress-strain of the coupon of the different part of the section, they concluded that due to the cold forming strength increases in the corner part of the section.

Van den Berg, G.J. and Van der Merwe, P. (1992) performed an extensive research of the corner properties of different grades of stainless steel with a variety of r_i/t. Based on the analogy with Karren's corner model (Karren, K.W.1967), they proposed an equation for the prediction of corner 0.2% proof strength $\sigma_{0.2,c}$ for stainless steel alloys which are given below:

$$\sigma_{0.2,c} = \frac{B_c \sigma_{0.2,v}}{\left(\frac{r_i}{t}\right)^m} \tag{1.18}$$

in which

$$B_c = 3.289\left(\frac{\sigma_{u,v}}{\sigma_{0.2,v}}\right) - 0.861\left(\frac{\sigma_{u,v}}{\sigma_{0.2,v}}\right)^2 - 1.34 \tag{1.19}$$

$$m = 0.06\left(\frac{\sigma_{u,v}}{\sigma_{0.2,v}}\right) + 0.031 \tag{1.20}$$

Where, $\sigma_{0.2,v}$ and $\sigma_{u,v}$ are the 0.2% proof strength and ultimate strength of virgin material respectively.

In the recent years, Gardner, L. (2002) studied data of three square hollow section (SHS) and two rectangular hollow section (RHS) roll-formed stainless steel members and noted an approximately linear relationship between the 0.2% proof strength $\sigma_{0.2,c}$ of the formed corners and the ultimate strength $\sigma_{u,f}$ of the flat faces. The other test results of Rasmussen, K. J. R. and Hancock, G. J. (1993) on material cut from a completed roll-formed section shows the same trends. So, a simple for the prediction of corner material strength in roll-formed sections are given below:

$$\sigma_{0.2,c} = 0.85\sigma_{u,f} \tag{1.21}$$

This equation is recalibrated by Ashraf, M. et al. (2005), against all available test data and the new final simplified relationship only for the cold rolled stainless steel sections are given below.

$$\sigma_{0.2,c} = 0.82\sigma_{u,f} \tag{1.22}$$

As the previous equation is valid for only the cold rolled stainless steel section, and the mechanical properties of $\sigma_{u,f}$ is not always available, Ashraf, M. et, al. (2005), proposed two power models to predict corner strength in stainless steel sections based on all available test data which follow the methodology of Karren K. W.(1967). The first evolution is the relationship between the corner 0.2% proof strength $\sigma_{0.2,c}$ and virgin material 0.2% proof strength $\sigma_{0.2,v}$ and the second expression is the relationship between the corner 0.2% proof strength $\sigma_{0.2,c}$ and virgin material ultimate strength $\sigma_{u,v}$ are given by:

$$\sigma_{0.2,c} = \frac{1.881\sigma_{0.2,v}}{\left(\frac{r_i}{t}\right)^{0.194}} \tag{1.23}$$

and

$$\frac{\sigma_{0.2,c}}{\sigma_{u,v}} = \frac{C_1}{\left(\frac{r_i}{t}\right)^{C_2}} \tag{1.24}$$

The coefficient, C_1 and C_2 depends on the ratio of $\sigma_{u,v}/\sigma_{0.2,v}$ with,

$$C_1 = -0.382\left(\frac{\sigma_{u,v}}{\sigma_{0.2,v}}\right) + 1.711 \tag{1.25}$$

$$C_2 = 0.176\left(\frac{\sigma_{u,v}}{\sigma_{0.2,v}}\right) - 0.1496 \tag{1.26}$$

To investigate the full scenario of the change of the material properties at the corner of the section, Ashraf, et, al. (2005), also evaluate the ultimate strength $\sigma_{u,c}$ at the corner from the predicted 0.2% proof strength $\sigma_{0.2,c}$ and the strength of the virgin materials. The expression is given by:

$$\sigma_{u,c} = 0.75\sigma_{0.2,c}\left(\frac{\sigma_{u,v}}{\sigma_{0.2,v}}\right) \tag{1.27}$$

Cruise, R.B. and Gardner, L. (2008) modified the expression of Ashraf, et, al. (2005) by refitting the models to include more data from the test and recently published data to predict the enhanced corner strength of the press-braked and cold-rolled sections, denoted as $\sigma_{0.2,pb,c}$ and $\sigma_{0.2,cr,c}$ respectively. The expression are given by,

$$\sigma_{0.2,pb,c} = \frac{1.673\sigma_{0.2,\text{mill}}}{\left(\frac{r_i}{t}\right)^{0.126}} \tag{1.28}$$

$$\sigma_{0.2,cr,c} = 0.83\sigma_{\text{ult},f} \tag{1.29}$$

Rossi, B. et, al. (2013), have presented a new predictive model for predicting the strength increases in cold-formed sections as a result of plastic deformation during production by assessing the proposed predictive models developed by Cruise, R.B. and Gardner, L. (2008) and Rossi, B. (2008). Here, to validate the predictions from the models, a complete database of the tensile coupon tests from the Afshan, S. et, al. (2013) and existing experimental programmes were used. The average plastic strain of the cold-rolling fabrication process was broken down into four key steps:

(A) coiling of the sheet material,
(B) uncoiling of the sheet material,
(C) forming into a circular section and
(D) subsequent deforming into a square or rectangular section.

Assuming the linear variation of the strain through sheet thickness and the bending neutral axis coincides with the material mid thickness they have proposed the average plastic strain through thickness at the corner region $\varepsilon_{c,av}$ are given by:

$$\varepsilon_{c,av} = 0.5[(t/2)/R_c] \tag{1.30}$$

Where, $R_c = r_i + t/2$

From these new strain measures, the strength enhancement in cold-formed structural sections was predicted by the proposed power law model given by:

$$\sigma = p\varepsilon^q \qquad \text{for, } 0 \le \varepsilon \le \varepsilon_u \tag{1.31}$$

Where, the parameters, p and q, are calibrated by the function passes through the 0.2% proof stress and corresponding total strain ($\varepsilon_{t,0.2}$, $\sigma_{0.2}$) and the ultimate tensile stress and corresponding total strain (ε_u, σ_u) points.

$$p = \frac{\sigma_{0.2.\text{mill}}}{\varepsilon_{t,0.2}^q} \tag{1.32}$$

$$q = \frac{ln(\sigma_{0.2,\,\mathrm{mill}} / \sigma_{u,\,\mathrm{mill}})}{ln(\varepsilon_{t,\,0.2} / \varepsilon_u)} \tag{1.33}$$

$$\varepsilon = \varepsilon_{c,\,av} + \varepsilon_{t,\,0.2} \tag{1.34}$$

This new proposed model provides a good agreement with the test data, which is easy to use in structural calculations and is suitable to any metallic structural sections.

1.4.2.2. Strength Increase in the Flat Faces

The expressions for the prediction of strength enhancement in the faces of the cold-rolled box sections on the structural stainless steel design by Cruise, R.B. and Gardner, L. (2008). From the experimental data of them and the other publications, it can be seen that the material strength of the flat portion of press-braking sections is close to that of the unformed sheet material and the strength in the corner regions where large plastic deformations occur during formation process is well above the unformed sheet material. However, in the cold rolled box section, the stress increases are also observed in the flat faces of the section due to the initial formation of the circular tube followed by crushing into the box faces. Considering the level of cold work, they have proposed the equations for the prediction of the 0.2% proof stress ($\sigma_{0.2,f}$) and the ultimate stress ($\sigma_{\mathrm{ult},f}$) at the face of the cold rolled box section which are given below:

$$\sigma_{0.2,f} = \frac{0.85\sigma_{0.2,\mathrm{mill}}}{-0.19 + \frac{1}{12.42\left(\frac{\pi t}{2(b+d)}\right)+0.83}} \tag{1.35}$$

$$\sigma_{\mathrm{ult},f} = \sigma_{\mathrm{ult,mill}}\left(0.19\left(\frac{\sigma_{0.2,f}}{\sigma_{0.2,\mathrm{mill}}}\right) + 0.85\right) \tag{1.36}$$

Where,

$$\varepsilon_f = \frac{\pi t}{2(b+d)} \tag{1.37}$$

is the strain experienced at the section face during the forming of a box from a circular tube.

Rossi, B. et, al. (2013), described that the flat faces of cold-rolled sections experience coiling and uncoiling in the rolling direction followed by bending and unbending, in the direction perpendicular to rolling direction. So, the step (C) forming into the circular shape has the greatest influence of the plastic deformation in the flat faces. Assuming the linear variation of the of the strain through sheet thickness and the bending neutral axis coincides with the material mid thickness they have proposed the average plastic strain through thickness of the flat faces $\varepsilon_{f,av}$ is given by:

$$\varepsilon_{f,av} = [(t/2)/R_{coiling}] + [(t/2)/R_f] \tag{1.38}$$

Where, $R_f = (b+h-2t)/\pi$

1.4.2.3. Strength Enhancement in the Whole Section

Rossi, B. et, al. (2013) have also express the enhancement 0.2% proof strength of the cross-section following the Cruise, R. B. and Gardner, L. (2008) confinement of enhanced corner strength for the press-breaking and cold-rolling formation.

For press-breaking section:

$$\sigma_{0.2,section} = \frac{(\sigma_{0.2,c,pred} A_{c,pb}) + (\sigma_{0.2,mill}(A - A_{c,pb}))}{A} \tag{1.39}$$

For cold-rolling section:

$$\sigma_{0.2,section} = \frac{(\sigma_{0.2,c,pred} A_{c,rolled}) + (\sigma_{0.2,f,pred}(A - A_{c,rolled}))}{A} \tag{1.40}$$

Where,

$A_{c,pb} = A_c = (n_c \pi t/4)(2r_i + t)$

$A_{c,rolled} = A_c + 4n_c t^2$,

A = the gross section area and n_c is the number of 90^0 bend.

Afshan, S. et, al. (2013) describes an experimental programme in a wide range cold formed structural sections containing Square Hollow Sections (SHS), Rectangular Hollow Sections (RHS) and Circular Hollow Section (CHS) to measure the level of strength enhancement of cold-formed structural sections, covering both carbon steel and a variety of stainless steel grades. By combining the test data with the previous existing stress – strain data on cold-formed stainless steel sections from the literature, they have proposed the revised values for the model parameters n, $n'_{0.2,u}$ and $n'_{0.2,1.0}$ and Young's modulus of elasticity E for commonly used stainless steel grades. They have recommended a single value of E ($195*10^3$ N/mm^2) for the stainless steel grades which are considered in this paper and also confirmed the accuracy of the expression of the CEN1996, EN 1993-1-4 Annex C for determining the strain (ε_u) at the ultimate tensile stress (σ_u).

$$\varepsilon_u = 1 - \frac{\sigma_{0.2}}{\sigma_u} \tag{1.41}$$

Where, $\sigma_{0.2}$ is the 0.2% proof stress.

1.4.3. Residual Stresses

1.4.3.1. Experimental Works

Residual stresses are important in cold-formed sections to predict their behaviour and strength. The zone of tensile residual stress on the inside surface of the bend is a possible source of fatigue cracking under cyclic loading and this region is more susceptible to stress corrosion. For this major concerning issue, the residual stresses were often measured in the laboratory and most of the existing results are for carbon steel sections. Rasmussen, K. J. R. and Hancock, G. J. (1993) and Jandera, M. et, al. (2008) have measured the residual stresses on stainless steel tubular sections but their study did not lead to any idealized model for residual stresses in stainless steel. The existing experimental studies of residual stresses in carbon steel sections are described below.

There are different methods for determining the residual stresses in the laboratory which can be categorized into three groups: non-destructive methods, semi-destructive methods and destructive methods.

In the non-destructive methods, X-ray diffraction (XRD) is a technique based on the principal that inter-planar spacing of the atomic planes is changed within a specimen when subjected to stresses. But it is difficult to predict the stresses due to cold working because it causes the change of texture and grain size of the material. Another method called neutron diffraction is more sophisticated than XRD due to its much greater penetration capacity. A recent innovation of ultrasonic technique based on the principal that residual stresses can cause the changes in velocity and attenuation of ultrasonic waves applied to the specimens.

Hole-drilling is the most commonly used semi-destructive method. The hole is usually less than 1/8 inch (3.175 mm) in both diameter and depth which may not impair the structural integrity of the test specimens and based on the principal that drilling of hole on the stress field locally relaxes the residual stresses, thus ensuing in strain released by hole-drilling. The other methods which are occasionally used named indentation method, trepanning method and Gunnert's method.

Destructive method are the most common mechanical method for measuring the residual stresses, removing the portion of metal by cutting, drilling, grinding and etching etc. The sectioning method (saw-cutting) were commonly used for the previous experimental works, which gave more reliable value of measured residual stresses but with limitation that it needs more time and cost.

Batista, E. M. and Rodrigues, F. C. (1992) have measured the longitudinal residual stresses distribution in both roll-formed and press-braked channel sections with the same cross-sectional geometry by the sectioning method. From their observation, they have concluded that residual stresses in roll-formed sections were larger than those in press-braked sections and the magnitude of residual stresses depends on the amount of cold work.

Weng, C. C. and Pekoz, T. (1990) have measured longitudinal residual stresses in cold-formed channel sections and found that residual stresses in corner regions were higher than those in flat portions (webs, flanges and lips). They have also observed that the inner surface of the section was subjected to compressive residual stresses while the outer surface was subjected to tensile residual stresses.

Abdel-Rahman, N. and Sivakumaran, K. S. (1997) have found the similar observation as that of Weng, C. C. and Pekoz, T. (1990) and they have only considered the longitudinal residual stresses, as the magnitude of the transverse residual stresses are small on the sheet surface. From these ideologies, most of existing studies on the modelling of residual stresses have been focused only for longitudinal residual stresses.

Weng, C. C. and Pekoz, T. (1990) and Abdel-Rahman, N. and Sivakumaran, K. S. (1997) respectively proposed two different idealized distributions for longitudinal residual stresses in channel sections from their experimental result. In these two model the residual stress variation through thickness are based on the assumption that the longitudinal residual stresses varies linearly across the plate thickness with the maximum tensile value on the outer surface and its maximum compressive value on the inner surface of the section. In these two studies, the magnitudes of the tensile and compressive surface longitudinal residual stresses were same, because they have considered only the bending, neglecting the membrane component of residual stresses.

In case of distribution of longitudinal residual stresses through the perimeter they have given different idealizations. According to Weng, C. C. and Pekoz, T. (1990), the longitudinal residual stresses are distributed uniformly through the perimeter of the section by neglecting the increase of residual stresses at corners, and the maximum longitudinal residual stress is taken to be 50% of the yield stress of the flat material. On the other hand, Abdel-Rahman, N. and Sivakumaran, K. S. (1997) have divided a cold-rolled channel section into two zones: a flat zone and a corner zone. The magnitude of the longitudinal surface residual stress in the corner zone is taken to be 40% of the yield stress of the flat material, and the longitudinal surface residual stress in the flat zone is assumed to have a

magnitude varying from 12% to 18% of the yield stress of the flat material depending on steel grades.

Schafer, B. W. and Peköz, T. (1998) idealized longitudinal residual stresses across the plate thickness by considering both of a bending component and a membrane component, assuming that the linear variation of the stresses through thickness. They have collected and studied the available experimental data of residual stresses in various cross sections formed by both the roll-forming and proposed that the longitudinal residual stresses in various parts of a cold-formed section can be modelled by the corresponding statistical means. From their static analysis, the membrane component can be ignored provided that the increase of yield strength due to the cold work of forming is not modelled.

In existing experimental studies which are described previously, only surface residual stresses were measured due to the small plate thickness, with the assumption of linear variation of stress through the thickness because it is difficult to examine the variation of residual stress across the thickness for thin sheets.

Key, P. W. and Hancock, G. J. (1993) carried out an experimental study on residual stresses in thick cold-rolled square hollow sections (SHS), and proposed idealized distributions of both longitudinal and transverse residual stresses of the section. Due to a greater plate thickness they were able to measure the complex residual stress variations through-thickness and the both longitudinal and transverse residual stresses in SHS sections.

1.4.3.2. Theoretical Approach

The experimental measurements of residual stresses in cold-formed thin-walled sections are time-consuming, difficult and with limited accuracy that the variation of stress cannot be obtained accurately. Also, the experimental result of thicker plate have illustrated that the variation of stress through the thickness were in a complex. Furthermore, clear relationships between residual stresses and various steps of the fabrication process (coiling, uncoiling including flattening and formation of sections by

cold rolling or press-breaking) cannot be established by an examination of the measurement results.

Ingvarsson, L. (1975) and Kato, B. and Aoki, H. (1978) modelled the pure plastic bending of a wide plate as a plane strain problem by means of an incremental numerical process, with the steel assumed to obey the von Mises yield criterion and the Prandtl-Reuss flow rule.

Rondal, J. (1987) presented a similar numerical analysis of the pure plastic bending of wide plates, and then proposed an approximate approach of deriving residual stresses in channel sections based on the results from his pure bending analysis. Complex residual stress variations were shown through the plate thickness for the all three numerical analysis.

It is most prevailing thing to model the manufacturing process of cold formed section to predict the residual stresses. Before cold forming either by roll forming or press braking, the flat sheet already has the experience the coiling, uncoiling and flattening process. So, the residual stresses in a cold-formed section resulting from the coiling, uncoiling and flattening process and the cold-forming process. For predicting residual stresses in cold formed section, Quach, W. M. (2005) has done the analytical analysis for the pure bending of wide plates with different amounts of straining in the two orthogonal directions which involve the residual stresses from the coiling and uncoiling including flattening and from the cold bending processes.

2. OBJECTIVES

The main objectives of the thesis work are to:

1) develop an analytical model for the structural behaviour of cold formed member considering residual stresses and plastic strain developed in the section.
2) validate the developed model with the numerical and experimental data.
3) predict the mechanical properties of the material using existing test of cold formed stainless steel.
4) compare the results with the existing predictive formulas for cold formed stainless steel sections.

3. ANALYTICAL MODELLING

Maple 18.01 is used in this analysis. It is powerful mathematical software developed by Maplesoft company in Waterloo, Ontario, Canada. In this software it is easy to enter the mathematical equations by using the traditional mathematical notations. Here the mathematic are live so if something is changed and re-executed in the problem, it gives the new results according to the changes. So if once the equation is write in proper way then the parametric study can be done in easier way. Other important thing is that for so many output data, it can be represented in a tabular and graphical form and also can be exported in the Excel file.

3.1. AXIAL EXPRESSION

The terminology used for denoting the stress and strain in different direction of cold formed sheet should be quoted before the analysis. In this study, the direction of coiling and uncoiling of sheet is referred to as longitudinal direction, denoted by 'z' axis. The width direction of the sheet is referred to as transverse direction, denoted by 'x' axis. The direction normal to the sheet is referred to as through-thickness direction, denoted by 'y' axis. For more convenient, a cold form sheet with notating the directions is given in Fig. 3.1 below, where t is the thickness of the sheet and D is the coil diameter.

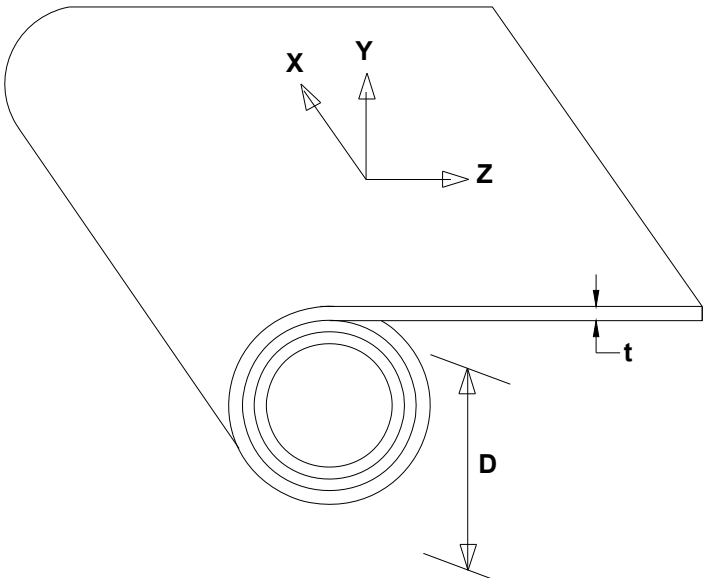

Figure 3.1: Direction of sheet axis.

The advantages of choosing these directions, mainly the longitudinal direction of the sheet remain the longitudinal direction of cold formed member. In the coiling and uncoiling process bending occurs in the longitudinal direction of the sheet. On the other hand, in the press-breaking process and cold rolling of box sections the bending occurs in the transverse direction, and the outer surface of the coiled sheet becomes the inner surface of the cold formed member.

3.2. ANALYTIC SOLUTION FOR COILING AND UNCOILING

3.2.1. Assumptions

1) The stainless steel is considered as isotropic material.

2) The flat steel sheet is assumed to be free from residual stresses before it is coiled for storage.

3) The stress-strain curve of the steel sheet is assumed to possess as of the virgin material before coiling the sheet.

4) The coiling of sheet and its subsequent uncoiling and flattening is modelled as plane strain pure bending in the y-z plane.

3.2.2. Geometric Properties

The thickness of the stainless steel sheet t = 2mm

Coiling radius, $r = D/2$ = 250 mm

Coiling curvature, κ_c = 1/250

3.2.3. Material Modelling

To validate the analytical model, the commonly used austenitic stainless steel grade 304 is used same as used in Quach, W.M. (2005) model. The material is assumed to be isotropic nonlinear strain-hardening material with the mechanical properties for longitudinal tension which is specified in Appendix B of AS/NZS 4673 Standard [AS/NZS (2001)] are given below:

The 0.2% proof stress, $\sigma_{0.2}$ = 205.0 MPa,

Initial elastic modulus, $E_0 = 195.0*10^3$ MPa,

The strain-hardening exponent, n = 7.5

The tangent modulus at the 0.2% proof stress (Eq. 1.7) $E_{0.2}$ = 12771.56 MPa

Poisson's ratio, v = 0.3

The non-dimensional parameter with respect to 0.2% proof stress,

$$e = \sigma_{0.2}/ E_0 = 205.0/(195.0*10^3) = 0.00105.$$

As the nonlinear stress-strain behaviour of stainless steel alloys described by the Ramberg-Osgood relationship can closely approximate measured stress-strain curves up to the 0.2% proof stress $\sigma_{0.2}$, a new 3-stage stress-strain model is used for the analytical model, which is developed by Quach, W. M. (2005). This 3- stage model which can measure the full range of stress-strain curve for both tensile and compressive strain is given below in Eq. 3.1. In the equation the upper sign is used for tension and lower sign for compression.

$$\varepsilon = \begin{cases} \dfrac{\sigma}{E_0} + 0.002\left(\dfrac{\sigma}{\sigma_{0.2}}\right)^n, & \sigma \le \sigma_{0.2} \\ \dfrac{\sigma-\sigma_{0.2}}{E_{0.2}} + \left[0.008 + (\sigma_{1.0}-\sigma_{0.2})\left(\dfrac{1}{E_0}-\dfrac{1}{E_{0.2}}\right)\right]\left(\dfrac{\sigma-\sigma_{0.2}}{\sigma_{1.0}-\sigma_{0.2}}\right)^{n'_{0.2,1.0}} + \varepsilon_{0.2}, & \sigma_{0.2} < \sigma \le \sigma_{2.0} \\ \dfrac{\sigma-a}{b \mp \sigma}, & \sigma > \sigma_{2.0} \end{cases} \quad (3.1)$$

For determining the strain from the above Eq. 3.1, besides the basic material properties got from the AS/NZS (2001), the other required properties are calculated by using the following expression which are found by analysing the previous tension coupon test data [Quach, W. M. (2005)].

The expression for 1.0% proof stress $\sigma_{1.0,}$

$$\frac{\sigma_{1.0}}{\sigma_{0.2}} = 0.542\frac{1}{n} + 1.072 \quad (3.2)$$

$$\Rightarrow \sigma_{1.0} = 205(0.542/7.5+1.072) = 234.57 \text{ MPa}$$

The expression for $n'_{0.2.1.0}$,

$$n'_{0.2,1.0} = 12.255\left(\frac{E_{0.2}}{E_0}\right)\left(\frac{\sigma_{1.0}}{\sigma_{0.2}}\right)+1.037 \tag{3.3}$$

$$= 12.255(12771.56/195.0*10^3)(234.57/205.0)+ 1.037$$

$$= 1.953$$

The expression for 2.0% proof stress $\sigma_{2.0,}$

$$\sigma_{2.0} = \sigma_{0.2} + (\sigma_{1.0} - \sigma_{0.2})A^{1/n'_{0.2,1.0}}\left[1 - \frac{(1/E_{0.2} - 1/E_0)\sigma_{0.2}}{B}\right]^{1/n'_{0.2,1.0}} \tag{3.4}$$

$$=205+(234.57-205)*5.654^{(1/1.953)}[1-((1/12771.56-1/195.0*10^3)*205/0.033)]^{(1/1.953)}$$

$$= 257.64 \text{ MPa}$$

Where,

$$A = \frac{B}{0.008 + e(\sigma_{1.0}/\sigma_{0.2} - 1)(1 - E_0/E_{0.2})} \tag{3.5}$$

$$= 0.033/[0.008+0.00105(234.57/205.0 -1)(1-195.0*10^3/12771.56)]$$

$$= 5.654$$

$$B = 0.018 + e\left(\frac{E_0}{E_{0.2}} - 1\right) \tag{3.6}$$

$$= 0.018+0.00105(12771.56/195.0*10^3-1) = 0.033$$

The expression for ultimate strength $\sigma_{u,}$ and corresponding strain ε_u

$$\frac{\sigma_u}{\sigma_{0.2}} = \frac{1}{0.2 + 185e} \tag{3.7}$$

$$\Rightarrow \sigma_u = 205/(0.2+185*0.00105) = 520 \text{ MPa}$$

$$\varepsilon_u = 1 - \frac{\sigma_{0.2}}{\sigma_u} \tag{3.8}$$

$$= 1-(205/520) =0.605> 0.6, \text{ so use } 0.6$$

The expression of constant *a* and *b*,

$$a = \sigma_{2.0}\left(1 \pm \varepsilon_{2.0}\right) - b\varepsilon_{2.0} \tag{3.9}$$

$$= 257.64(1+0.0213) - 983.05*0.0213$$

$$= 242.17$$

$$b = \frac{\sigma_u\left(1 \pm \varepsilon_u\right) - \sigma_{2.0}\left(1 \pm \varepsilon_{2.0}\right)}{\varepsilon_u - \varepsilon_{2.0}} \tag{3.10}$$

$$= [520(1+0.6) - 257.64(1+0.0213)]/(0.6-0.0213)$$

$$= 983.05$$

$$\varepsilon_{2.0} = \frac{\sigma_{2.0}}{E_0} + 0.02 \tag{3.11}$$

$$= (257.64/195.0*10^3)+0.02 = 0.0213$$

In calculating the constants *a* and *b*, here it is used the upper sign, as the analysis is done for tension.

As in the coupon test, due to the longitudinal straining the width and thickness shrink, there is a variation of cross-section. The nominal or engineering stress and strain are calculated based on the original dimension of the material. Hence the term true stress and strain are calculated based on the actual dimensions of the material. The continuous monitoring of the thickness and width during the test is a tedious and complex task. The true stress σ_t and true strain ε_t can be calculated from the nominal stress σ_n and nominal strain ε_n by using the following relationship:

$$\sigma_t = \sigma_n\left(1 \pm \varepsilon_n\right) \tag{3.12a}$$

$$\varepsilon_t = \pm\ln\left(1 \pm \varepsilon_n\right) \tag{3.12b}$$

By using the 3-stage stress-strain expression the true and nominal stress-strain diagram for austenitic steel are given in Fig.3.2 below.

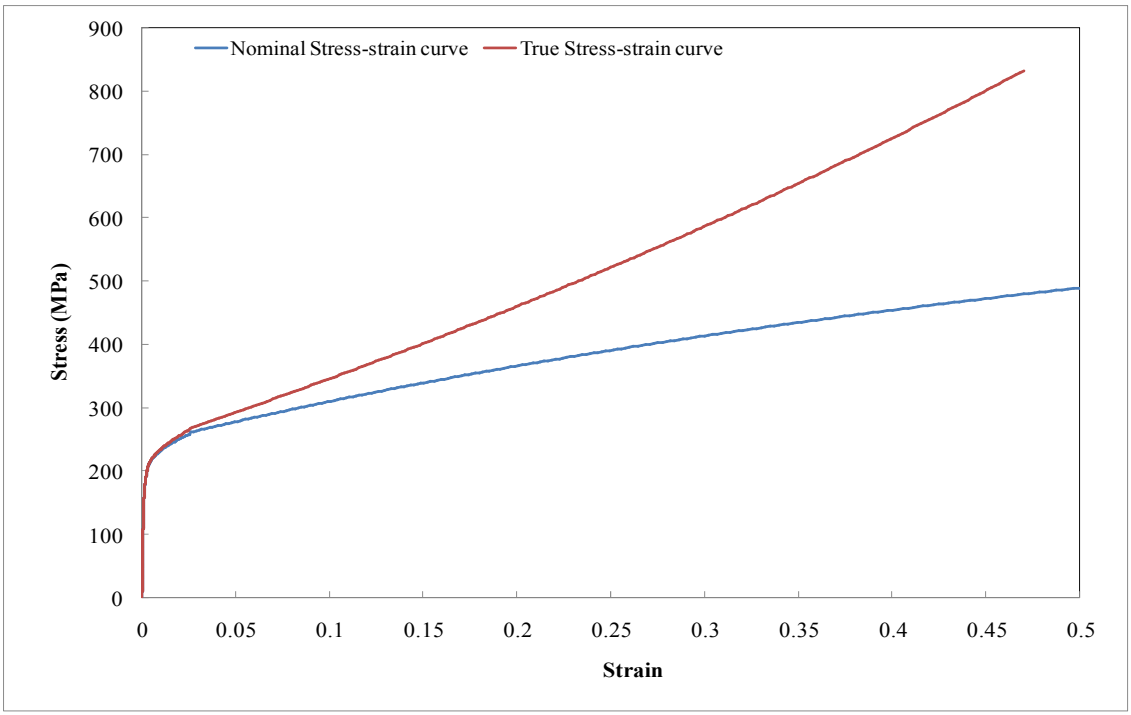

(a) Full stress-strain diagram

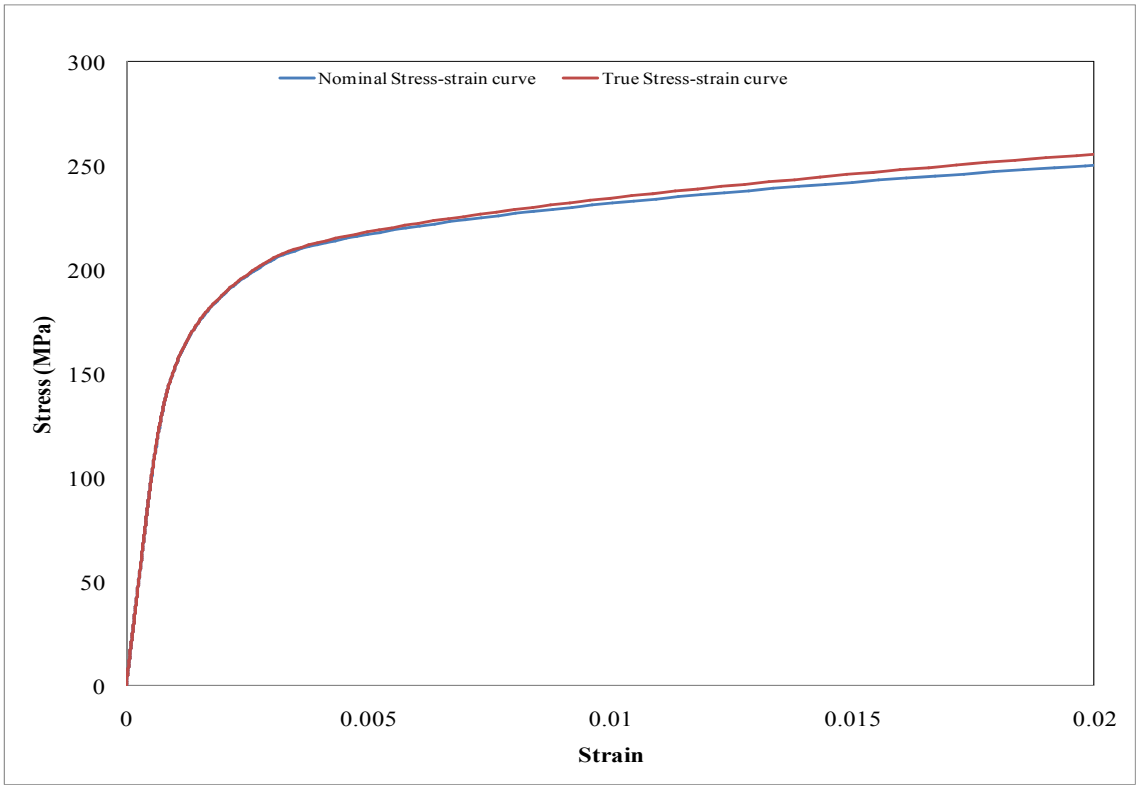

(b) Initial state of the stress-strain diagram

Figure 3.2: Stress-strain curves of the austenitic stainless steel (tensile coupon test).

From the above Fig. 3.2, it is shown that at the initial stage there is no significant difference between the nominal stress-strain and the true stress-strain curve. So at small and intermediate strain levels, nominal stress-strain curves obtained from coupon tests can accurately describe the stress-strain behaviour of materials. But in the full stress-strain curve, the variation between the nominal stress-strain and the true stress-strain curve are significant. The deviation at large strain is due to the fact of that the nominal stress-strain curve does not take into account the changes of cross sections of test coupons. Hence, the stress-strain behaviour of the material at large strains cannot be accurately described by the nominal stress-strain relationship.

3.2.4. For Coiling

Through thickness an arbitrary point in the sheet undergoes elastic or elastic-plastic deformation due to coiling of steel sheet, depending on the coiling curvature κ_c and its location 'y' away from the neutral axis of the section.

The in-plane strain under a plane strain condition in the x direction (width) and a plane stress condition in the y direction (thickness) for elastic material points across the thickness are given by:

$$\varepsilon_{z,c} = \frac{\left(\sigma_{z,c} - \nu\sigma_{x,c}\right)}{E_0} \tag{3.12a}$$

$$\varepsilon_{x,c} = \frac{\left(\sigma_{x,c} - \nu\sigma_{z,c}\right)}{E_0} = 0 \tag{3.12b}$$

Where,

E_0 is the initial elastic modulus,

ν is the Poisson's ratio,

$\sigma_{x,c}$ and $\sigma_{z,c}$ are the stresses in the x and z directions due to coiling of steel respectively.

$\varepsilon_{x,c}$ and $\varepsilon_{z,c}$ are the corresponding strains.

So, the elastic coiling stress in the z and x direction at any arbitrary location of '*y*' from the neutral axis with respect to the longitudinal strain $\varepsilon_{z,c}$ due to bending in the z direction are given below

$$\sigma_{z,c} = \frac{E_0}{\left(1-\nu^2\right)}\varepsilon_{z,c} \tag{3.13a}$$

$$\sigma_{x,c} = \frac{\nu E_0}{\left(1-\nu^2\right)}\varepsilon_{z,c} \tag{3.13b}$$

with

$$\varepsilon_{z,c} = \kappa_c y \tag{3.13c}$$

For material points undergoing plastic straining, the Von Mises yield criterion is satisfied

$$\bar{\sigma} = \sigma_{yc} \tag{3.14}$$

Where,

σ_{yc} is the instantaneous yield stress reached at the end of coiling,

and $\bar{\sigma}$ is the equivalent stress, for the plane stress condition in the through-thickness direction given by

$$\bar{\sigma} = \sqrt{\sigma_{z,c}^2 + \sigma_{x,c}^2 - \sigma_{x,c}\sigma_{z,c}} \tag{3.15}$$

For a material point at the onset of yielding, where the initial yield stress equals the instantaneous yield stress at the end of coiling (σ_{y0}= σ_{yc}), the von Mises yield criterion can be expressed as

$$\sqrt{\sigma_{z,c}^2 + \sigma_{x,c}^2 - \sigma_{x,c}\sigma_{z,c}} = \sigma_{y0} \tag{3.16}$$

The longitudinal stress at which material start yielding is expressed as

$$\varepsilon_{z,cy} = \pm\sigma_{y0}\left(1-\nu^2\right)\Big/\left(E_0\sqrt{1-\nu+\nu^2}\right) \tag{3.17}$$

'+' sign indicate that the strain is in tension (i.e. y>0)

Under a definite coiling curvature κ_c the central core of the material remains elastic and the thickness of the core is the twice of the value given in the following expression.

$$y_{cy} = \sigma_{y0}\left(1-\nu^2\right)\Big/\left(E_0\kappa_c\sqrt{1-\nu+\nu^2}\right) \tag{3.18}$$

Hence, the point through thickness, for $|y| < y_{cy}$ is in the elastic zone and followed the Eq. 3.13 for stress calculation. For $|y| > y_{cy}$, the zone is plastic and the stresses obey the Von Mises yield criterion in which the coiling stresses of any point can then be obtained as

$$\sigma_{z,c} = \pm\frac{\sigma_{yc}}{\sqrt{1-\omega_c+\omega_c^2}} \tag{3.19a}$$

$$\sigma_{x,c} = \pm\frac{\omega_c\sigma_{yc}}{\sqrt{1-\omega_c+\omega_c^2}} \tag{3.19b}$$

Where,

$$\omega_c = \sigma_{x,c}/\sigma_{z,c} \tag{3.20}$$

As the material is considered as isotropic, the relationship between the equivalent stress and equivalent plastic strain is described by the uniaxial stress-strain relationship given by the function

$$\sigma = F(\varepsilon) \text{ or } \varepsilon = f(\sigma) \tag{3.21}$$

That is,

$$\bar{\sigma} = \sigma, \text{ when } \bar{\varepsilon}_p = \varepsilon_p \tag{3.22a}$$

and

$$d\bar{\sigma} = d\sigma, \text{ when } d\bar{\varepsilon}_p = d\varepsilon_p \tag{3.22b}$$

For strain-hardening materials, σ_{yc} and ω_c are related to each other. To establish their relationship, the stress ratio ω_c and its increment $d\omega_c$ can be expressed in terms of the stress σ and the stress increment $d\sigma$ from the uniaxial stress-strain curve.

For material points under plastic straining, the slope of the equivalent stress-equivalent plastic strain relation H' is equal to the corresponding slope of the uniaxial stress-plastic strain curve:

$$H' = \frac{d\bar{\sigma}}{d\bar{\varepsilon}_p} = \frac{d\sigma}{d\varepsilon_p} = \left(\frac{d\varepsilon}{d\sigma} - \frac{1}{E_0} \right)^{-1} \tag{3.23}$$

The ratio of the stress increment is expressed as

$$\Omega_c = \frac{4\nu H'\left(1-\omega_c+\omega_c^2\right) - E_0\left(2-\omega_c\right)\left(2\omega_c-1\right)}{E_0\left(2\omega_c-1\right)^2 + 4H'\left(1-\omega_c+\omega_c^2\right)} \tag{3.24}$$

Hence, the stress increment ratio as a function of stress is given by

$$d\omega_c = \frac{2\left(1-\omega_c+\omega_c^2\right)\left(\Omega_c-\omega_c\right)}{\sigma\left[\left(2-\omega_c\right)+\Omega_c\left(2\omega_c-1\right)\right]} d\sigma \tag{3.25}$$

The equivalent plastic for a given coiling curvature κ_c is given by

$$\bar{\varepsilon}_{p,c} = \varepsilon_{p,c} = \varepsilon_{yc} - \frac{\sigma_{yc}}{E_0} \tag{3.26}$$

Where, σ_{yc} and ε_{yc} are the instantaneous yield stress and the corresponding strain reached at the end of coiling.

The longitudinal increment coiling strain consist of both elastic strain increment and plastic strain increment with respect to stress increment is given by

$$d\varepsilon_{z,c} = \pm\left\{\begin{array}{l}\dfrac{\left[(1-2\omega_c)^2 - 2\nu(1-2\omega_c)(2-\omega_c)+(2-\omega_c)^2\right]\sigma}{2E_0(1-2\omega_c)\left(1-\omega_c+\omega_c^2\right)^{3/2}}d\omega_c \\ +\dfrac{(1-\omega_c^2)(1-2\nu)}{E_0(1-2\omega_c)\left(1-\omega_c+\omega_c^2\right)^{1/2}}d\sigma\end{array}\right\} \tag{3.23}$$

The limiting value of coiling curvature denoting κ_{cy} at which the extreme surface of the sheet start to yield is found by substituting $\varepsilon_{z,c} = \kappa_{cy}\, t/2$ in Eq. 3.17.

$$\kappa_{cy} = 2\sigma_{y0}(1-\nu^2)\Big/\left(E_0 t\sqrt{1-\nu+\nu^2}\right) \tag{3.24}$$

The value of κ_{cy} depends on the material properties of the sheet. If the value of $\kappa_{cy} > \kappa_c$ no plastic bending occurs due to coiling and the residual stress after uncoiling will be zero. On the other hand, if $\kappa_{cy} < \kappa_c$ the yielding occurs in coiling process and resulting the residual stresses at the end of the coiling and uncoiling process.

3.2.5. For Uncoiling including Flattening

When $\kappa_{cy} < \kappa_c$, the natural uncoiling of a coiled sheet leads to a sheet with a small residual curvature, but in practice this curvature is removed before or during cold forming. In the present analysis, flattening is assumed to take place before cold forming to remove the residual curvature by applying the curvature equal to coiling curvature (κ_c) in magnitude but opposite in direction. Hence the uncoiling curvature is defined as

$$\kappa_u = -\kappa_c \tag{3.25}$$

The total stress at any point after such uncoiling including flattening is found by adding the stresses due to coiling and uncoiling of the sheet.

$$\sigma_{z,r} = \sigma_{z,c} + \sigma_{z,u} \tag{3.26a}$$

$$\sigma_{x,r} = \sigma_{x,c} + \sigma_{x,u} \tag{3.26b}$$

The uncoiling stress remains elastic until the reverse bending curvature exceed the uncoiling curvature limit κ_{uy}. The uncoiling elastic stress is given by:

$$\sigma_{z,u} = \frac{E_0}{\left(1-\nu^2\right)}\kappa_u y \tag{3.27a}$$

$$\sigma_{x,u} = \frac{\nu E_0}{\left(1-\nu^2\right)}\kappa_u y \tag{3.27b}$$

The uncoiling curvature limit κ_{uy} can be expressed as

$$\kappa_{uy} = -\frac{\sigma_{yc}\left(1-\nu^2\right)\left[2-\nu+(2\nu-1)\omega_c\right]}{E_0|y|\left(1-\nu+\nu^2\right)\sqrt{1-\omega_c+\omega_c^2}} \tag{3.28}$$

The total longitudinal strain of any point at the onset of reverse yielding (shown as point UE in Fig. 3.3) during uncoiling is

$$\varepsilon_{z,uy} = \left(\kappa_c + \kappa_{uy}\right)y \tag{3.29}$$

The corresponding uncoiling stresses are

$$\sigma_{z,uy} = \frac{E_0}{\left(1-\nu^2\right)}\kappa_{uy} y \tag{3.30a}$$

$$\sigma_{x,uy} = \frac{\nu E_0}{\left(1-\nu^2\right)}\kappa_{uy} y \tag{3.30b}$$

and the corresponding stress ratio

$$\omega_{uy} = \frac{\left[\left(1-\nu^2\right)\omega_c - \nu(2-\nu)\right]}{\left[(1-2\nu)\omega_c - \left(1-\nu^2\right)\right]} \tag{3.31}$$

Hence, when $\kappa_c \leq |\kappa_{uy}|$, the uncoiling stresses

$$\sigma_{z,u} = -\frac{E_0}{\left(1-\nu^2\right)}\kappa_c y \tag{3.32a}$$

$$\sigma_{x,u} = -\frac{\nu E_0}{\left(1-\nu^2\right)}\kappa_c y \tag{3.32b}$$

When, $\kappa_c > |\kappa_{uy}|$, reverse yielding will occurs and the total stress after uncoiling including flattening is

$$\sigma_{z,r} = \mp\frac{\sigma_{yr}}{\sqrt{1-\omega_u+\omega_u^2}} \tag{3.33a}$$

$$\sigma_{x,r} = \mp\frac{\omega_u\sigma_{yr}}{\sqrt{1-\omega_u+\omega_u^2}} \tag{3.33b}$$

with,

$$\omega_u = \sigma_{x,r}/\sigma_{z,r} = \left(\sigma_{x,c}+\sigma_{x,u}\right)/\left(\sigma_{z,c}+\sigma_{z,u}\right) \tag{3.34}$$

Similar to coiling, the equivalent plastic strain after uncoiling

$$\bar{\varepsilon}_{p,r} = \varepsilon_{p,r} = \varepsilon_{yr} - \frac{\sigma_{yr}}{E_0} \tag{3.35}$$

in which the subscript $'r'$ refers to the end of the uncoiling stage, and σ_{yr} and ε_{yr} are the instantaneous yield stress and the corresponding strain reached at the end of flattening with their relationship defined by the function in Eq. 3.21.

As like the coiling, the increment of the stress ratio during uncoiling can be expressed as

$$d\omega_u = \frac{2\left(1-\omega_u+\omega_u^2\right)\left(\Omega_u-\omega_u\right)}{\sigma\left[\left(2-\omega_u\right)+\Omega_u\left(2\omega_u-1\right)\right]}d\sigma \tag{3.34}$$

in which is the ratio of stress increments $\Omega_u = d\sigma_{x,r}/\, d\sigma_{z,r}$ is given by

$$\Omega_u = \frac{4\nu H'\left(1-\omega_u+\omega_u^2\right)-E_0\left(2-\omega_u\right)\left(2\omega_u-1\right)}{E_0\left(2\omega_u-1\right)^2+4H'\left(1-\omega_u+\omega_u^2\right)} \tag{3.35}$$

Here, H' is defined in Eq. 3.23 as for coiling.

The equation for longitudinal strain increment during uncoiling can also be obtained as

$$d\varepsilon_{z,u} = \pm\left\{\begin{array}{l} -\dfrac{\left[\left(1-2\omega_u\right)^2-2\nu\left(1-2\omega_u\right)\left(2-\omega_u\right)+\left(2-\omega_u\right)^2\right]\sigma}{2E_0\left(1-2\omega_u\right)\left(1-\omega_u+\omega_u^2\right)^{3/2}}d\omega_u \\ -\dfrac{\left(1-\omega_u^2\right)\left(1-2\nu\right)}{E_0\left(1-2\omega_u\right)\left(1-\omega_u+\omega_u^2\right)^{1/2}}d\sigma \end{array}\right\} \tag{3.36}$$

3.2.6. Verification of Model

Maple 18.01 is used for the analytic analysis of stainless steel sheet. Here, the thickness of the sheet is equally divided into 28 parts to observe the residual stress and plastic strain distribution through thickness. To verify this analytical model for coiling and uncoiling, the result of the model is compared with the analytical solution of Quach, W.M. (2005). An austenitic stainless steel grade 304 sheet of 2 mm thickness is taken and all the other material and geometrical properties are kept same as used is Quach, W.M. (2005) analysis. The material is modelled in 3 stages considering nonlinearity which is described above to provide the nominal stress-strain behaviour until the ultimate state. As in the coiling-uncoiling process, the produced strain level is small, so the nominal stress-strain curves obtained from coupon tests can accurately describe the stress-strain behaviour. In the small strain level (initial stress-strain curve), the difference between the true stress-strain curve

and the nominal stress-strain curve is negligible. For this reason, in this study, 3-stage nominal stress-strain relationship is used for determining the residual stresses and equivalent plastic strain in coiling and uncoiling stage.

The results of longitudinal and transverse residual stresses and equivalent plastic strain are seen to be very close agreement with the Quach, W.M. (2005) solution. Hence, it reveals that the analytical model by using the Maple is valid.

Due to the round shape stress-strain behaviour of the stainless steel, there is no elastic coiling stage and the stress path of the extreme fibre undergoes plastic strain. During this stage, across the whole thickness there is an inelastic straining for which the coiling stress distribution and the equivalent plastic strain are nonlinear.

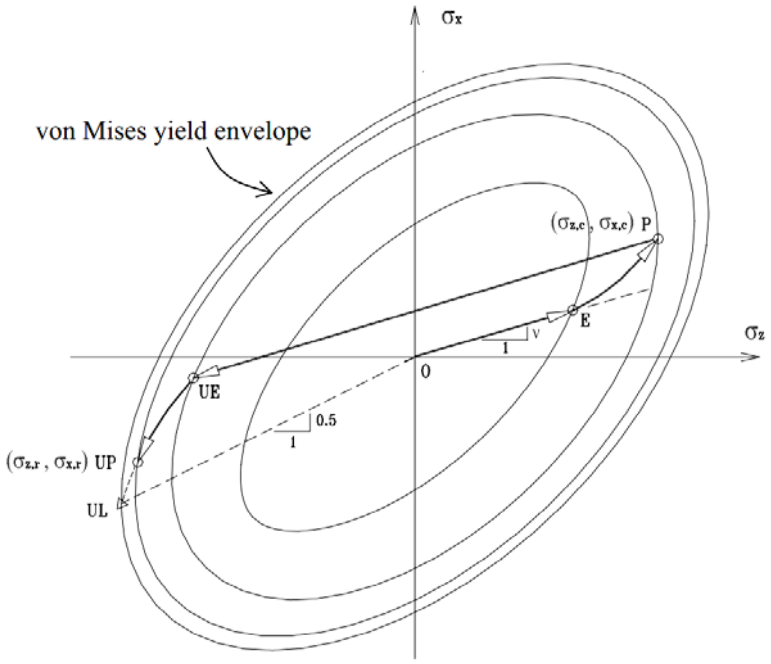

Figure 3.3: Stress path of a surface point of a strain-hardening steel strip during the coiling-uncoiling process [Quach, W. M. (2005)].

Hence, for stainless steel there is no existence of linear OE line in von Mises yield envelop which is shown in Fig. 3.3. E coincides to the point O. So the stress path of a surface point of the austenitic stainless steel due to coiling follow the nonlinear path OP, representing P the end of the coiling stage.

The maximum value of longitudinal and transverse residual stresses occurs at the sheet surface with a value of 1.202 $\sigma_{0.2}$ and 0.582 $\sigma_{0.2}$ respectively which are in Tab. 3.1 below. In the Quach, W.M. (2005), the value of longitudinal and transverse residual stresses the sheet surface were 1.206 $\sigma_{0.2}$ and 0.584 $\sigma_{0.2}$ respectively. The variation of the values is less than 0.4% and it is neglected. The residual stresses decrease gradually from sheet surface to the mid point of thickness reaching zero value.

Table 3.1: Residual stresses and equivalent plastic strain through thickness at the end of coiling.

y/t	$\sigma_{z,c}$	$\sigma_{x,c}$	$\varepsilon_{p,c}$	$\sigma_{z,c}/\sigma_{0.2}$	$\sigma_{x,c}/\sigma_{0.2}$
0.5000	246.489	119.372	0.00293	1.202	0.582
0.4643	244.739	117.741	0.00267	1.194	0.574
0.4286	242.398	115.462	0.00237	1.182	0.563
0.3929	240.048	113.148	0.00213	1.171	0.552
0.3571	235.932	109.448	0.00183	1.151	0.534
0.3214	230.639	105.088	0.00155	1.125	0.513
0.2857	224.720	100.068	0.00129	1.096	0.488
0.2500	218.161	94.417	0.00105	1.064	0.461
0.2143	209.141	86.697	0.00078	1.020	0.423
0.1786	198.237	77.770	0.00054	0.967	0.379
0.1429	183.083	66.622	0.00032	0.893	0.325
0.1071	160.386	53.177	0.00013	0.782	0.259
0.0714	119.985	36.644	0.00002	0.585	0.179
0.0357	61.320	18.400	0.00000	0.299	0.090
0.0000	0.000	0.000	0.00000	0.000	0.000
-0.0357	-61.320	-18.400	0.00000	-0.299	-0.090
-0.0714	-119.985	-36.644	0.00002	-0.585	-0.179
-0.1071	-160.386	-53.177	0.00013	-0.782	-0.259
-0.1429	-183.083	-66.622	0.00032	-0.893	-0.325
-0.1786	-198.237	-77.770	0.00054	-0.967	-0.379
-0.2143	-209.141	-86.697	0.00078	-1.020	-0.423
-0.2500	-218.161	-94.417	0.00105	-1.064	-0.461
-0.2857	-224.720	-100.068	0.00129	-1.096	-0.488
-0.3214	-230.639	-105.088	0.00155	-1.125	-0.513
-0.3571	-235.932	-109.448	0.00183	-1.151	-0.534
-0.3929	-240.048	-113.148	0.00213	-1.171	-0.552
-0.4286	-242.398	-115.462	0.00237	-1.182	-0.563
-0.4643	-244.739	-117.741	0.00267	-1.194	-0.574
-0.5000	-246.489	-119.372	0.00293	-1.202	-0.582

From the table data (Tab. 3.1), graph (Fig. 3.4) is drawn between normalized distance through thickness with respect to thickness (y/t) and Normalized residual stress with respect to 0.2% proof stress ($\sigma_{z,c}/\sigma_{0.2}$ and $\sigma_{x,c}/\sigma_{0.2}$). It reveals from the Fig. 3.4 that the distribution of the residual stresses for both tension and compression develop two inelastic zones respectively in the upper half and lowers half of the thickness. In the middle one fourth thickness zone the variation is linear. The longitudinal residual stresses in the upper and lower quarter thickness are greater than 0.2% proof stress, $\sigma_{0.2}$.

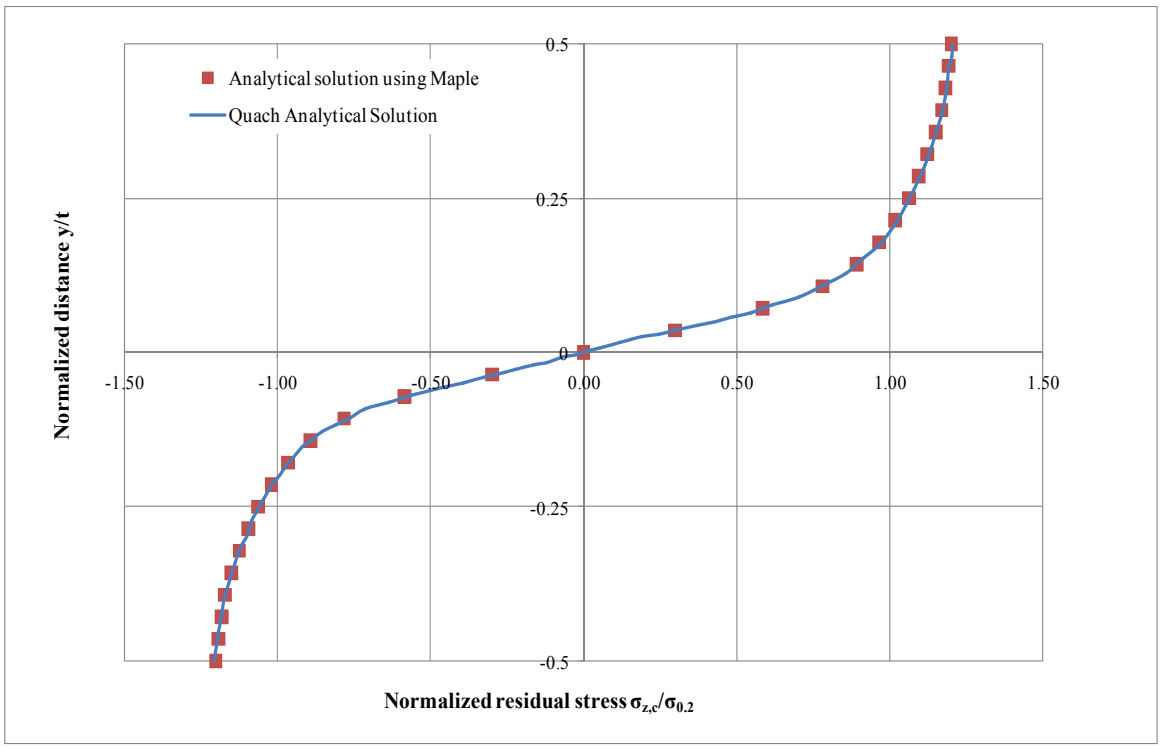

(a) Longitudinal coiling stresses

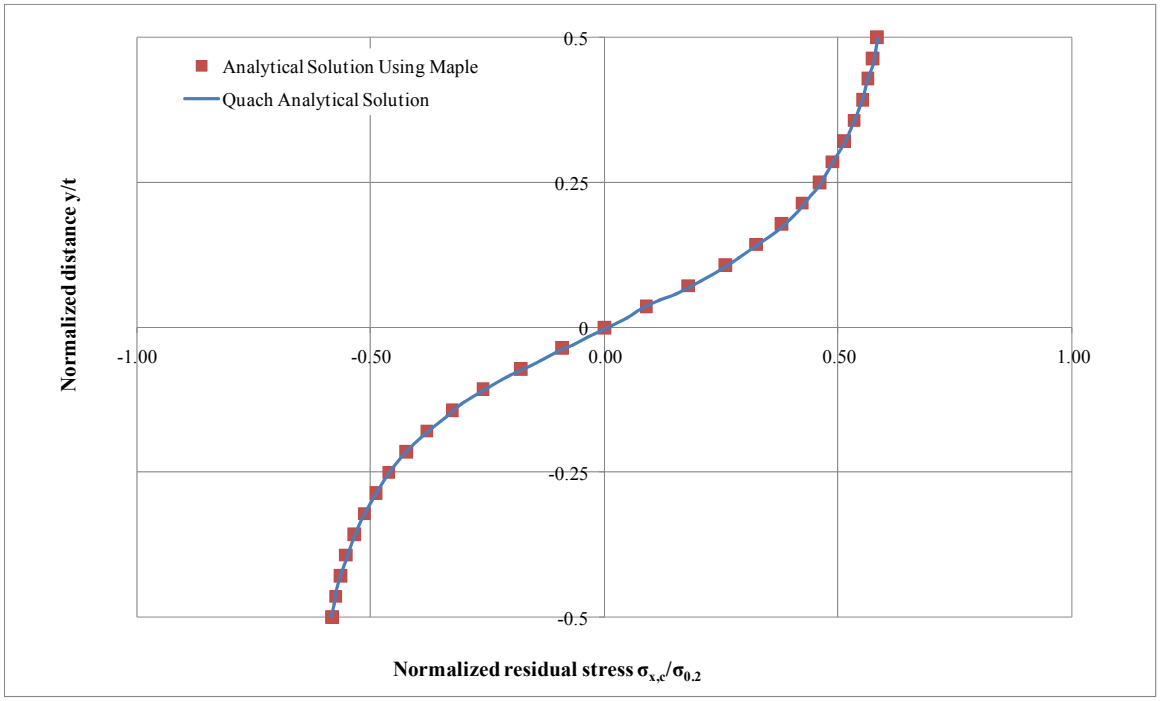

(b) Transverse coiling stresses

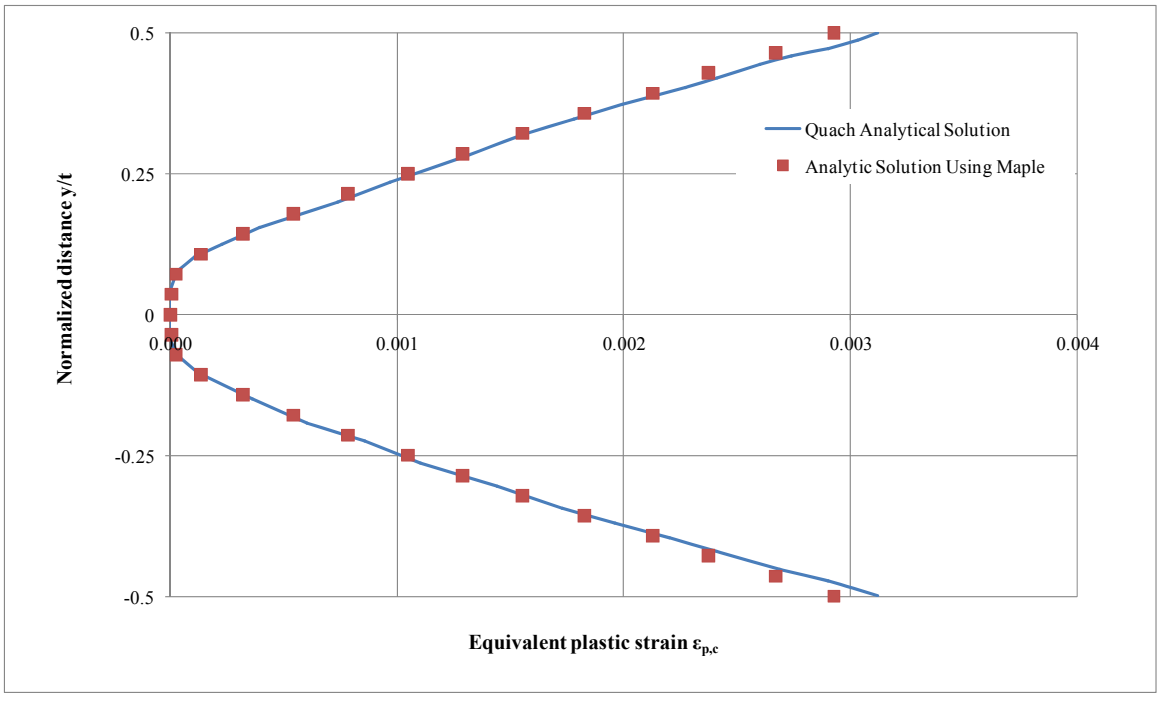

(c) Equivalent plastic strain after coiling

Figure 3.4: Comparison of residual stresses and equivalent plastic strain between Quach analytical solution and analytical solution using Maple due to coiling of Austenitic sheet.

The unloading stresses are elastic, until the reverse bending curvature exceeds a threshold curvature value. A curvature limit κ_{uy}, beyond which uncoiling stresses are no longer elastic, can be defined to indicate the onset of reverse yielding. In the von Mises yield envelop the onset of reverse yielding point is denoted by UE. In this stage there is no additional plastic stress introduced. After this stage the yield surface again starts to expand from the prior, which developed at the end of coiling representing the reverse yielding following the stress path UE to UP in the von Mises yield envelope.

At the end of this stage the maximum value of longitudinal and transverse residual stresses occurs at the sheet surface with a value of 1.237 $\sigma_{0.2}$ and 0.518 $\sigma_{0.2}$ respectively which are in Tab. 3.2 below. In the Quach, W.M. (2005), the value of longitudinal and transverse residual stresses the sheet surface were 1.244 $\sigma_{0.2}$ and 0.529 $\sigma_{0.2}$ respectively. The variation of the values can be neglected. The residual stresses decrease gradually from sheet surface to the mid point of thickness reaching zero value with two inelastic zones in the upper half and lower half respectively. The longitudinal stresses are greater than the 0.2% proof stress of annealed material up to the upper and lower quarter portion from the surface.

Table 3.2: Residual stress and equivalent plastic strain through thickness at the end of uncoiling including flattening.

y/t	$\sigma_{z,u}$	$\sigma_{x,u}$	$\varepsilon_{p,u}$	$\sigma_{z,u}/\sigma_{0.2}$	$\sigma_{x,u}/\sigma_{0.2}$
0.5000	-253.513	-106.286	0.00471	-1.237	-0.518
0.4643	-251.512	-103.001	0.00430	-1.227	-0.502
0.4286	-247.722	-94.739	0.00368	-1.208	-0.462
0.3929	-243.509	-85.370	0.00314	-1.188	-0.416
0.3571	-238.682	-76.977	0.00261	-1.164	-0.375
0.3214	-230.718	-63.210	0.00204	-1.125	-0.308
0.2857	-219.945	-50.652	0.00156	-1.073	-0.247
0.2500	-205.939	-36.019	0.00109	-1.005	-0.176
0.2143	-158.206	-23.507	0.00078	-0.772	-0.115
0.1786	-107.885	-14.067	0.00054	-0.526	-0.069
0.1429	-61.815	-6.847	0.00032	-0.302	-0.033
0.1071	-23.288	-1.925	0.00013	-0.114	-0.009
0.0714	-2.464	-0.091	0.00002	-0.012	0.000
0.0357	0.095	0.033	0.00000	0.000	0.000
0.0000	0.000	0.000	0.00000	0.000	0.000
-0.0357	-0.095	-0.033	0.00000	0.000	0.000
-0.0714	2.464	0.091	0.00002	0.012	0.000
-0.1071	23.288	1.925	0.00013	0.114	0.009
-0.1429	61.815	6.847	0.00032	0.302	0.033
-0.1786	107.885	14.067	0.00054	0.526	0.069
-0.2143	158.206	23.507	0.00078	0.772	0.115
-0.2500	205.939	36.019	0.00109	1.005	0.176
-0.2857	219.945	50.652	0.00156	1.073	0.247
-0.3214	230.718	63.210	0.00204	1.125	0.308
-0.3571	238.682	76.977	0.00261	1.164	0.375
-0.3929	243.509	85.370	0.00314	1.188	0.416
-0.4286	247.722	94.739	0.00368	1.208	0.462
-0.4643	251.512	103.001	0.00430	1.227	0.502
-0.5000	253.513	106.286	0.00471	1.237	0.518

From the table data (Tab. 3.2), graph is drawn between normalized distance through thickness with respect to thickness (y/t) and normalized residual stress with respect to 0.2% proof stress ($\sigma_{z,c}/\sigma_{0.2}$ and $\sigma_{x,c}/\sigma_{0.2}$). It shows from the Fig. 3.5 that the distribution of the residual stresses for both tension and compression develop two inelastic zones respectively in the lower half and upper half of the thickness.

The developed plastic strain through thickness in this stage also matches with the Quach, W.M. (2005) analytical solution.

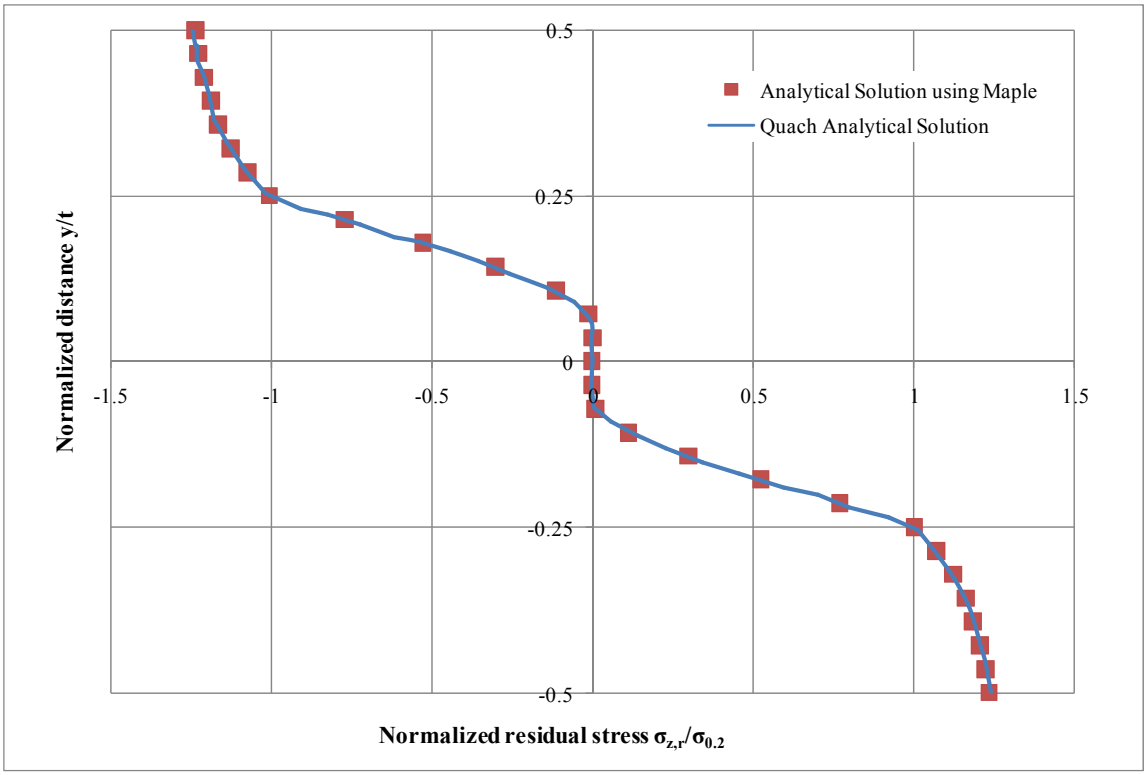

(a) Final longitudinal residual stress

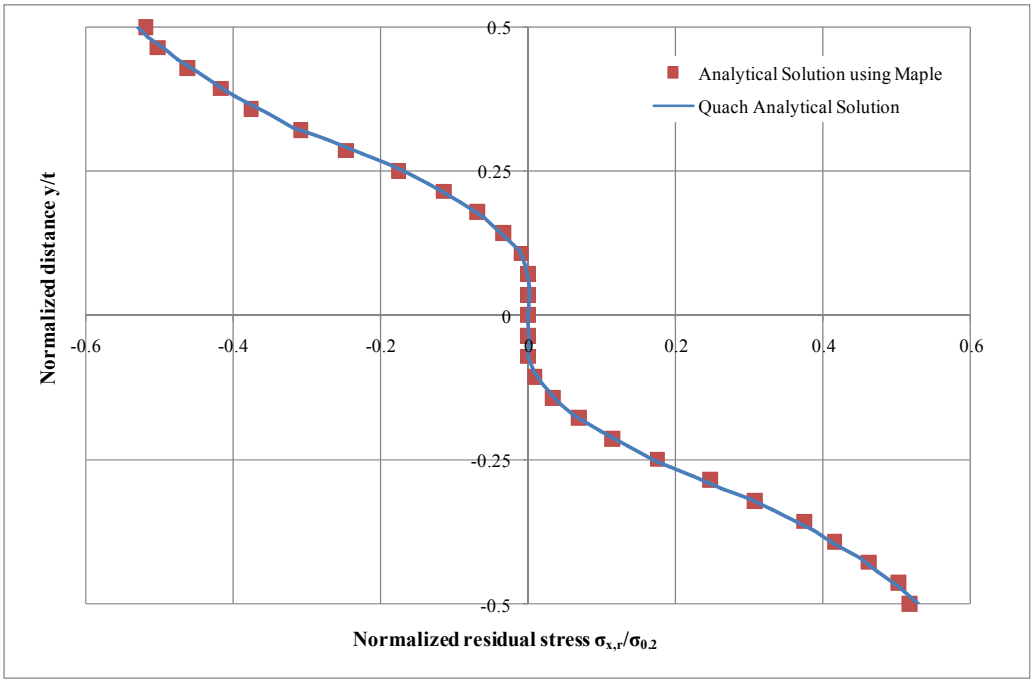

(b) Final transverse residual stress

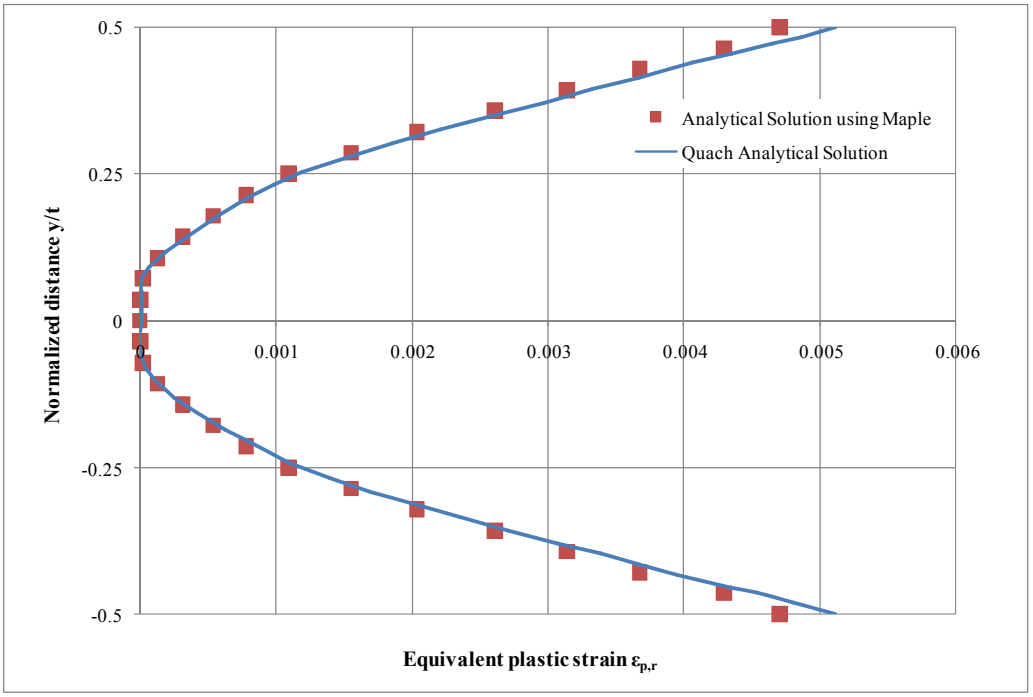

(c) Equivalent plastic strain after flattening

Figure 3.5: Comparison of residual stresses and equivalent plastic strain between Quach analytical solution and analytical solution using Maple due to uncoiling including flattening of Austenitic sheet.

3.3. ANALYTICAL SOLUTION DUE TO COLD BENDING

As the cold-formed sections are thin, so through thickness the variations of residual stresses due to cold bending are difficult to measure in the laboratory and only surface residual stresses were measured in most experimental studies assuming that it varies linearly through the thickness of the sheet. The measurement was also time consuming and of limited accuracy which is described in the literature review. From these limitations, it is necessary to model the cold forming process for predicting the residual stresses throughout the thickness or across the cross-section in the cold formed members.

Here, the analytical modelling proposed by Quach, W. M. (2005) is presented for the press braking type of cold-formed members. These equations are used to validate the analytical modelling using Maple 18.01. As like coiling and uncoiling process described above, the flat steel strip can be assumed to be free from residual stresses before it is coiled for storage. So the residual stress calculation due to press braking come from two distinct sources i.e. the coiling-uncoiling process and the cold bending of press-braking operations. The solution for first stage coiling-uncoiling process is described above. As is described in the literature review that in the press-braking operations cold work is confined to the corner regions of a press-braked section so the residual stresses in the flat portions are mainly derived from the coiling and uncoiling of the steel sheet and can be determined by means of the analytical solution for the coiling-uncoiling process.

The stresses in various directions are designated by the same terminology used in the coiling-uncoiling process. It is important to quote that in the manufacturing process of cold formed section by press-braking, the outer surface of a coiled sheet becomes the inner surface of the lipped channel section produced from the sheet. The manufacturing process due to press braking is shown in Fig. 3.6 below.

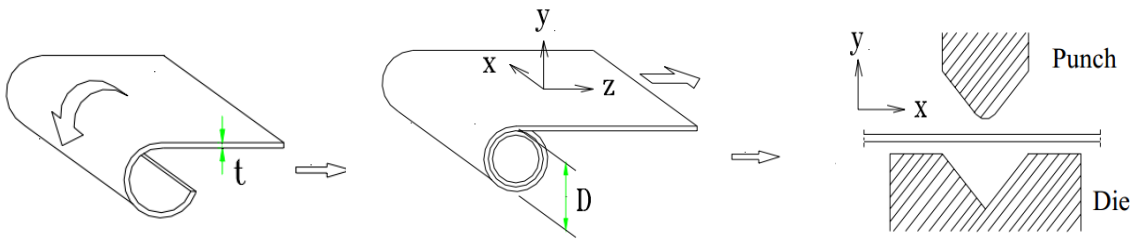

(a) Coiling *(b) Uncoiling including flattening* *(c) Press braking*

Figure 3.6: Manufacturing process of press-braked sections.

3.3.1. Material Modelling

The analytical solution presented here is based on the plain strain bending of the sheet into large curvature similar to the coiling and uncoiling process stated above for small curvature. As the bending curvature at the corner of a pressed braked section is much larger than the coiling curvature, the residual stresses in the corner due to cold work does not affected by the residual stress induced by the coiling-uncoiling process. According to the cold formed open section specified in AISI Cold -Formed Steel Specification (AISI (1996)), the ratio of centre line radius R_c to thickness of the sheet t, (R_c/t) varies from 2 to 6.

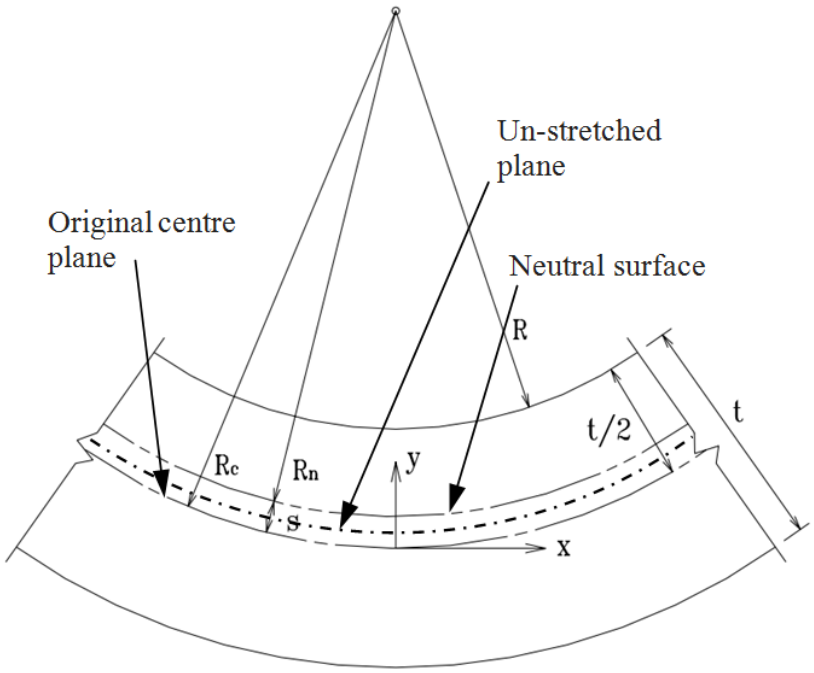

Figure 3.7: Schematic diagram of a sheet under pure bending with a large curvature.

Yu and Zhang (1996) proposed that in case of pure bending of wide plate for large bending curvature at the corner say as R_c/t <10, the strain induced is large, so the use of nominal stress-strain properties does not give the accurate result. Hence, the true stress-strain properties is adopted in case of analytical solution of cold bending of sheet into the corner, where nominal stress-strain properties are used in the coiling and uncoiling processes.

3.3.2. Theory of Cold Bending of Sheet

Hill, R. (1950) described the elementary theory of sheet bending the cold bending of sheet assuming that if the final radius of curvature is greater than four or five times the thickness of sheet then it is assumed that the strains are so small that the transverse stresses induced by the curvature are negligible. It is also assumed that the neutral surface coincides with the central plane of the sheet throughout the bend. He examined the state of stress and the movement of the neutral surface and individual elements, while the strains are of any magnitude. His analysis is restricted to only for the bending of wide sheet or bar, where the strain in the width direction is negligible. The neutral surface initially coincides with the central plane, and indicates the inner surface during the bending. All fibres to the tension side of the central plane are extended while all fibres in the inner side (inside the radius R_c) are progressively compressed.

Due to the movement of central plane toward the inner surface during bending, at some intermediate stages fibres are overtaken by the neutral surface first feel compression and afterward tension with the progress of bending. The reversal straining occurs in the zone between the neutral surface and the original central fibre. At each stage of bending there is one surface where the fibre feels the same amount of shortening and extension which is represented as unstretched surface of resultant change of length is zero (Fig. 3.7).

The strain due to cold bending of sheet into the corner depends on the location of fibre through thickness 'y' away from the current middle surface of the sheet, the distance 's' between the neutral surface and the current middle surface, and the bending curvature κ_b. Where, $\kappa_b = 1/R_c$. By the assumption of zero strains at the neutral surface, the true transverse strain due to cold bending can be expressed as

$$\varepsilon_{x,b} = \ln\left(1+\left(\frac{s-y}{R_c-s}\right)\right) \tag{3.37}$$

Similar to coiling and uncoiling, the in-plane stresses are taken into account ignoring the stresses through thickness in case of both elastic and inelastic material fibre across the thickness. For elastic material points, the longitudinal and transverse stresses are

$$\sigma_{z,b} = \frac{\nu E_0}{\left(1-\nu^2\right)}\varepsilon_{x,b} \tag{3.38a}$$

$$\sigma_{x,b} = \frac{E_0}{\left(1-\nu^2\right)}\varepsilon_{x,b} \tag{3.38b}$$

The transverse strain at which a fibre start to yield is expressed as

$$\varepsilon_{x,by} = \pm\sigma_{y0}\left(1-\nu^2\right)/\left(E_0\sqrt{1-\nu+\nu^2}\right) \tag{3.39}$$

Here, + sign indicate that the strain is in tension (i.e. $y<s$).

The stresses of any point undergoing plastic straining due to cold bending can be expressed as

$$\sigma_{z,b} = \pm\frac{\omega_b\sigma_{yb}}{\sqrt{1-\omega_b+\omega_b^2}} \tag{3.40a}$$

$$\sigma_{x,b} = \pm\frac{\sigma_{yb}}{\sqrt{1-\omega_b+\omega_b^2}} \tag{3.40b}$$

in which,

$$\omega_b = \sigma_{z,b}/\sigma_{x,b} \tag{3.40c}$$

The equivalent plastic strain due to cold bending can be given by

$$\bar{\varepsilon}_{p,b} = \varepsilon_{yb} - \frac{\sigma_{yb}}{E_0} \tag{3.41}$$

in which the subscript b is used to refer to cold bending, σ_{yb} and ε_{yb} are the instantaneous yield stress and the corresponding strain reached at the end of cold bending. The strain ε_{yb} is determined from the stress σ_{yb} following by the stress-strain relationship $\varepsilon=f(\sigma)$.

Through thickness the value of σ_{yb} and ω_b varies which can be determined numerically using their inter-relationship and the known boundary values are expressed below. The increment of stress ratio for the inelastic material point is expressed by the following expression.

$$d\omega_b = \frac{2\left(1-\omega_b+\omega_b^2\right)\left(\Omega_b-\omega_b\right)}{\sigma\left[\left(2-\omega_b\right)+\Omega_b\left(2\omega_b-1\right)\right]}d\sigma \tag{3.42}$$

In which, the ratio of stress increment $\Omega_b = d\sigma_{z,b}/\, d\sigma_{x,b}$ can be expressed as

$$\Omega_b = \frac{4\nu H'\left(1-\omega_b+\omega_b^2\right)-E_0\left(2-\omega_b\right)\left(2\omega_b-1\right)}{E_0\left(2\omega_b-1\right)^2+4H'\left(1-\omega_b+\omega_b^2\right)} \tag{3.43a}$$

where, the slope of the equivalent stress to equivalent plastic strain can be expressed as

$$H' = \frac{d\bar{\sigma}}{d\bar{\varepsilon}_p} = \frac{d\sigma}{d\varepsilon_p} = \left(\frac{d\varepsilon}{d\sigma}-\frac{1}{E_0}\right)^{-1} \tag{3.43b}$$

3.3.3. Cold Bending of Stainless Steel

The procedure which is stated above can be used for cold bending of stainless steel sheet. But there is one problem of the mechanical properties of the stainless steel in the large strain level differs from the small strain level. For coiling-uncoiling stage the induced strain is small so the nominal stress-strain curve obtained from the coupon test can be put

accurately in the analytical solution. At larger strains, the nominal stress-strain relationship deviates from the "real" stress-strain response which is described above in the material modelling section with stress-strain diagram in Fig. 3.2. Hence, at large curvature, the stress strain relationship $\varepsilon=f(\sigma)$, is to be represented by the relationship between true stress σ_t and true strain ε_t.

From the relation between the true stress-strain and the nominal stress-strain which is expressed in Eq. 3.12, the true plastic strain can be expressed as

$$\varepsilon_{tp} = \varepsilon_t - \frac{\sigma_t}{E_0} = \pm\ln(1\pm\varepsilon_n) - \frac{\sigma_n(1\pm\varepsilon_n)}{E_0} \tag{3.44}$$

Where, '+' sign correspond to tension and '-' sign correspond to compression and σ_n, ε_n, σ_t, ε_t, ε_{tp} are the absolute value for both tension and compression coupon test.

As true stress-strain relationship is used for large straining, the slope of the equivalent stress-equivalent plastic strain relation H' for inelastic material points can be expressed by the same as used in coiling by replacing the term $d\varepsilon/d\sigma$ with $d\varepsilon_t/d\sigma_t$.

The strain rate $d\varepsilon_t/d\sigma_t$ can be expressed in term of nominal stress σ_n and nominal strain ε_n by the following formula.

$$\frac{d\varepsilon_t}{d\sigma_t} = \frac{d\varepsilon_n/d\sigma_n}{(1\pm\varepsilon_n)[(1\pm\varepsilon_n)\pm\sigma_n(d\varepsilon_n/d\sigma_n)]} \tag{3.45}$$

Hence, the new expression for slope H' is

$$H' = \frac{d\bar{\sigma}}{d\bar{\varepsilon}_p} = \left[\frac{d\varepsilon_n/d\sigma_n}{(1\pm\varepsilon_n)[(1\pm\varepsilon_n)\pm\sigma_n(d\varepsilon_n/d\sigma_n)]} - \frac{1}{E_0}\right]^{-1} \tag{3.46}$$

Where, $d\varepsilon_n/d\sigma_n$ is the strain rate of the nominal stress-strain curve.

To determine the increment of stress ratio of Eq. 3.42, it is needed the stress increment $d\sigma$, which are calculated from the nominal stress σ_n and the increment of stress $d\sigma_n$ by using the following expression.

$$\frac{d\sigma_t}{d\sigma_n} = \begin{cases} 1 \pm \left[\dfrac{2\sigma_n}{E_0} + 0.002(n+1)\left(\dfrac{\sigma_n}{\sigma_{0.2}} \right)^n \right], & \sigma_n \le \sigma_{0.2} \\ 1 \pm \left\{ \begin{array}{l} \varepsilon_{0.2} + \dfrac{(2\sigma_n - \sigma_{0.2})}{E_{0.2}} + \left[(n'_{0.2,1.0}+1)\sigma_n - \sigma_{0.2} \right] \cdot \\ \left[0.008 + (\sigma_{1.0} - \sigma_{0.2})\left(\dfrac{1}{E_0} - \dfrac{1}{E_{0.2}} \right) \right] \dfrac{(\sigma_n - \sigma_{0.2})^{n'_{0.2,1.0}-1}}{(\sigma_{1.0} - \sigma_{0.2})^{n'_{0.2,1.0}}} \end{array} \right\}, & \\ & \sigma_{0.2} < \sigma_n \le \sigma_{2.0} \\ 1 \pm \dfrac{(2\sigma_n - a)(b \mp \sigma_n) \pm \sigma_n(\sigma_n - a)}{(b \mp \sigma_n)^2}, & \sigma_n > \sigma_{2.0} \end{cases} \tag{3.47}$$

So, from Eq. 3.47 for the small increment of nominal stress ($d\sigma_n$), the increment for true stress ($d\sigma_t$) is calculated first and then value of increment of stress ratio $d\omega_b$ in Eq. 3.42 is calculated from the resulting stress increment $d\sigma_t$.

It is noted that due to the nonlinear behaviour of stainless steel, there is no initial yield stress (σ_{y0} =0). So the $\varepsilon_{x,by}$ in Eq. 3.39 becomes zero and it reveals that there is no elastic straining through the thickness of stainless steel sheet.

In the Maple 18.01, cold bending of austenitic steel sheet of thickness 1.8 mm and bending radius, R =3.96 mm is analysed by using the both nominal stress-strain and true stress-strain relationship of materials. The basic material properties are same as used in the coiling-uncoiling process analysis. The variation of residual stresses in longitudinal ($\sigma_{z,b}$) and transverse ($\sigma_{x,b}$) direction and the equivalent plastic strain ($\varepsilon_{p,b}$) for both cases are presented as tabular (Tab. 3.3) and graphical form (Fig. 3.8) below.

Table 3.3: Residual stress and equivalent plastic strain through thickness due to cold bending of sheet.

y/t	For nominal stress-strain (σ_n and ε_n)			For true stress-strain (σ_t and ε_t)		
	$\sigma_{z,b}$	$\sigma_{x,b}$	$\varepsilon_{p,b}$	$\sigma_{z,b}$	$\sigma_{x,b}$	$\varepsilon_{p,b}$
0.5000	-219.46	-439.36	0.2032	-297.25	-596.40	0.1823
0.4643	-214.55	-429.55	0.1887	-280.90	-563.49	0.1691
0.4286	-208.78	-418.00	0.1718	-265.97	-533.47	0.1561
0.3929	-203.29	-407.03	0.1559	-251.90	-505.18	0.1429
0.3571	-198.10	-396.64	0.1415	-238.68	-478.62	0.1298
0.3214	-192.03	-384.52	0.1256	-225.75	-452.64	0.1165
0.2857	-186.26	-372.97	0.1107	-213.67	-428.39	0.1033
0.2500	-180.49	-361.42	0.0962	-202.17	-405.30	0.0902
0.2143	-174.71	-349.88	0.0822	-191.24	-383.36	0.0771
0.1786	-168.65	-337.75	0.0676	-180.60	-362.00	0.0636
0.1429	-162.30	-325.05	0.0531	-170.24	-341.21	0.0501
0.1071	-156.24	-312.92	0.0400	-160.16	-321.01	0.0367
0.0714	-149.32	-299.07	0.0251	-150.95	-302.53	0.0237
0.0357	-137.71	-276.55	0.0117	-137.04	-275.40	0.0104
0.0000	39.65	128.53	0.0000	90.96	213.98	0.0009
-0.0357	138.89	278.86	0.0127	141.74	284.63	0.0138
-0.0714	149.89	300.22	0.0263	152.68	306.00	0.0262
-0.1071	155.67	311.77	0.0387	161.32	323.32	0.0383
-0.1429	161.15	322.74	0.0505	170.24	341.21	0.0501
-0.1786	166.92	334.29	0.0636	179.44	359.69	0.0621
-0.2143	171.83	344.10	0.0753	188.36	377.59	0.0735
-0.2500	177.02	354.49	0.0877	197.57	396.06	0.0846
-0.2857	181.64	363.73	0.0990	206.77	414.54	0.0954
-0.3214	186.84	374.12	0.1120	215.97	433.01	0.1057
-0.3571	191.17	382.78	0.1228	226.04	453.22	0.1164
-0.3929	195.79	392.02	0.1348	235.81	472.85	0.1265
-0.4286	199.54	399.53	0.1454	244.72	490.75	0.1361
-0.4643	204.16	408.77	0.1578	255.63	512.69	0.1459
-0.5000	207.91	416.27	0.1679	266.26	534.05	0.1554

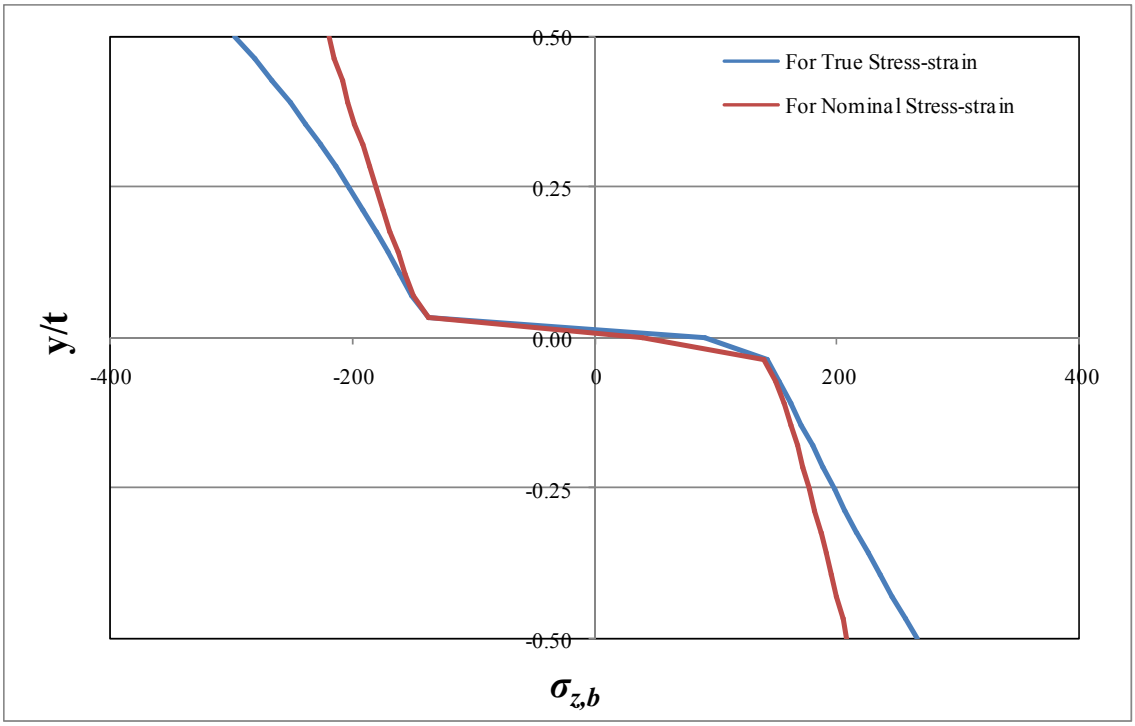

(a) Longitudinal residual stresses

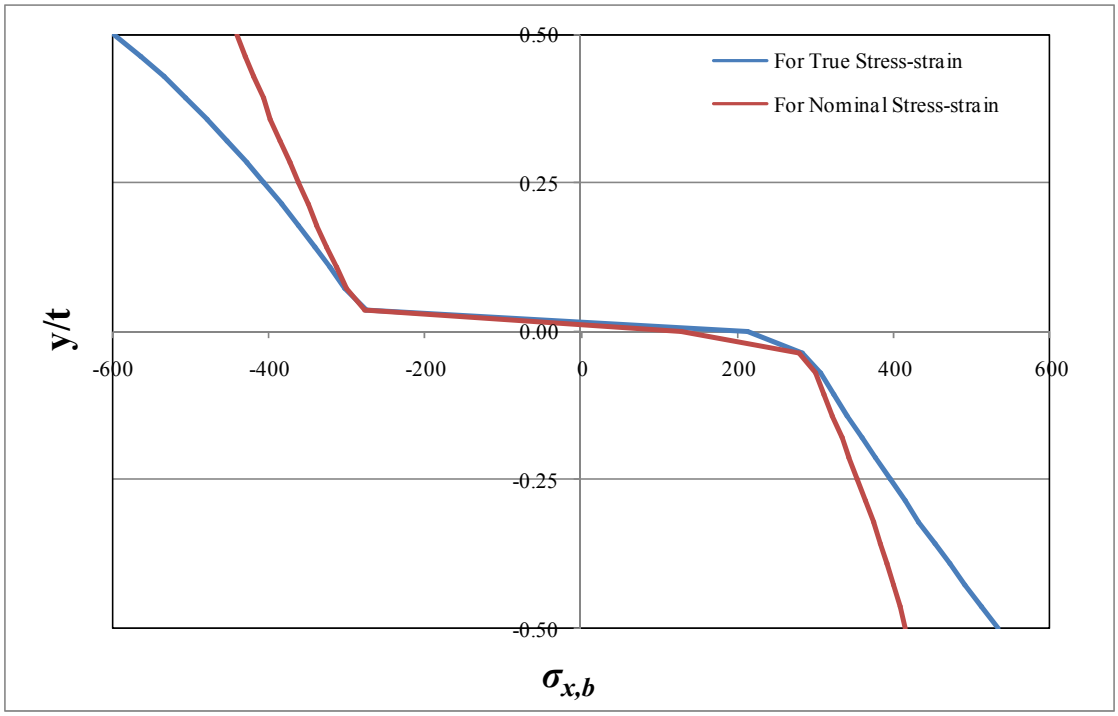

(b) Transverse residual stresses

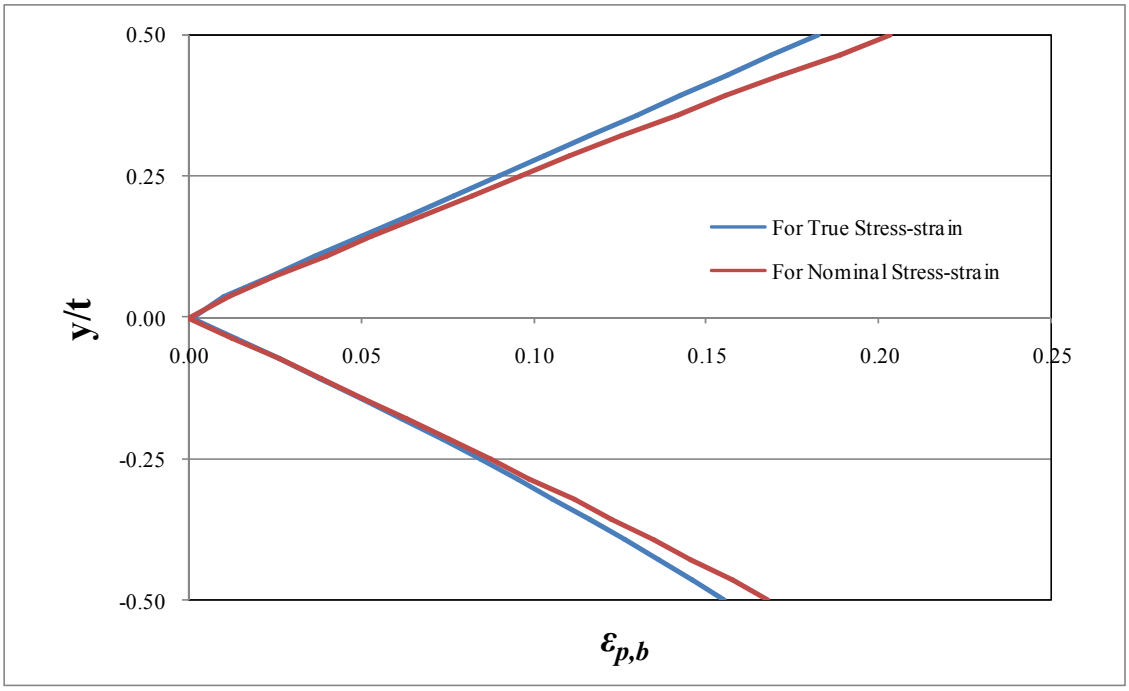

(c) Equivalent plastic strain

Figure 3.8: Comparison of residual stresses and equivalent plastic strain due to cold bending by using nominal and true stress-strain relationship of austenitic steel.

3.3.4. Validation of Analytical Solution due to Cold Bending

For validating the analytical modelling due to cold bending in the transverse direction (x axis) of sheet duplex stainless steel of grade UNS31803 alloy is used. In this analysis the mechanical properties of the steel is taken from the test result of Rasmussen, K. J. R. et, al. (2003) based on compression coupon tests shown in Tab. 3.4.

Table 3.4: Mechanical properties of duplex stainless steel of grade UNS31803 alloy tested by Rasmussen, K.J.R. et, al. (2003)

Specimen	E_0 (GPa)	$\sigma_{0.01}$(MPa)	$\sigma_{0.2}$ (MPa)	e	n
LC	181.65	275	527	0.00290	4.6
TC	210.00	380	617	0.00294	6.2
DC	205.00	460	610	0.00298	10.6
LC = Longitudinal compression coupon, TC = Transverse compression coupon, DC = Diagonal compression coupon.					

The solution is based on the true stress-strain behaviour of the material because in the previous section it is observed the variation of results by using the nominal and true stress-strain due to large strain. In this analysis coiling-uncoiling process is also included in the longitudinal direction (z axis) with a coiling radius 750 mm, but due to the small straining, nominal stress-strain relationship is used. The thickness of sheet is taken, t = 1.80 mm with the bending radius to thickness ratio (R_c/t) as 2.5. As the coiling radius is high, so the residual stress developed by the coiling-uncoiling process is negligible and the developed stress is mainly due to the cold bending. The cold bending of sheet are in the transverse direction, hence the material properties taken in the Maple analysis are for transverse coupon test (TC) considering isotropy of material which is represented in the Tab. 3.4 above.

The longitudinal and transverse residual stresses variations through thickness are presented below in a graphical form. The result is verified with the result of Quach, W.M. (2005), shown in Fig. 3.9 where the material anisotropy is considered based on the material properties of the longitudinal, transverse and diagonal compression coupon tests. The residual stresses are normalized by dividing the residual stresses with a value $\sigma_{0.2L}$ = 527 MPa which is the 0.2% proof stress in the longitudinal direction got form compression coupon tests.

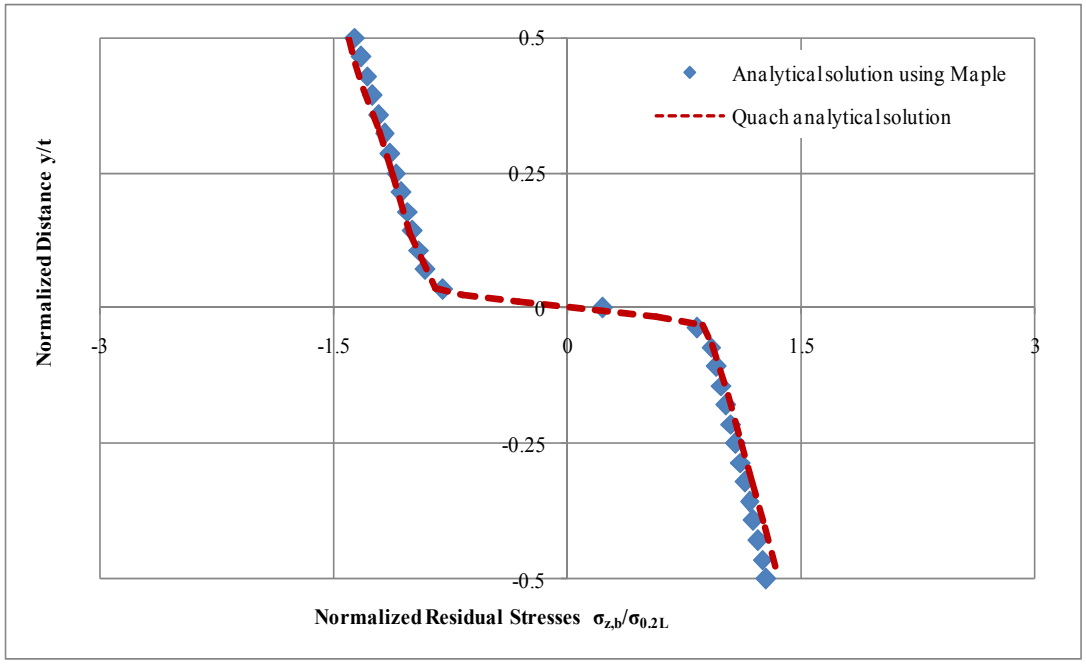

(a) Longitudinal residual stresses

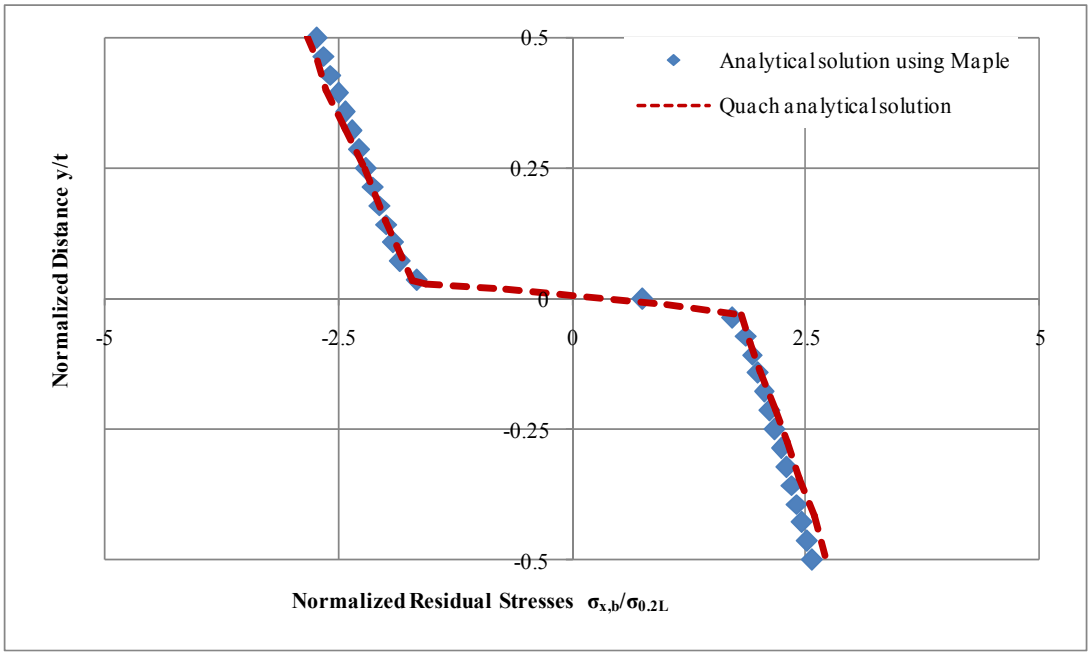

(b) Transverse residual stresses

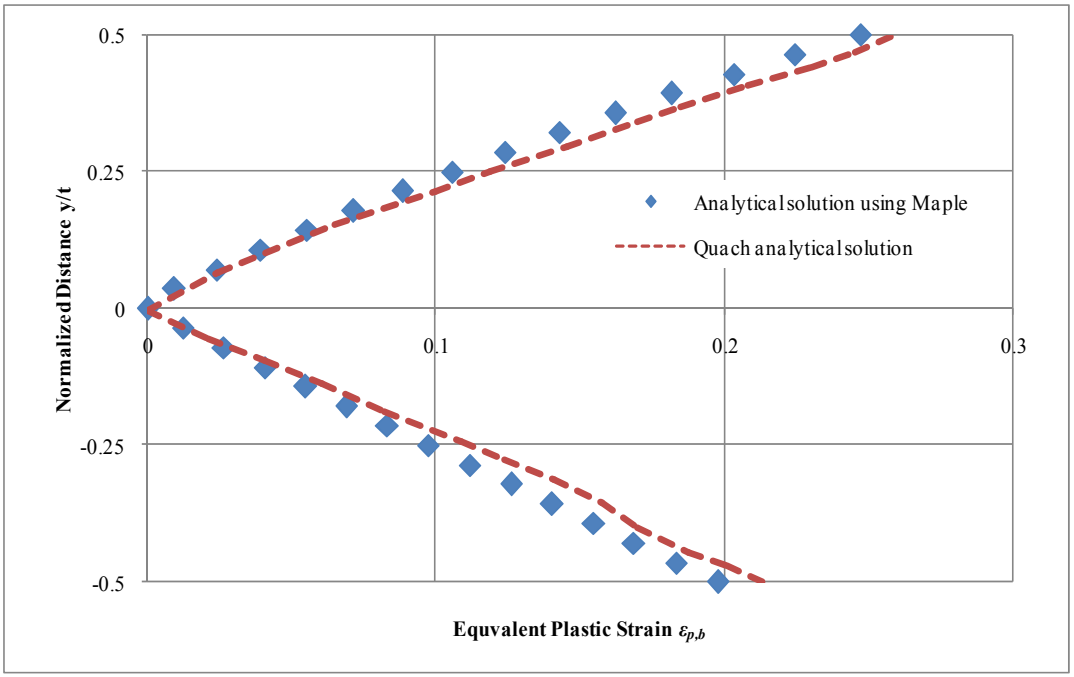

(c) Equivalent plastic strain

Figure 3.9: Comparison of residual stresses and equivalent plastic strain between Quach analytical solution and analytical solution using Maple due to cold bending of Duplex sheet.

3.3.5. Validation of Analytical Solution for Complete Press-breaking (including springback)

The cold bending of steel sheet occurs by loading the sheet into the plastic range followed by elastic unloading known as springback. A typical press-braking operation for bending the steel plate to 90^0 by using die and punch is shown in Fig. 3.10. The inelastic loading stress, elastic unloading stress and the resulting residual stresses are shown in Fig. 3.11.

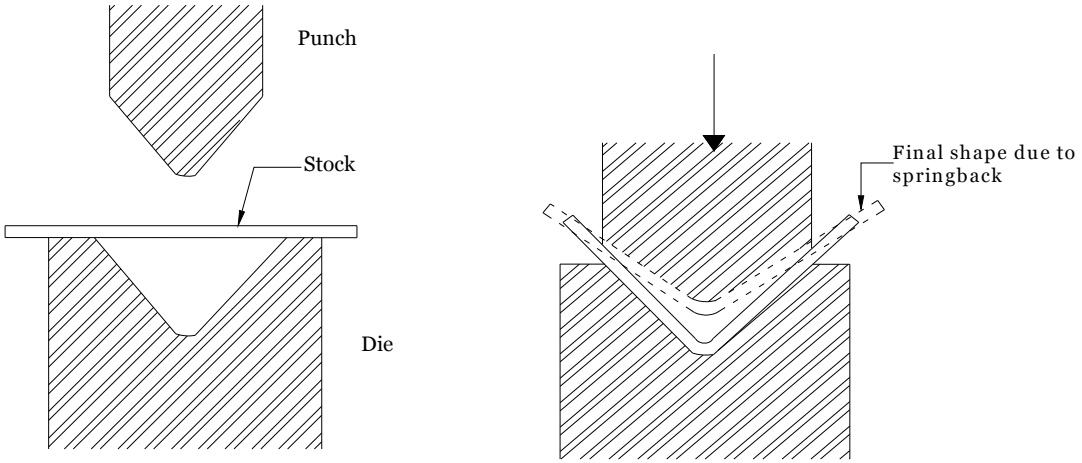

Figure 3.10: Press-braking operation and springback due to unloading.

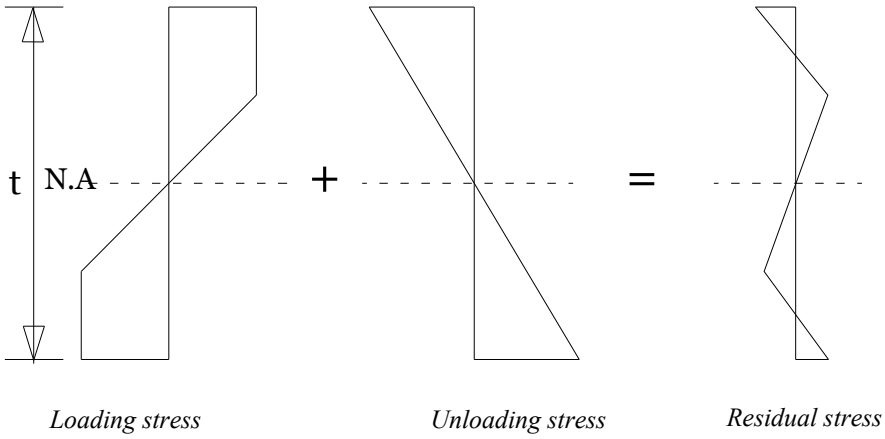

Figure 3.11: Loading, unloading and residual stresses in cold bent section.

For validating the analytical solution due to cold bending considering springback HY-80 carbon steel thick sheet of thickness 1 inch (25.4 mm). HY-80 has high yield strength, low carbon and low alloy steel with nickel, molybdenum and chromium. Weng, C. C. and

White, R. N. (1990) have done the experimental investigation of residual stress due to cold bending using the same material for different bending radius and angle. In the Maple analysis the inside bending radius R is taken as 5.5 $*t$. The material properties from the uniaxial tensile coupon test of Weng, C. C. and White, R. N. (1990) are given in a tabular form below in Tab. 3.5.

Table 3.5: Material properties for HY-80 steel [Weng, C. C. and White, R. N. (1990)].

σ_y (MPa)	σ_u (MPa)	E (MPa)	v	ε_u
593.23	737.92	$203.9*10^3$	0.3	0.244

In the Maple analysis, the carbon steel material is considered as elastic-linear strain hardening steel with a slope of the stress-strain curve in the strain hardening stage E_{st} = 598.61 Mpa.

Rossi, B. et, al. (2007) have done the numerical analysis using Matlab with equation proposed by Quach, W. M.(2005) due to cold bending considering springback of the same material and geometry described here. But Rossi, B. et, al. (2007) incorporate the behaviour of HY-80 steel as a nonlinear one by using the Swift law. The result from the Maple analysis is confronted with the experimental measurements of Weng, C. C. and White, R. N. (1990), Rossi, B. et, al. (2007) and Quach, W. M. (2005) finite element analysis side by side which are presented in Fig. 3.12 below. From the Fig. 3.12 it is shown that the result of Maple analysis is in close agreement with the Rossi, B. et, al. (2007) analysis and the Weng, C. C. and White, R. N. (1990) experimental result of residual stresses shows some difference with the Maple analysis. In the Quach, W. M. (2005) finite element analysis by Abaqus, he has considered the interaction between the steel section and the die/punch by modelling the die and punch with analytical rigid surfaces. For this reason, some differences are observed between the analytical and finite element solutions.

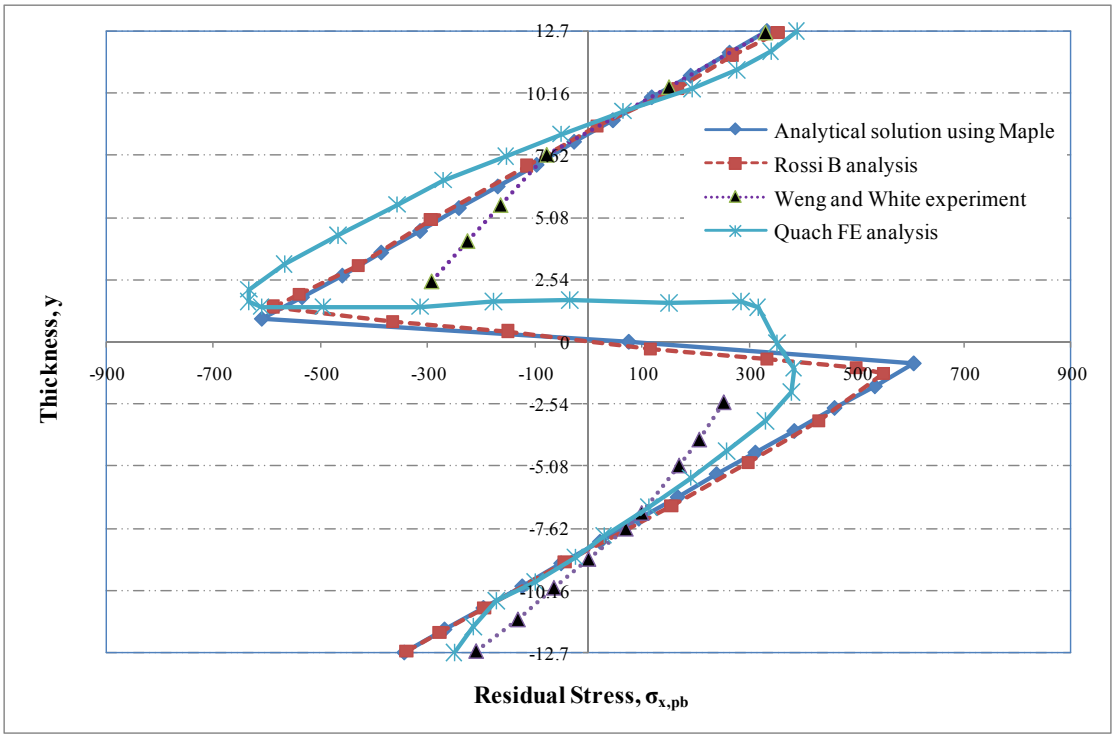

(a)Transverse residual stress

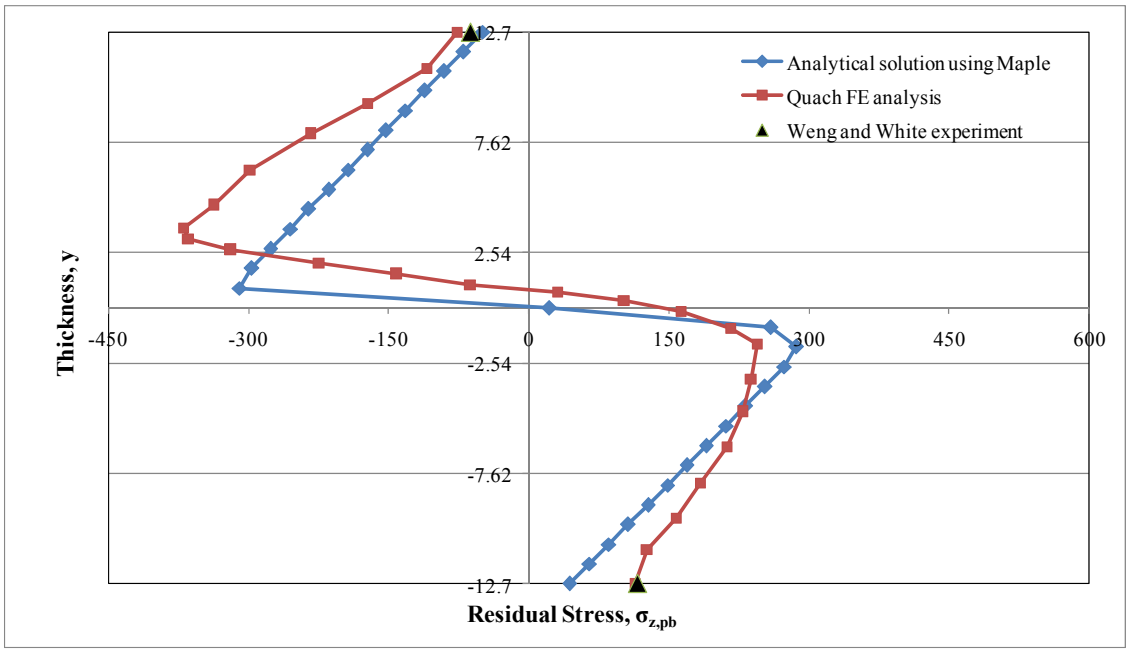

(b) Longitudinal residual stress

Figure 3.12: Comparison of residual stresses due to press-braking.

3.3.6. Increase of Strength due to Cold Forming

Gardner, L. (2002) has conducted the tensile and compressive coupon tests on material cutting from the corner and the flat faces of finished square hollow section (SHS) and Rectangular hollow section (RHS) to examine the new material properties of the cold bending section which differs from the material properties of the annealed materials (which is considered the material without any residual stresses). The change of the material properties of the flat face and the corner is analysed by using Maple 18.01 for the section SHS 80×80×4.

For this analytical modelling, the material is assumed to be an isotropic nonlinear strain-hardening material. The mechanical properties of the annealed material from the compression coupon test of the sheet are given in Tab. 3.6. In this table the symbol of coupon is represented as

TF = Tensile coupon test in the flat face of the section

TC = Tensile coupon test at corner of the section

A-CF = Compression coupon test of the flat annealed material.

Table 3.6: Measured material Properties for SHS 80×80×4 [Gardner, L (2002)].

Coupons SHS 80×80×4	E_0 (N/mm^2)	$\sigma_{0.2}$ (N/mm^2)	$\sigma_{1.0}$ (N/mm^2)	σ_u (N/mm^2)	ε_{pu}	*Modified R-O coefficient*		
						n	$n'_{0.2,u}$	$n'_{0.2,1.0}$
TF	186600	457	525	706	0.43	5.0	3.2	3.5
TC	215000	594	723	820	0.30	4.5	6.0	4.5
A-CF	206300	261	316	--	--	11.5	--	1.5

The material properties of the table are the weighted average value from the coupon tests by considering the nominal area of the material, so the stress-strain behaviour considering theses data represent the nominal stress-strain diagram. In the Maple analysis 3-stage stress strain model is used which can measure the full range of stress-strain curve described above. As the input material properties the coupon test data of A-CF in the table is used but here the data of ultimate stress (σ_u) and ultimate strain (ε_{pu}) is not available. For this reason, the ultimate data of TF is used by converting them for compression coupon test which are shown below.

$$\varepsilon_{u(ten)} = \varepsilon_{pu} + \sigma_u/E_0$$
$$= 0.43+(706/186600)$$
$$= 0.4338$$

$$\sigma_{u(com)} = \sigma_{u(ten)} [1+\varepsilon_{u(ten)}]^2$$
$$= 706[1+0.4338]^2$$
$$= 1450 \text{ MPa}$$

$$\varepsilon_{u(com)} = 1\text{-}1/(1+ \varepsilon_{u(ten)})$$
$$= 1\text{-}1/(1+0.4338)$$
$$= 0.3025$$

The tangent modulus at the 0.2% proof stress (Eq. 1.7) $E_{0.2}$ = 10756.16 MPa
Poisson's ratio v = 0.3
The non-dimensional parameter with respect to 0.2% proof stress

$$e = \sigma_{0.2}/E_0 = 261/(186.6*10^3) = 0.001265.$$

As the value of coil radius is unknown, it is not possible to provide an exact measure of the plastic strains associated with the coiling-uncoiling processes. Hence, the strain measured due to coiling and uncoiling is determined on the basis of an average coil radius $R_{coiling}$ = 450 mm, as recommended by Moen, C. D. et al. (2008). The other geometric properties are got from the specimen tested by Grander, L (2002). The data in Tab. 3.7 represent the average value of the five numbers of specimens of SHS 80×80×4.

Table 3.7: Geometric properties of the cold bend section [Grander, L. (2002)]

Specimen (SHS)	Depth, h (mm)	Breadth, b (mm)	Thickness, t (mm)	Internal corner radius, r_i (mm)	Area, A (mm^2)
80×80×4	79.84	79.84	3.756	4.38	1102.8

3.3.6.1. For Corner

The corner of the section is modelled in the Maple considering stages as the coiling, uncoiling including flattening of the sheet, cold bending of sheet to form the section including springback which are described above precisely. For analysing, through thickness the specimen is divided into 28 numbers for getting the variation of developed stresses and plastic strain. The material properties (stress-strain behaviour) of the corner of the cold bend section are determined by averaging the stress increment of the corner through thickness for the small increment of strain $\Delta\varepsilon=1*10^{-4}$ with a precision of 0.0001 upto the strain of 0.07. Here, in the maple analysis of cold bending due to the large curvature (induce large strain) the stress-strain behaviour is represented by the relationship between true stress σ_t and true strain ε_t.

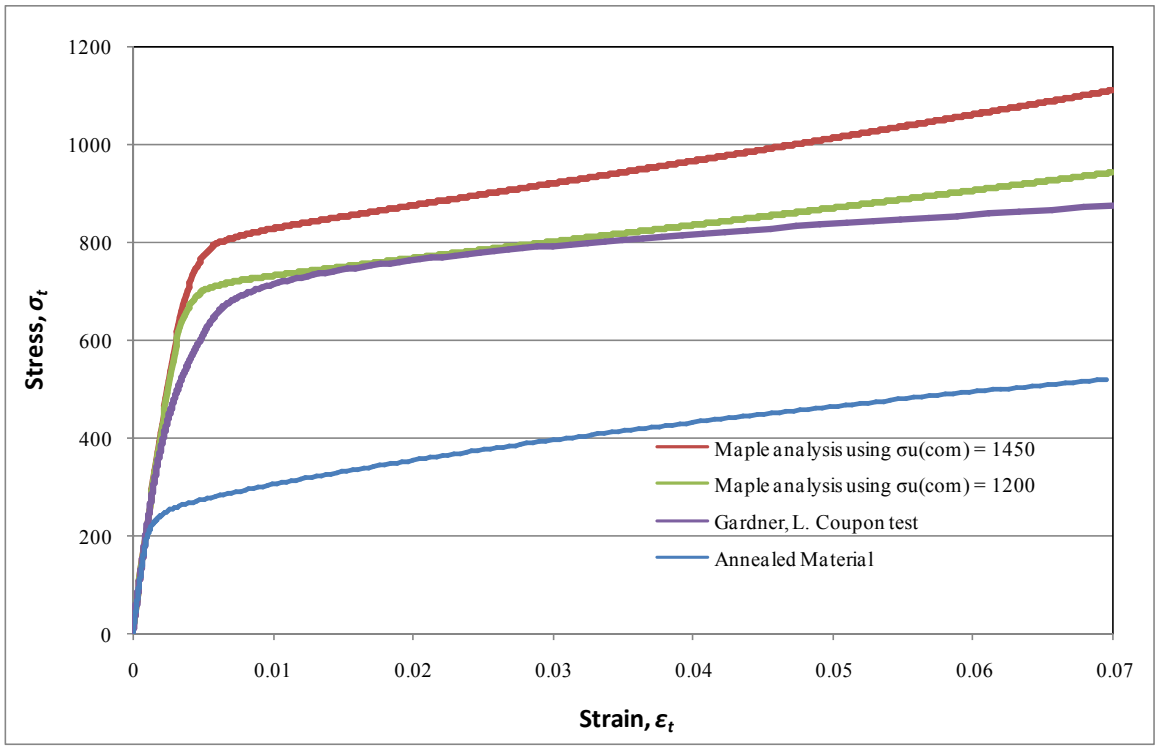

Figure 3.13: Comparison of Maple analysis and Test data of material behaviour due to cold bending at corner.

In the Maple analysis, due to the unavailability of the ultimate strength of the annealed material, it is taken as for the flat faces. Hence, by using the value of $\sigma_{u(com)}$ = 1450 MPa, the result of the Maple analysis after cold bending at corner is higher than the coupon test result of Gardner, L. (2002). By trial analysis, it is shown that the stress-strain behaviour

by using $\sigma_{u(com)}$ = 1200 MPa of the annealed material gives the similar behaviour as like the coupon test results which is shown in Fig. 3.13 above.

3.3.6.2. For Flat Face

The flat faces of the section is modelled in the Maple considering stages as the coiling, uncoiling including flattening of the sheet, forming into a circular sections and then making it flat including springback. The inner radius of the circle (R_i) is calculated from the section size given in Tab. 3.7 in the following way.

$$2\pi R_i = 4(79.84\text{-}3.756)$$
$$\Rightarrow R_i = 48.4 \text{ mm}$$

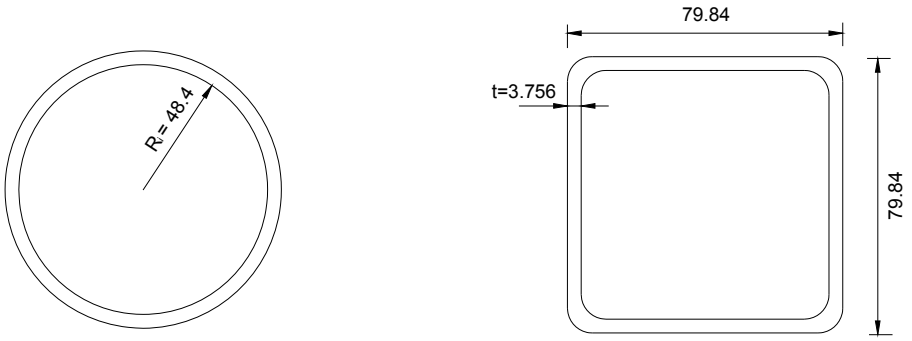

(a) circle making *(b) final SHS section*

Figure 3.14: Formation of square hollow section (SHS) by cold-rolling

For analysing, through thickness the specimen is divided into 28 numbers as like corner. The material properties (stress-strain behaviour) of the flat face is determined by averaging the stress increment of the flat faces through thickness for the as increment and precision of strain as corner upto the strain of 0.07. Here, in the maple analysis for the flat faces the ultimate strength is taken as $\sigma_{u(com)}$ = 1200 MPa of the annealed material. As the centre line radius 'R_c' of the circle (R_i+t/2=48.4+3.756/2 =50.278) is greater than the 10 times the thickness 't', then according to Yu, T. X. and Zhang, L. C. (1996) for pure bending of wide sheet, the nominal stress-strain relationship is used in the model and the shifting of the

neutral surface from the middle surface of the sheet is neglected. The result is represented in Fig. 3.15 with the Gardner, L. (2002) test result for comparison.

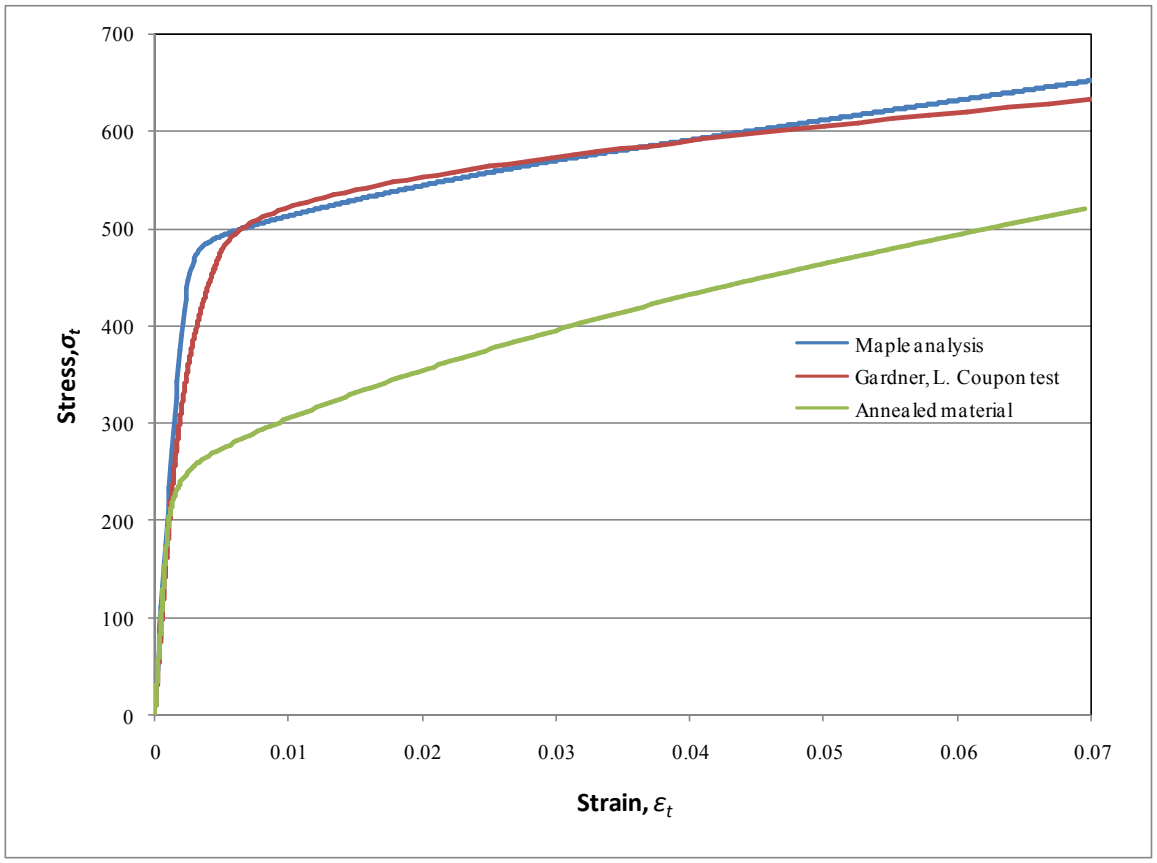

Figure 3.15: Comparison of Maple analysis and Test data of material behaviour due to cold bending at flat face.

4. TEST DATA ANALYSIS

4.1. PREVIOUS TENSILE TEST

The experimental programme has been carried out at the Czech Technical University in Prague (Marik, J. and Jandera, M. (2014)) consisting of tension coupon test of all type of stainless steel grades, say as austenitic (1.4404), ferritic (1.4003), duplex (1.4462) and relatively new grade lean-duplex (1.4162). The coupons were dimensioned and tested in accordance with EN ISO 6892-1. The tested specimens were collected from the cold rolled steel sheet strip of 1.5 mm and 2.0 mm thickness.

The materials were tested in both parallel and transverse to the rolling direction for getting the stress-strain behaviour. For the best accuracy at the initial part of the stress-strain diagram, the corresponding strain due to the increase of load was determined by using the electrical resistance strain gauges attached to both sides of the specimens and extensometer was used for higher strain ranges.

The stress-strain behaviour of the material were also determined by introducing the tensile plastic strain on the coupon and special wide specimen from which the coupons were machined subsequently for both parallel and transverse to the rolling direction of the sheet which is shown in Fig. 4.1. The induced plastic strain was equal to 1%, 3%, 5%, 10%, 15% and 50% for austenitic steel, for ferritic steel it was up to 20% and for the lean-duplex and duplex up to 15% plastic strain.

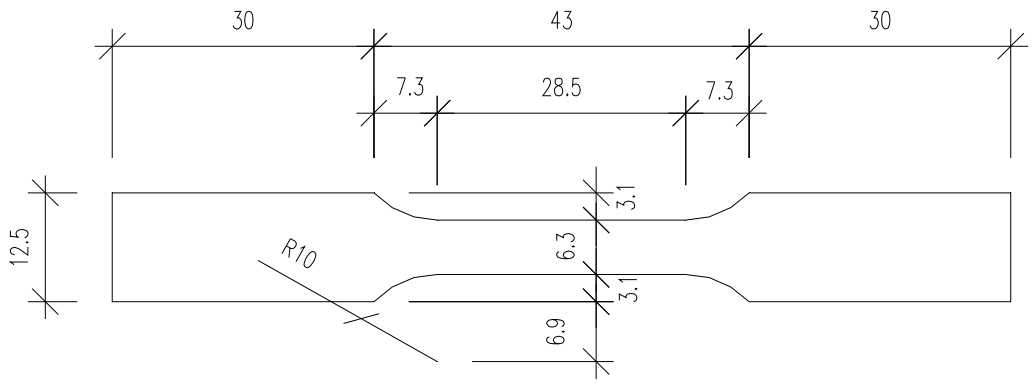

(a) dimension of coupon specimen

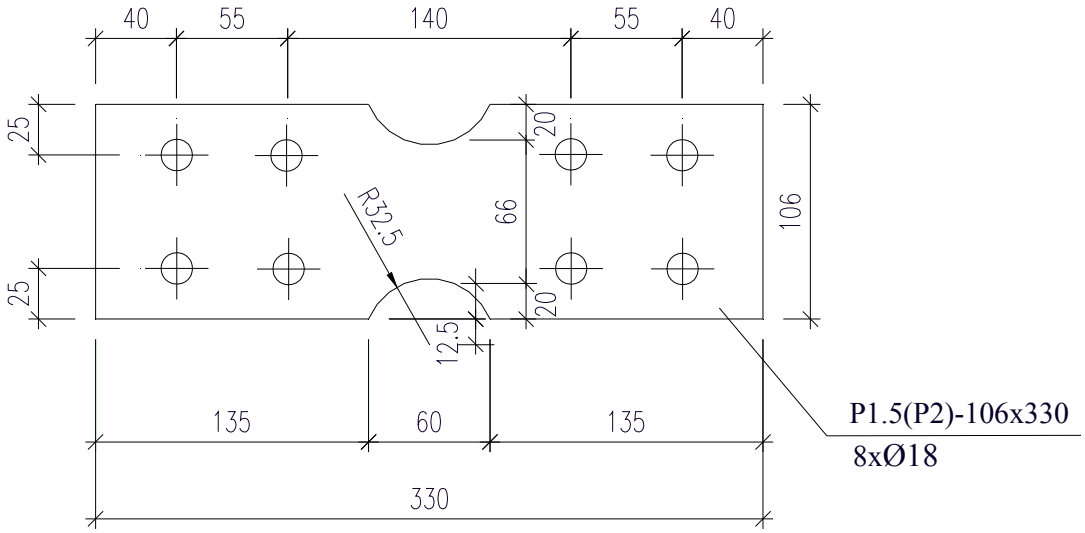

(b) wide specimen from which the coupons were cut

Figure 4.1: Detail drawing of tested coupons of stainless steel sheet.

4.2. INCREASED STRENGTH AT CORNER AND FLAT FACES

4.2.1. Austenitic Steel

For determining the effect of cold bending on the mechanical properties of sheet the data, a commonly used austenitic steel grade of 1.4404 is taken. The tensile material property of the sheet without introducing any plastic strain is shown in Tab. 4.1, which is considered the initial value of the material (annealed material properties) in the Maple. Here the tension coupon test was performed in both parallel to the rolling direction which is denoted by 'P' and the transverse to the rolling direction denoted by 'T' of the sheet. As anisotropy is not considered in the analysis, so the average value of the two directions is used.

Table 4.1: Summary of tensile material properties for austenitic steel sheet.

Grade	Rolling direction	E (GPa)	$\sigma_{0.2}$ (MPa)	$\sigma_{1.0}$ (MPa)	σ_u (MPa)	$\varepsilon_{pl,u}$ (%)	n	$n'_{0.2,1.0}$
1.4404	P	191.00	257.2	307.7	620.6	49.5	3.9	2.2
	T	199.80	279	322	635.1	57.1	8.8	2.3
Avg.		195.40	268.1	314.85	627.85	53.3	6.35	2.25

The cold bending of sheet occurs transverse to the rolling direction, so the data of plastic strain induce in the transverse to the roiling direction is presented in Tab. 4.2. In the table 'RD' means the rolling direction, 'LPSI' means the level (magnitude) of the induced plastic strain and 'PSI' means the plastic strain induced direction.

Table 4.2: 1.4404 grade tensile material properties for the coupons with induced plastic deformation.

RD	LPSI (%)	PSI	E (GPa)	$\sigma_{0.2}$ (MPa)	$\sigma_{1.0}$ (MPa)	σ_u (MPa)	$\varepsilon_{pl,u}$ (%)	n	$n'_{0.2,1.0}$
P	1	T	194.41	296.1	365.4	654.3	60.1	3.5	3
P	3	T	198.10	336.6	425.7	666.5	56.9	1.8	3.2
P	5	T	195.10	362.1	461	678	54.9	3.2	3.4
P	10	T	193.70	413.8	534.9	699.4	51.6	2.9	3.6
P	15	T	190.30	452.3	586	716.5	44.4	2.9	3.8
P	50	T	199.20	610	--	--	--	3.0	--
T	1	T	202.00	312.1	370.8	663.6	66.5	4.4	3
T	3	T	209.10	359.7	420.1	670.8	64.1	4.2	3.3
T	5	T	202.50	399.1	473.5	688.2	62.1	3.6	4.3
T	10	T	203.80	474.2	553.5	712.6	54.9	3.5	4.9
T	15	T	204.90	517.2	618.7	743.1	46.8	3.3	4.8
T	50	T	203.60	679.7	850.9	891.8	26.4	2.9	4.5

The values of material properties say as, modulus of elasticity (E), 0.2% proof strength ($\sigma_{0.2}$), 1.0% proof strength ($\sigma_{1.0}$), ultimate strength (σ_u), ultimate strain (ε_u), Ramberg-Osgood hardening exponent(n), compound Ramberg-Osgood model hardening exponent ($n'_{0.2,1.0}$) from the coupons with various percentage of induced plastic deformation are compared with the initial value of material. Then the data are plotted against with the induced plastic strain to get the equation of material properties with respect to initial value and induced plastic strain shown in Fig. 4.2. As for higher strain it is necessary to use the true stress-strain behaviour so the values of $\sigma_{0.2}$, $\sigma_{1.0}$, σ_u, ε_u are converted to true stress and strain.

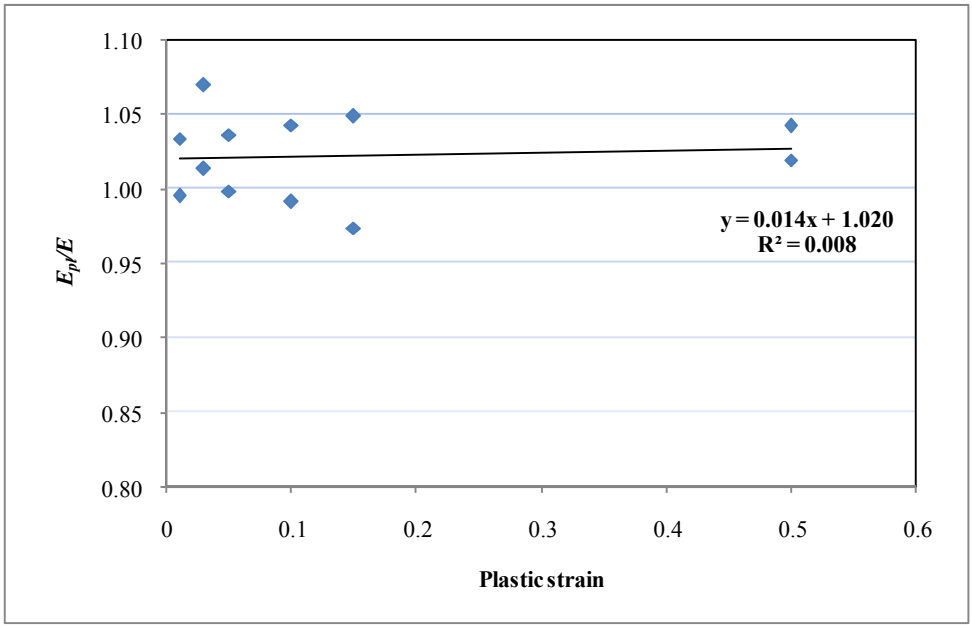

(a) For modulus of elasticity (E)

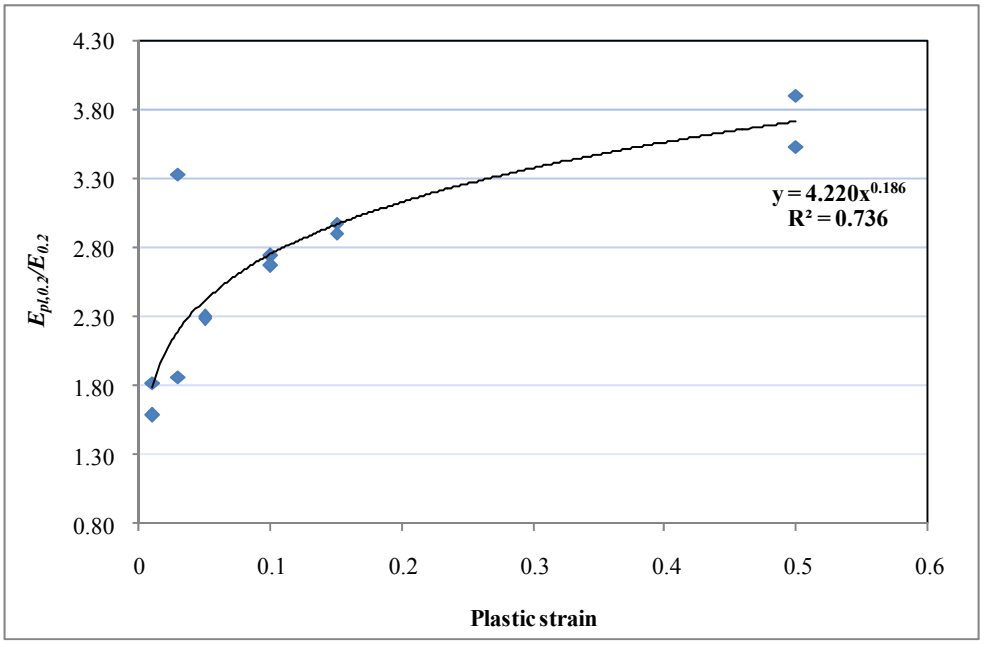

(b) For the tangent modulus at the 0.2% proof stress ($E_{0.2}$)

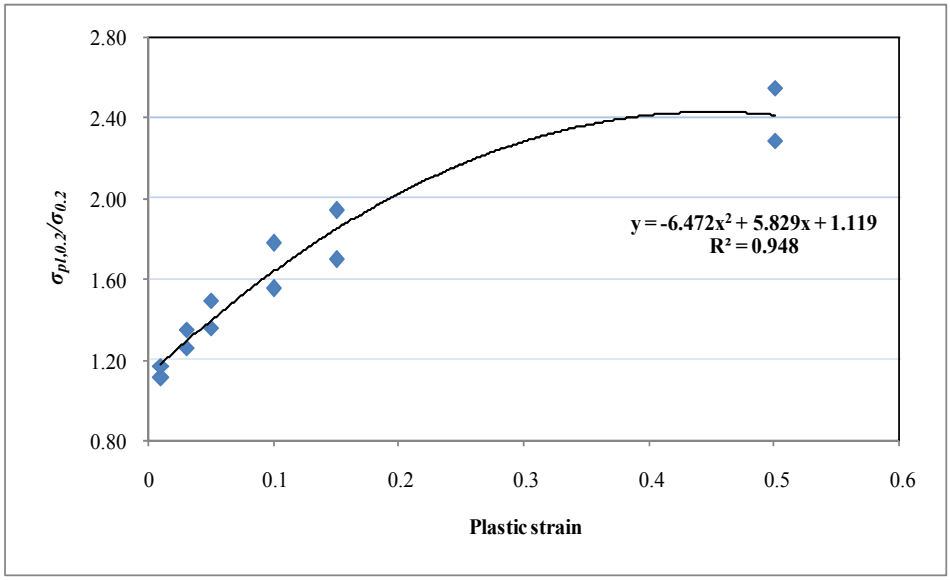

(c) For 0.2% proof stress ($\sigma_{0.2}$)

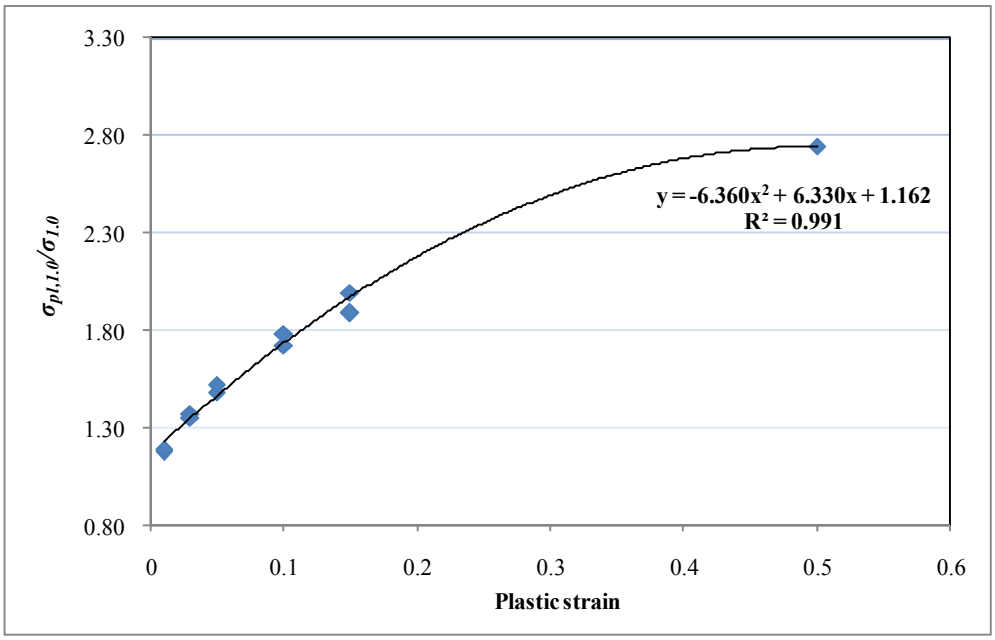

(d) For 1.0 % proof stress ($\sigma_{1.0}$)

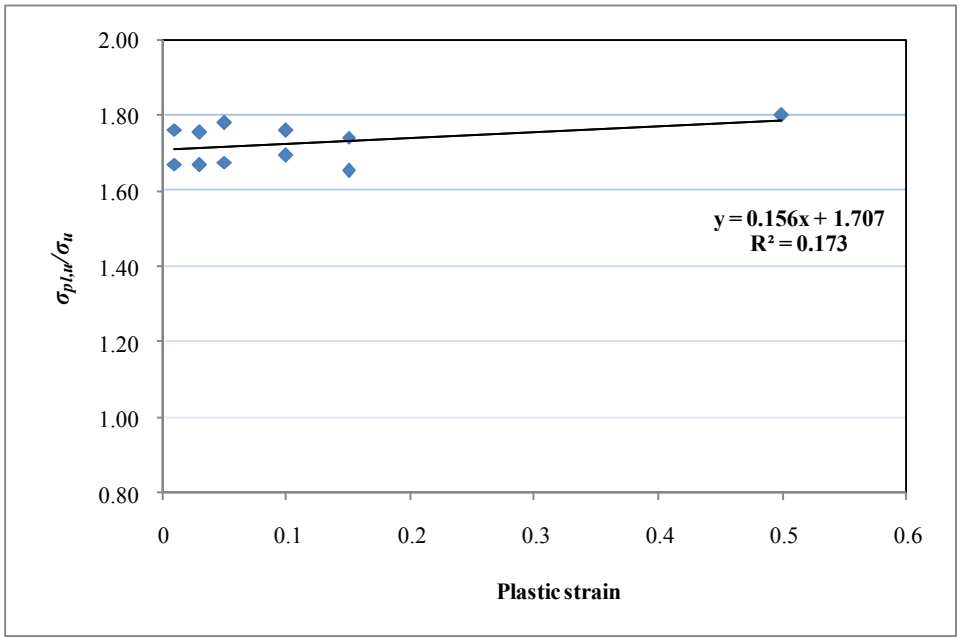

(e) For ultimate strength (σ_u)

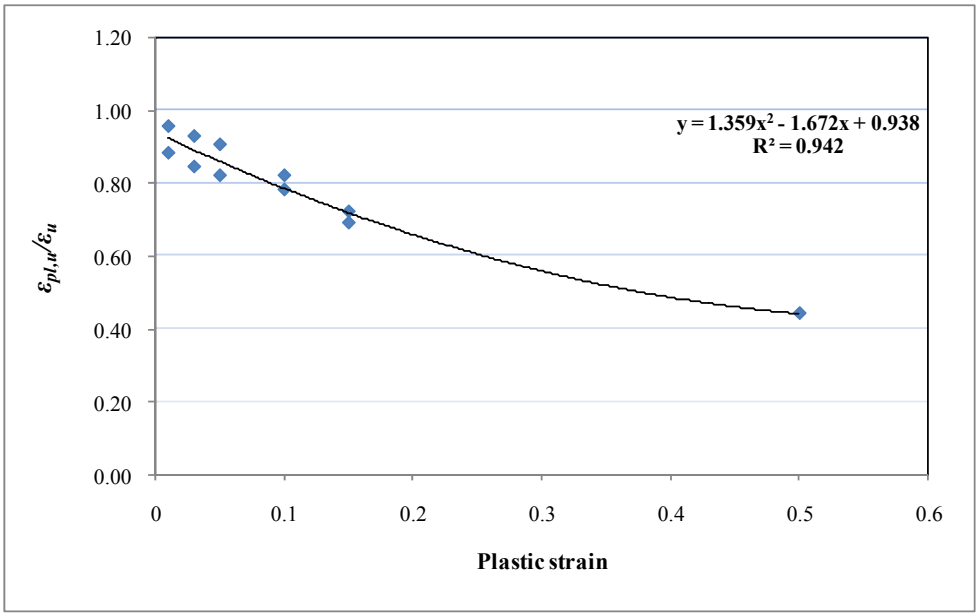

(f) For ultimate strain (ε_u)

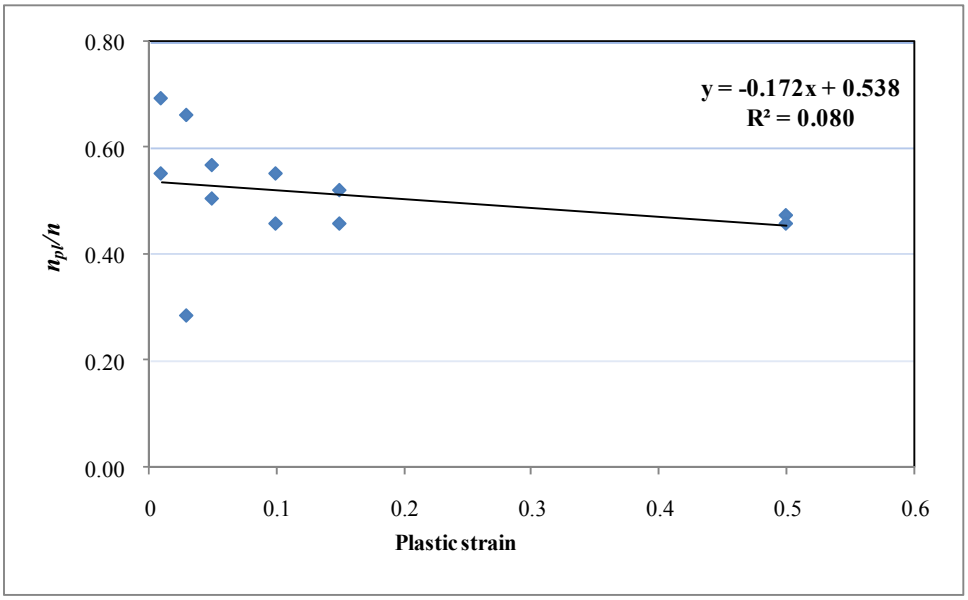

(g) For Ramberg-Osgood hardening exponent (n)

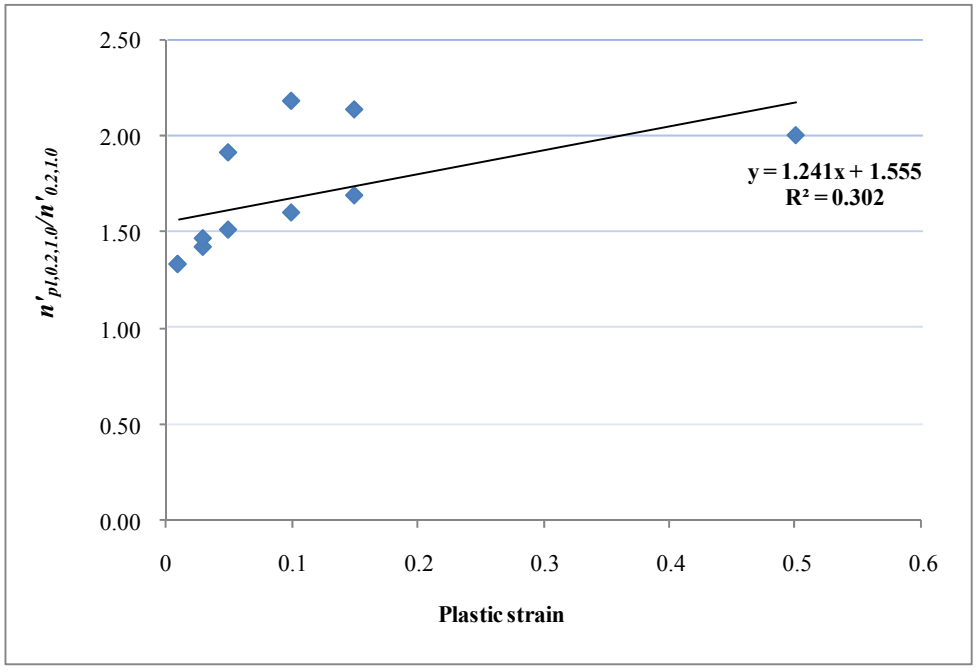

h) For compound Ramberg-Osgood hardening exponent ($n'_{0.2,1.0}$)

Figure 4.2: Variation of material properties with respect to induced plastic strain.

For ferritic, lean-duplex and duplex steel the variation of material properties correspond to induced plastic strain are expressed in the graphical form as like the austenitic steel in Annex B.

The value of coefficient of determination R^2 in case of modulus of elasticity (E), ultimate strength (σ_u) and Ramberg-Osgood hardening exponent (n) and compound Ramberg-Osgood hardening exponent ($n'_{0.2,1.0}$) are lower because the scattered data where it is more data up to the 15% plastic strain then the only data for 50% plastic strain.

The annealed material properties of the Gardner, L (2002), are nearly the same as the properties of austenitic (1.4404). So using the equation of material properties with respect to induced plastic strain, the corner and the flat part properties of the specimen due to cold forming is analysed in the Maple. Here, sheet is divided into 10 parts through thickness and the material properties is calculated from the value of plastic strain after cold bending for each part. Then with the new material properties, for small increment of strain, the stress is calculated and by averaging the data stress strain curve is plotted and compared with the Gardner, L. (2002) stress strain curve for the corner and flat part in the following Fig. 4.3 and Fig. 4.4.

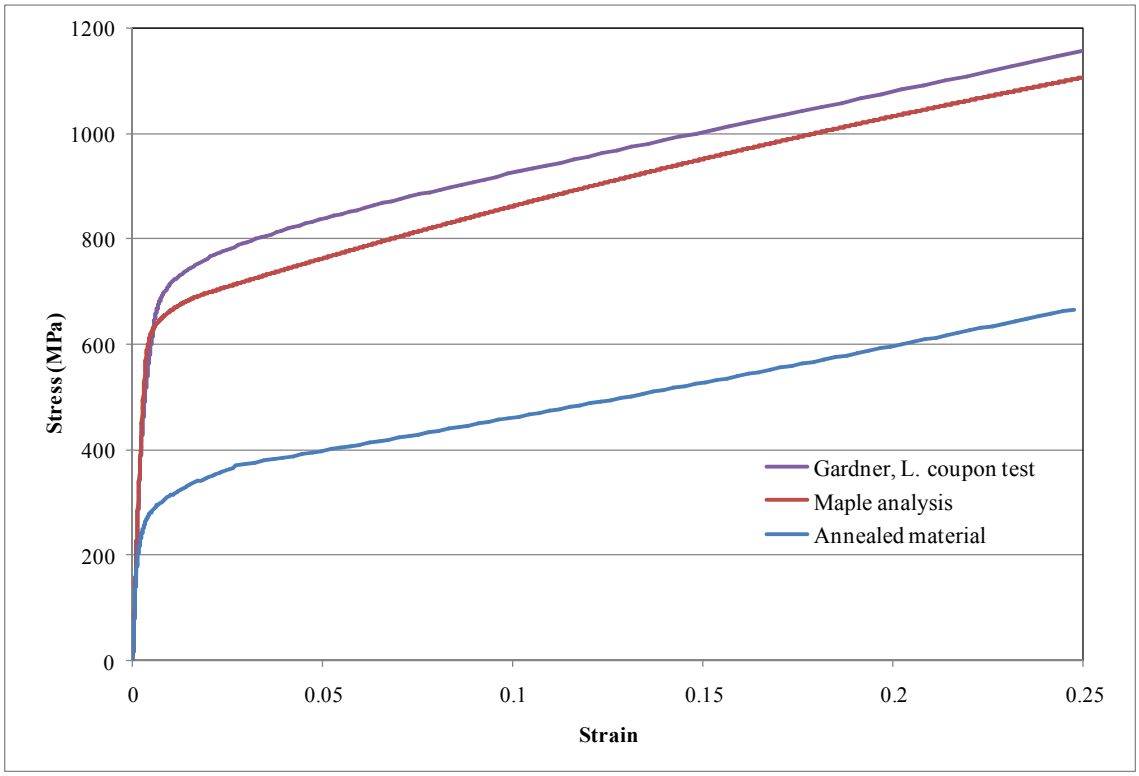

(a) Full stress-strain curve

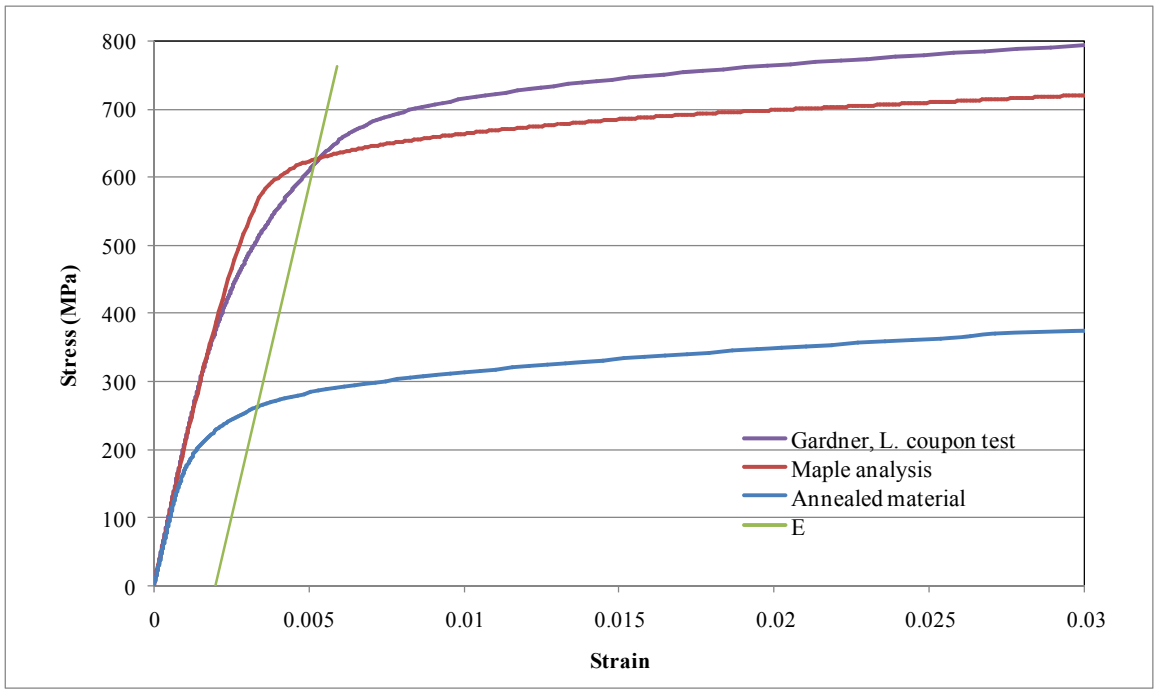

(b) Initial stage of the stress-strain curve

Figure 4.3: Stress strain diagram at corner of the specimen.

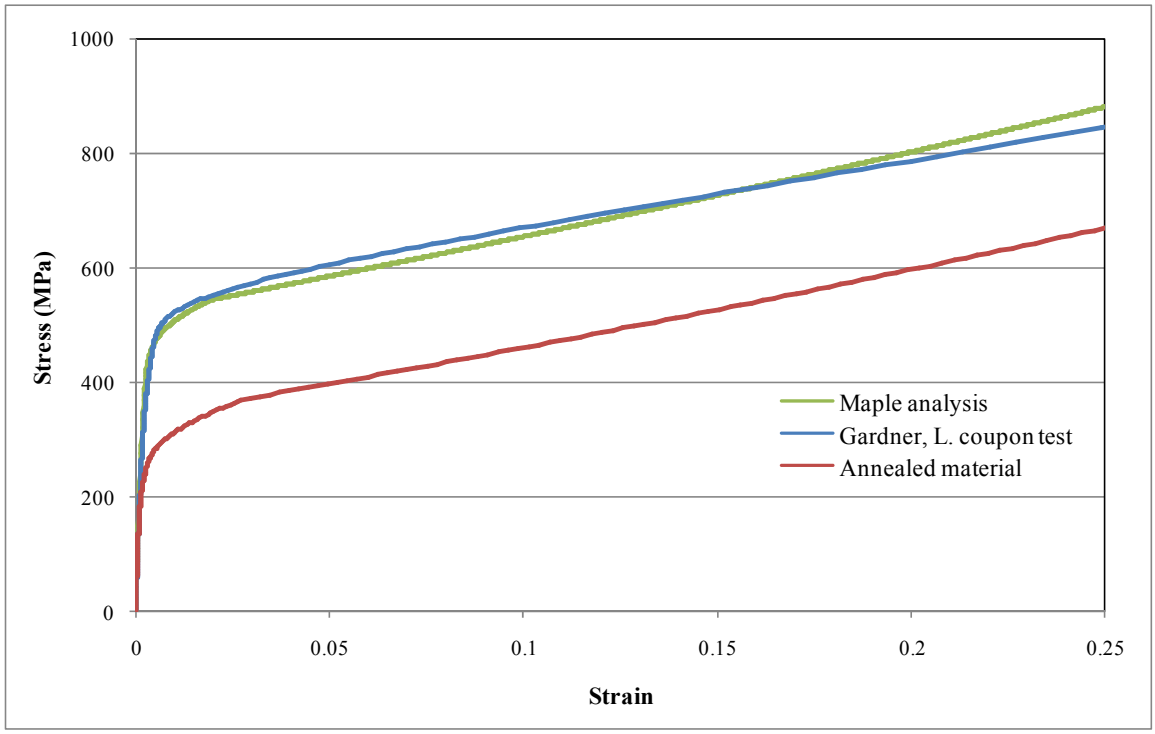

(a) Full stress-strain curve

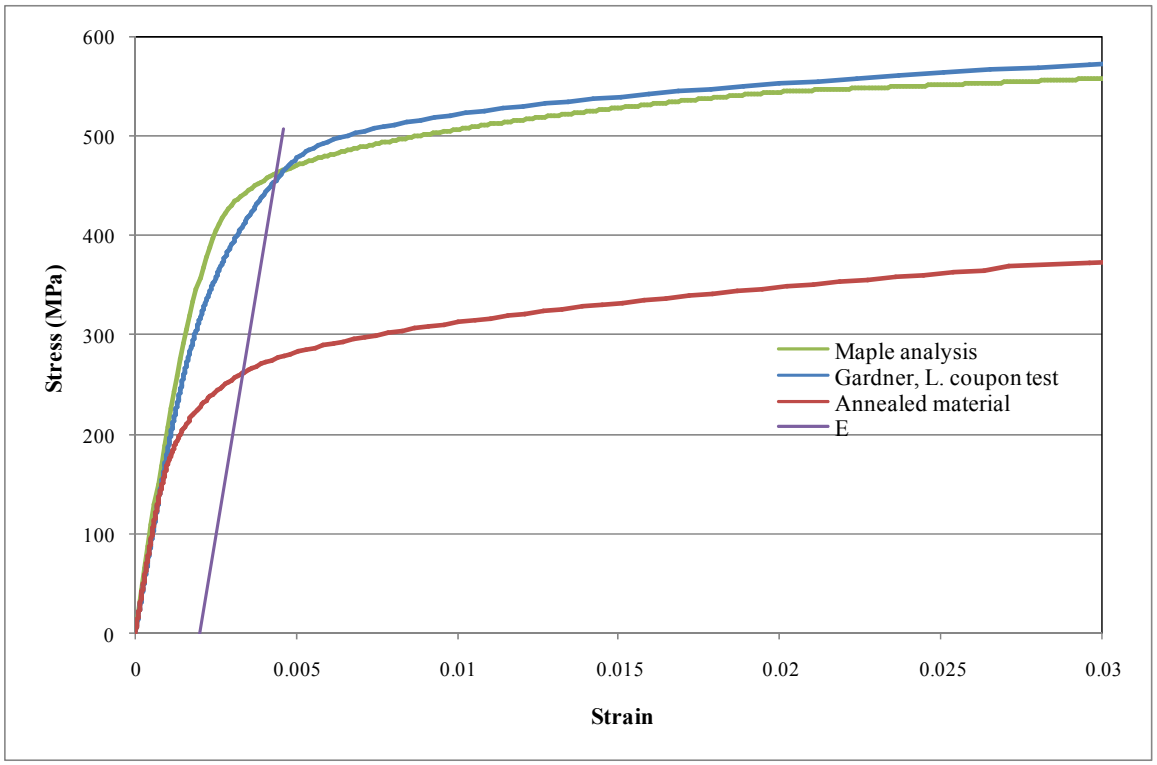

(b) Initial stage of the stress-strain curve

Figure 4.4: Stress strain diagram at flat face of the specimen.

For austenitic steel grade 1.4404, the Maple analysis by varying the ratio of internal radius of corner to thickness (r_i/t) is done to get the increased 0.2% proof strength. The thickness is taken as constant with a value of t equal to 2.0 mm. Here, for analysis the new material properties is set after the final formation of section. The material properties are defined with respect to the plastic strain which is developed due to cold forming process. The stress is get for small increment of strain ($\Delta\varepsilon = 1*10^{-4}$) from the analysis, which is represented as stress-strain diagram in Fig. 4.5. From the figure it is seen that with the increase of r_i/t, the mechanical properties is decreased. In the stainless steel the strength increase during cold forming is due to the strain hardening, so for small radius of curvature it experiences more straining. As the induced plastic strain in the section does not vary linearly through thickness, to account the nonlinear variation of strain the section is divided into ten parts. Finally average stress for the section is taken for getting the stress-strain relationship.

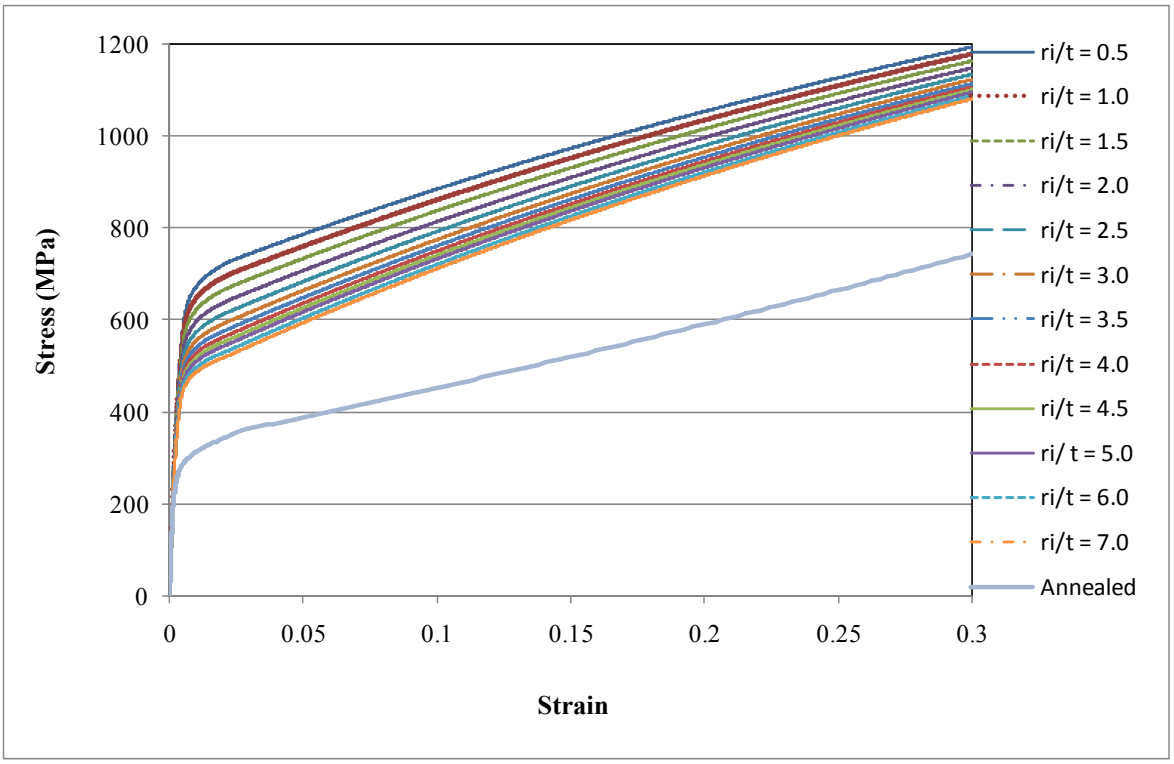

(a) Full stress-strain curve

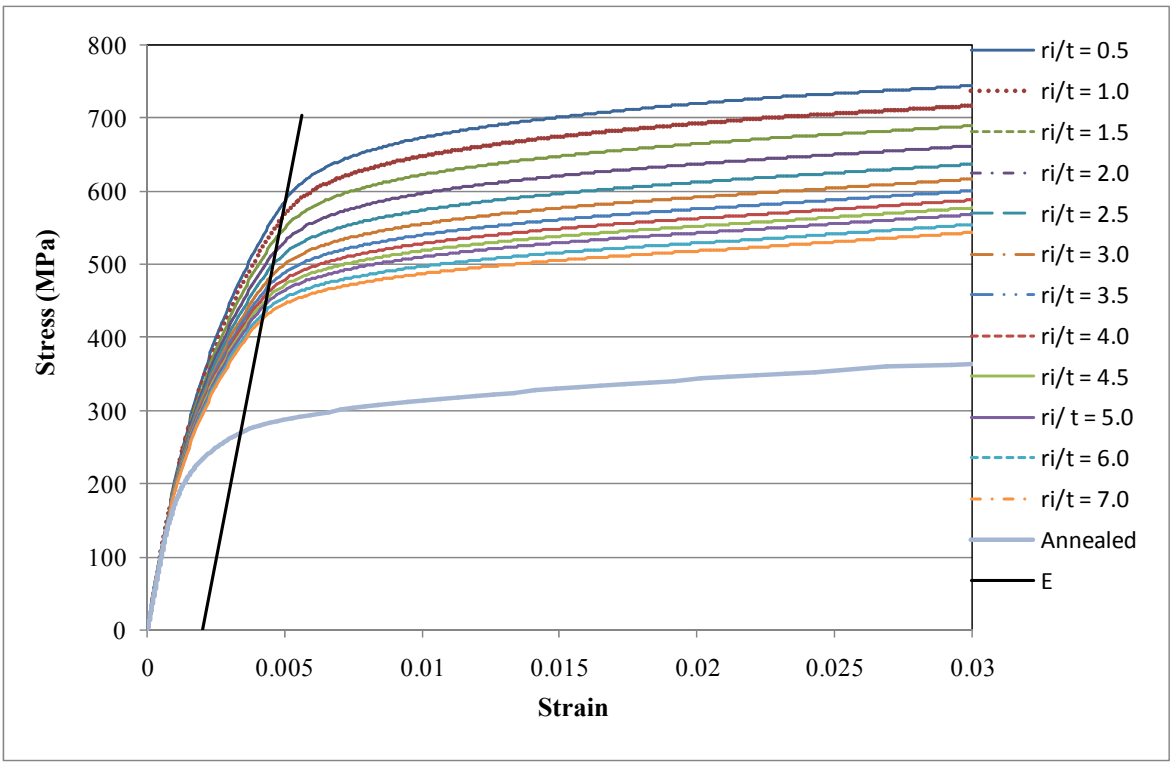

(b) Initial stage of the stress-strain curve

Figure 4.5: Variation of material properties for different r_i/t ratio at corner (austenitic steel).

From the stress-strain relationship of material after cold bending the 0.2% proof strength ($\sigma_{0.2}$) is calculated for each bending radius to thickness (r_i/t). The increased 0.2% proof strength at corner ($\sigma_{0.2,c}$) is graphically represented considering the strength affecting parameters as 0.2% proof strength of the annealed material ($\sigma_{0.2,a}$) , internal corner radius (r_i) and the thickness of sheet (t) to be cold formed. The ratio of 0.2% proof strength at corner and annealed material ($\sigma_{0.2,c}/\ \sigma_{0.2,a}$) is plotted against the ratio of internal corner radius and thickness (r_i/t) in Fig. 4.6 below. The value of r_i/t varies from 0.5 to 7.0 as all the previous test data of cold working are within this ranges.

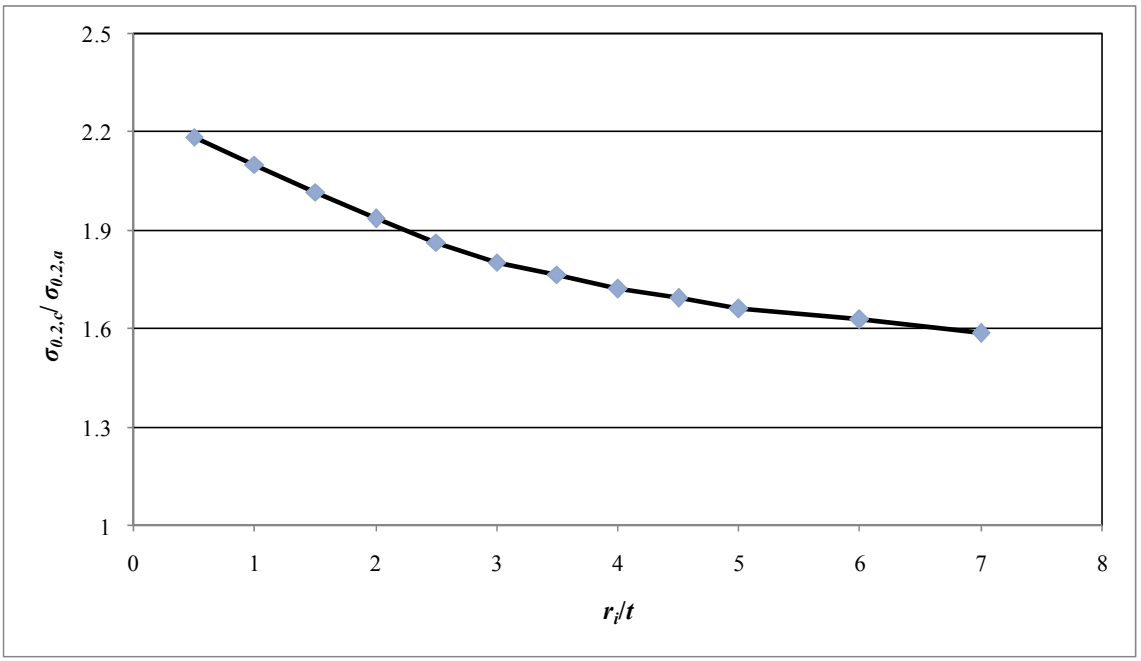

Figure 4.6: Variation of increased corner strength against r_i/t ratio due to cold bending (austenitic steel).

The previous model described in the literature review for predicting the corner properties of stainless steel considering the 0.2% proof strength of annealed material and the r_i/t are represented in graphical form to compare the result got from the analysis here.

Van den Berg, G. J. and Van der Merwe, P. (1992) proposed a model from the test result of stainless steel (ferritic steel grade (1.4512, 1.4016 and 1.4003) and austenitic steel grade 1.4301) for the prediction of corner 0.2% proof strength $\sigma_{0.2,c}$. They have considered the

parameters as $\sigma_{0.2,a}$ and $\sigma_{u,a}$ which are the 0.2% proof strength and ultimate strength of annealed material respectively and r_i/t.

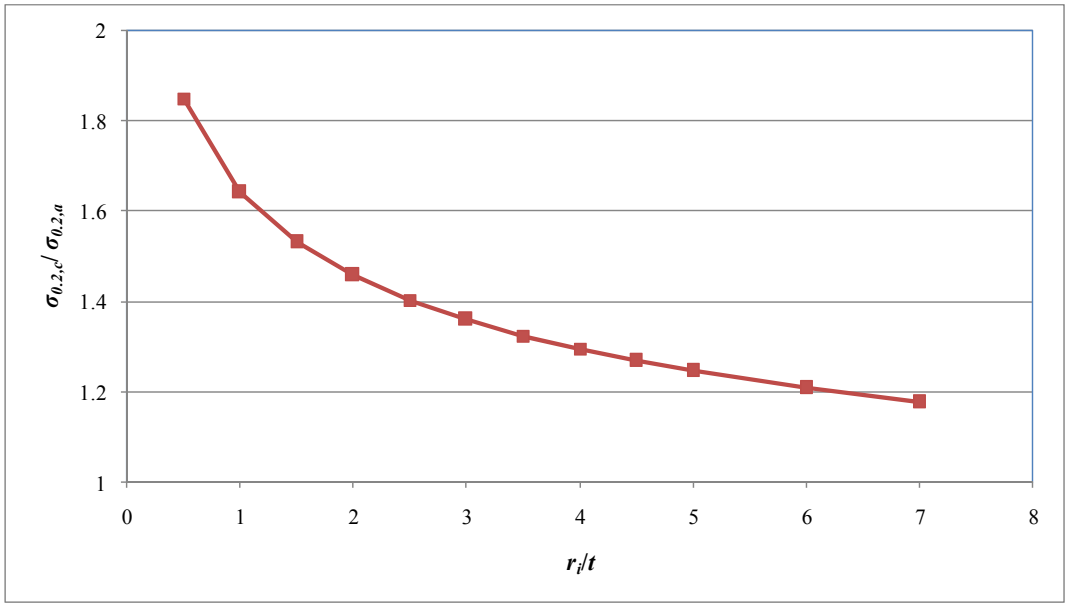

Figure 4.7: Van den Berg, G.J. and Van der Merwe, P. (1992) model.

Ashraf, M. et, al. (2005), proposed two power modes to predict corner strength in stainless steel sections based on all available test data of Coetzee, J. S. et, al. (1990), Van den Berg, G. J. and Van der Merwe, P. (1992), Rasmussen, K. J. R. and Hancock, G. J. (1993), Gardner, L. (2002). The first model named the simple power model which is independent to the ultimate strength of the annealed material and can be obtained by three parameters ($\sigma_{0.2,a}$, r_i, *and* t). In the second model named power model also considered the ultimate strength of the annealed material ($\sigma_{u,a}$). The model takes the stainless steel into account are austenitic steel grade of 1.4301, 1.4401, 1.4301 and ferritic steel grade of 1.4003, 1.4016, 1.4512.

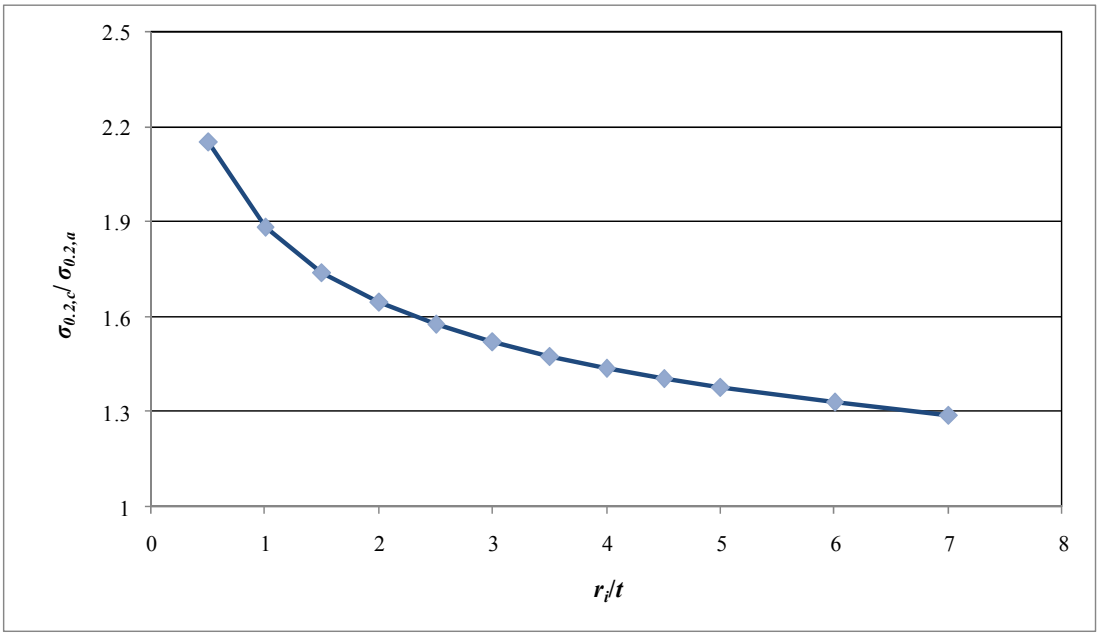

(a) independent to ultimate strength of annealed material ($\sigma_{u,a}$)

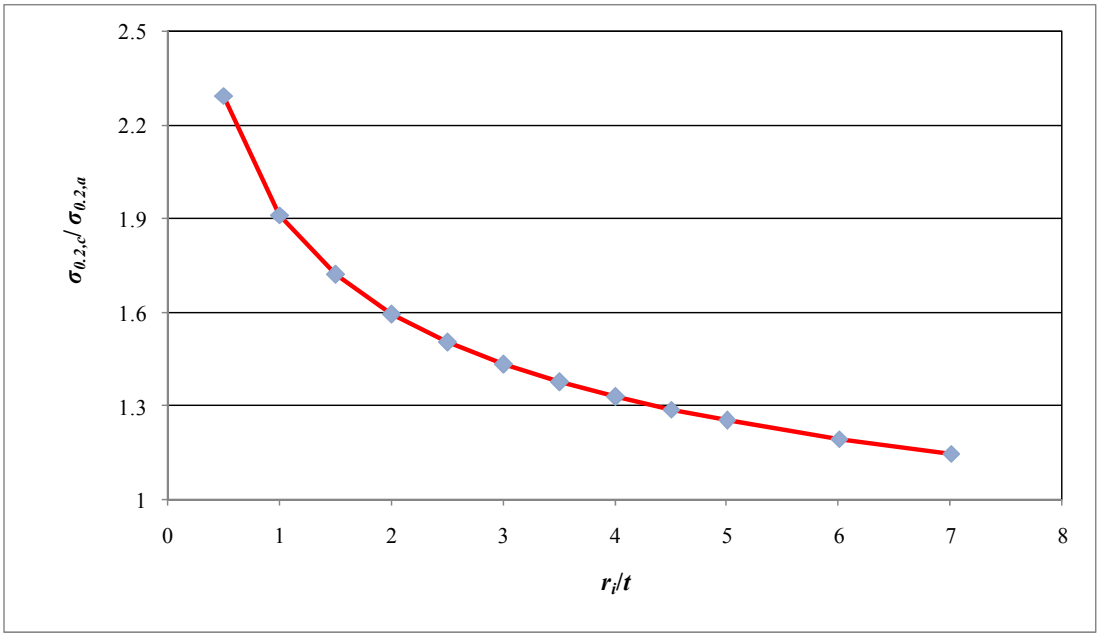

(b) considering ultimate strength of annealed material ($\sigma_{u,a}$)

Figure 4.8: Ashraf, M. et al. (2005) model.

Cruise, R.B. and Gardner, L. (2008) modified the expression of Ashraf, et, al. (2005) by their test data of austenitic steel grade 1.4301 and the previous published data.

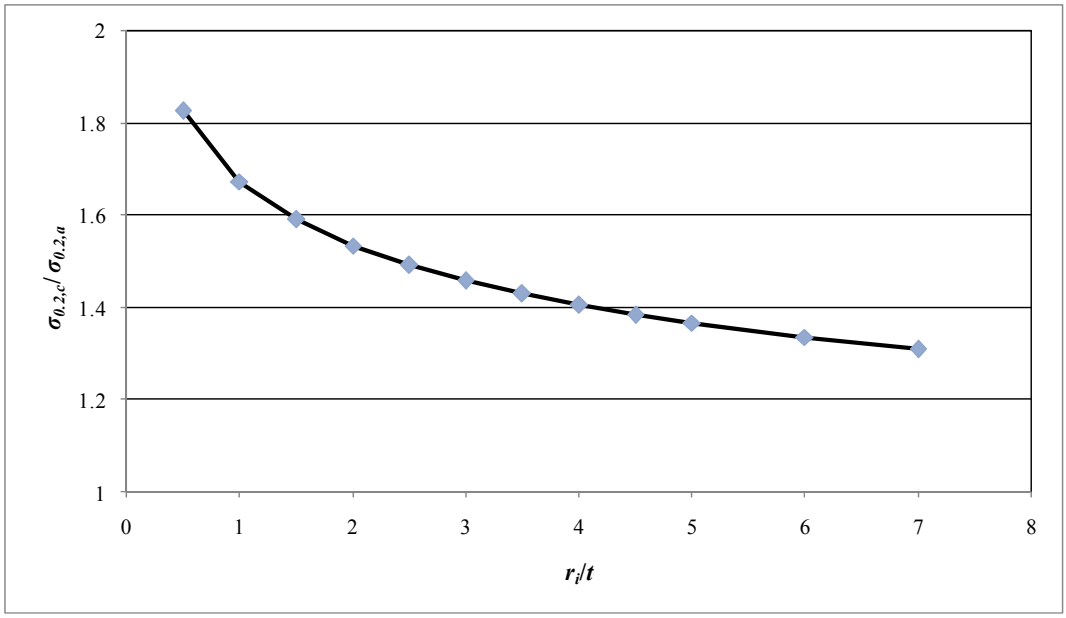

Figure 4.9: Cruise, R.B. and Gardner, L (2008) model.

Rossi, B. et, al. (2013) proposed a new power model where more stainless steel grade is considered consisting of austenitic steel grade of 1.4301, 1.4306, 1.4307, 1.4318, 1.4401, 1.4571, 1.4401, ferritic steel grade of 1.4016, 1.4003, duplex steel grade of 1.4462 and lean duplex steel grade of 1.4162.

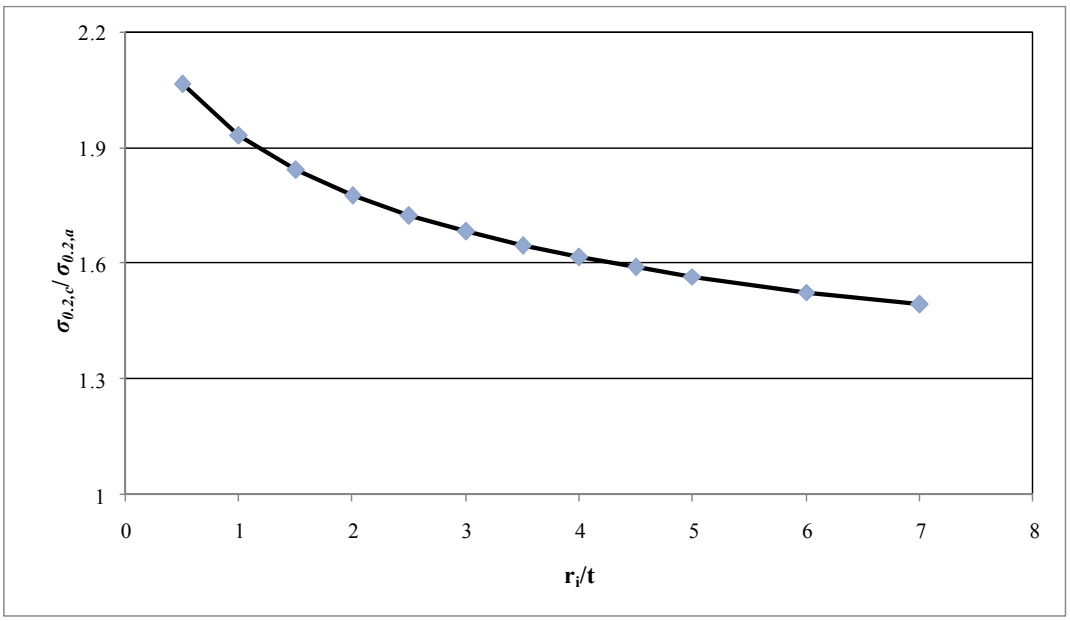

Figure 4.10: Rossi, B. et, al. (2013) model.

The comparison of these models with the analysed data for austenitic steel is shown in Fig. 4.11 below.

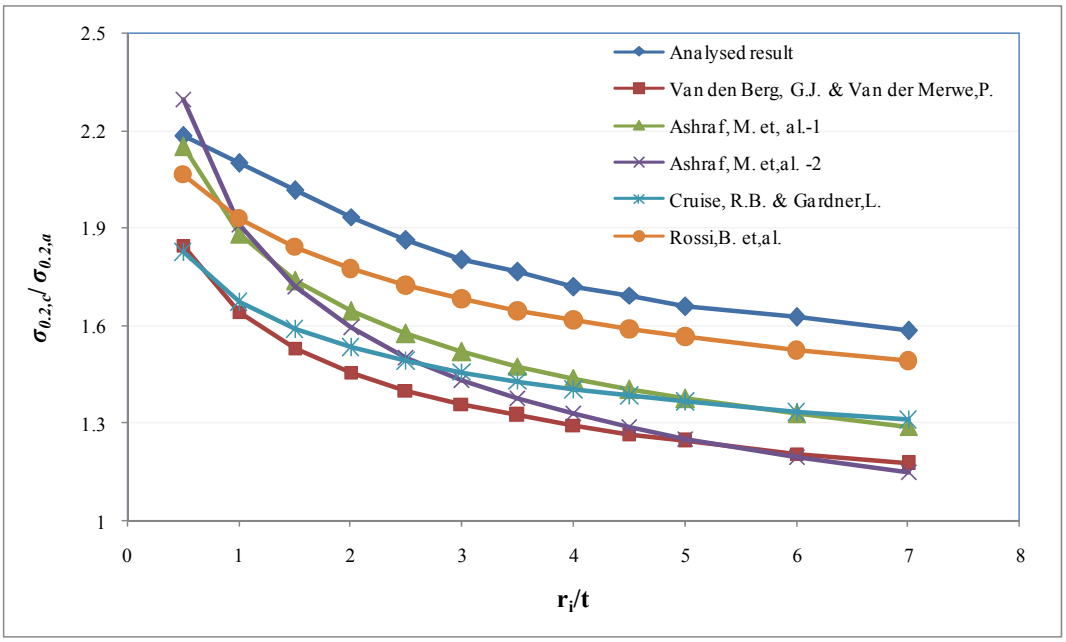

Figure 4.11: Comparison of models for predicting the corner strength increase (austenitic steel).

The strength at the flat face of the cold rolled section is determined using the Maple by varying the ratio of internal radius circle which indicate the geometry of the section before making the square or rectangular section to thickness (R_i/t) is done to get the increased 0.2% proof strength. Here, for analysis the new material properties is set after the flattening of circle and using the same equation as used for the corner. The stress is get for small increment of strain from the analysis, which is represented as stress-strain diagram in Fig. 4.12.

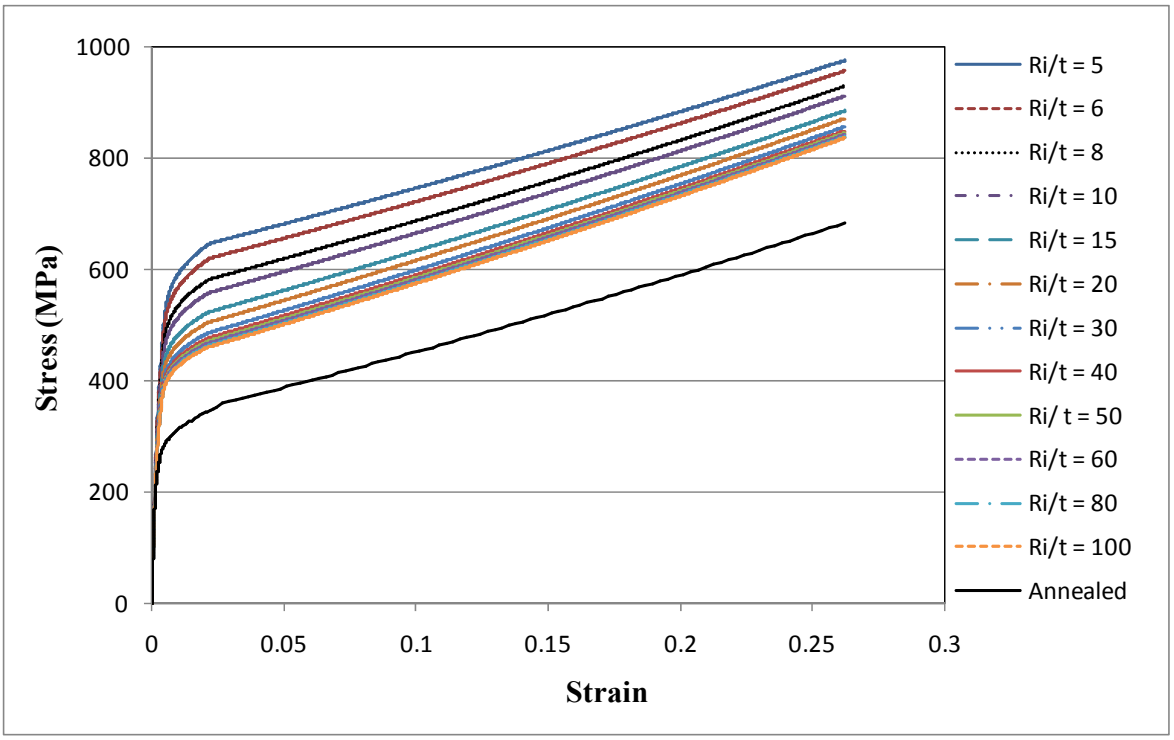

(a) Full stress-strain curve

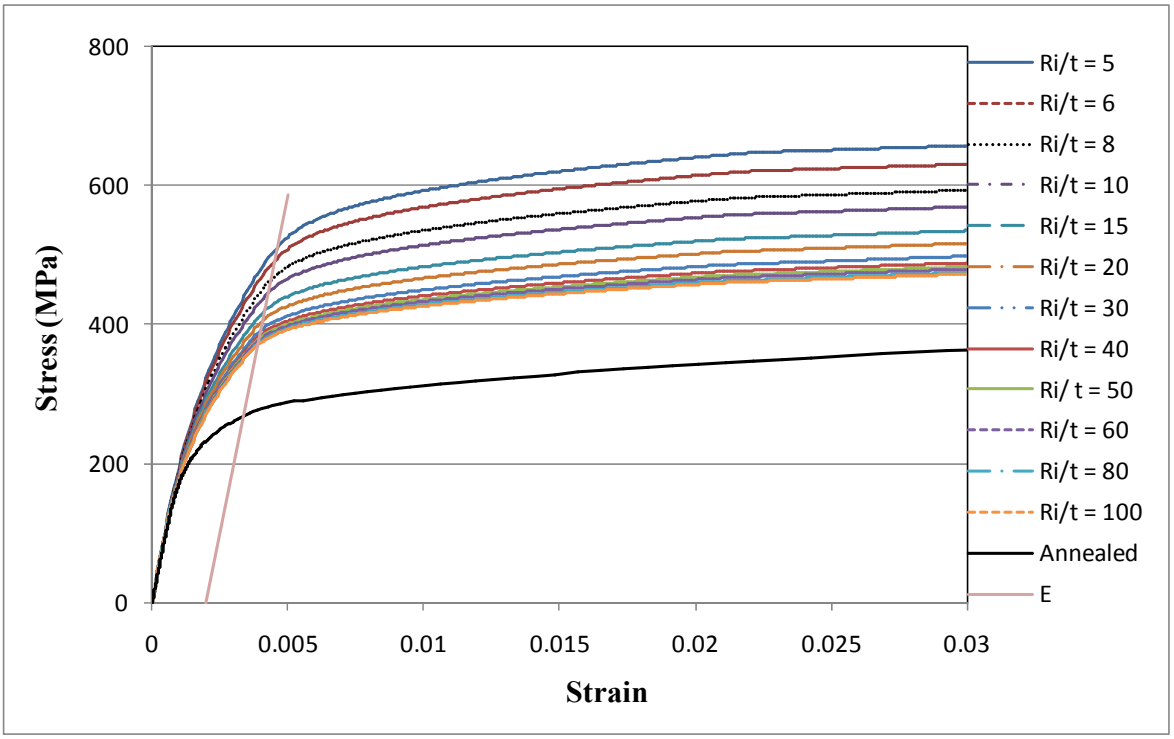

(b) Initial stage of the stress-strain curve

Figure 4.12: Variation of material properties for different R_i/t ratio at flat face (austenitic steel).

From the stress-strain relationship of material after making circle to flatten, the 0.2% proof strength ($\sigma_{0.2}$) is calculated for each circle radius to thickness (R_i/t). The ratio of 0.2% proof strength at flat faces and annealed material ($\sigma_{0.2,f}/\ \sigma_{0.2,a}$) is plotted against the ratio of internal circle radius and thickness (R_i/t) in Fig. 4.13 below. The value of R_i/t varies from 5 to 100 which can satisfy for all the square or rectangular section made by cold rolling. The increased 0.2% proof strength at flat face ($\sigma_{0.2,f}$) is graphically represented considering the strength affecting parameters as 0.2% proof strength of the annealed material ($\sigma_{0.2,a}$), internal circle radius (R_i) and the thickness of sheet (t) to be cold formed. Here the internal circle radius $R_i = (b+h-2t)/\pi$, where b is the width and h is the height of the section and t is the thickness of the sheet.

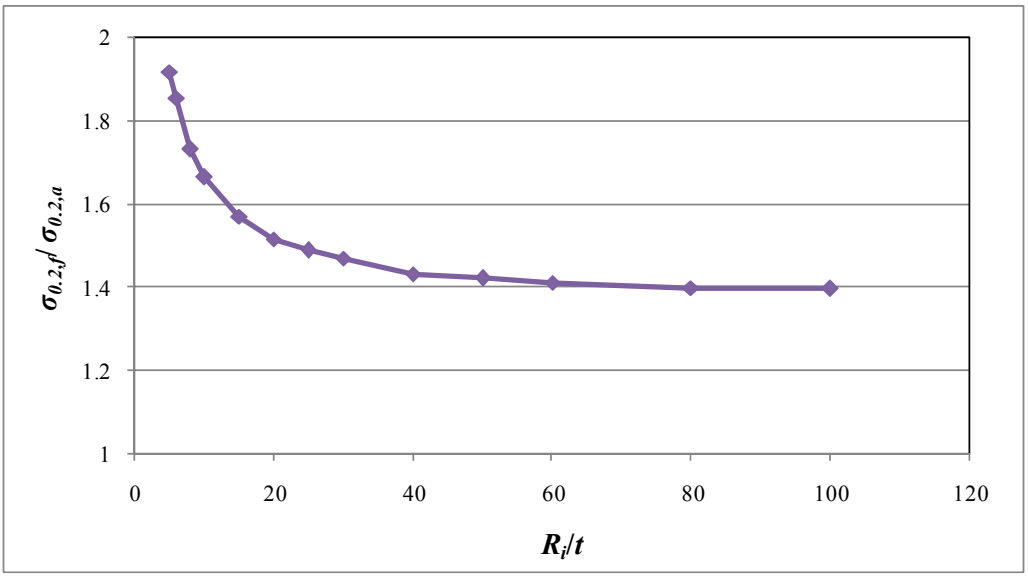

Figure 4.13: Variation of increased strength at flat faces against R_i/t ratio due to cold bending (austenitic steel).

The previous model [Cruise, R.B. and Gardner, L. (2008) and Rossi, B. et, al. (2013)] model described in the literature review for predicting the flat face properties of stainless steel considering the 0.2% proof strength of annealed material and the geometry of the section are represented in graphical form to compare the result got from the analysis here in Fig. 4.14 below.

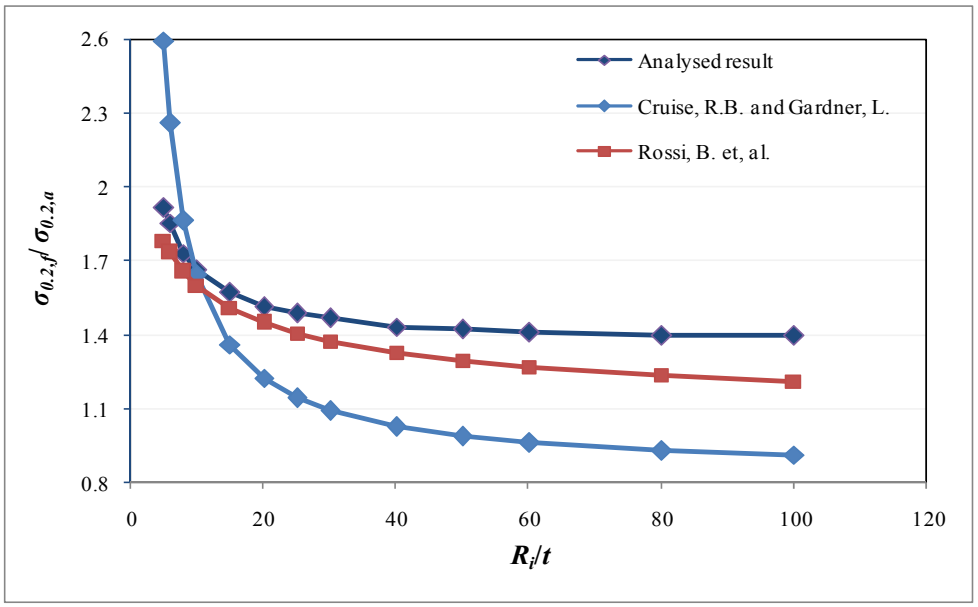

Figure 4.14: Comparison of predicted model for the strength increase at flat faces due to cold rolling (austenitic steel).

4.2.2. Ferritic Steel

The tensile material property of the sheet without introducing any plastic strain is shown in Tab. 4.3, which is considered the initial value of the material (annealed material properties) in the Maple.

Table 4.3: Summary of tensile material properties for ferritic steel sheet.

Grade	Rolling direction	E_0 (GPa)	$\sigma_{0.2}$ (MPa)	$\sigma_{1.0}$ (MPa)	σ_u (MPa)	$\varepsilon_{pl,u}$ (%)	n	$n'_{0.2,1.0}$
1.4003	P	198.3	326.7	357.1	492.3	18.0	8.4	1.8
	T	211.9	343.7	374.5	512.3	17.6	8.5	1.9
Avg.		205.1	335.2	365.8	502.2	17.8	8.45	1.85

As like austenitic steel, using the Tab. 4.4, the equation of material properties with respect to induced plastic strain is determined (Annex B) and theses relationship of material properties as set after final stage of cold bending.

Table 4.4: 1.4003 grade tensile material properties for the coupons with induced plastic deformation.

RD	LPSI (%)	PSI	E (GPa)	$\sigma_{0.2}$ (MPa)	$\sigma_{1.0}$ (MPa)	σ_u (MPa)	$\varepsilon_{pl,u}$ (%)	n	$n'_{0.2,1.0}$
P	1	T	192.1	354.1	407.2	455.0	--	9.2	3.1
P	3	T	202.6	420.2	469.1	503.2	--	4.0	4.0
P	5	T	194.6	453.7	517.7	526.5	--	3.9	5.0
P	10	T	189.2	492.0	581.4	581.4	11.7	3.3	5.0
P	15	T	184.9	585.7	649.6	650.6	7.6	5.3	5.0
T	1	T	190.7	368.0	415.7	528.0	15.7	6.3	2.5
T	3	T	207.3	408.2	481.7	534.1	44.9	3.4	4.9
T	5	T	197.6	464.7	518.2	551.0	21.7	4.7	4.5
T	10	T	197.2	561.1	612.3	632.4	9.7	4.2	4.0
T	15	T	201.8	577.1	--	643.5	6.5	4.1	4.0

The ratio of 0.2% proof strength at corner and annealed material ($\sigma_{0.2,c}/\ \sigma_{0.2,a}$) is plotted against the ratio of internal corner radius and thickness (r_i/t) in Fig. 4.15 below with the previous established predictive model.

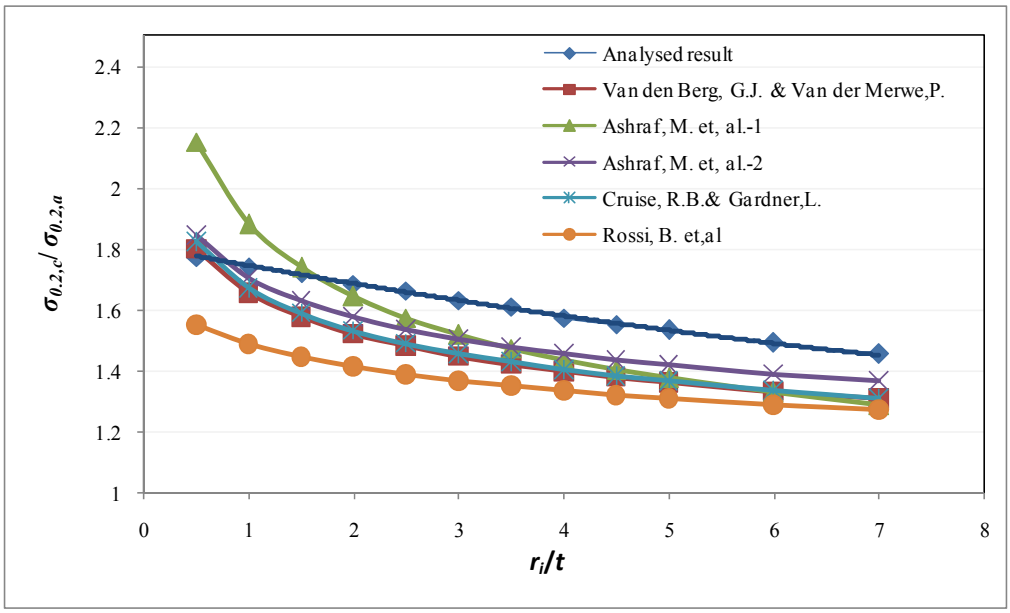

Figure 4.15: Variation of increased corner strength against r_i/t ratio due to cold bending (ferritic steel).

The ratio of 0.2% proof strength at flat faces and annealed material ($\sigma_{0.2,f}/\sigma_{0.2,a}$) is plotted against the ratio of internal circle radius to thickness (R_i/t) in Fig. 4.16 below.

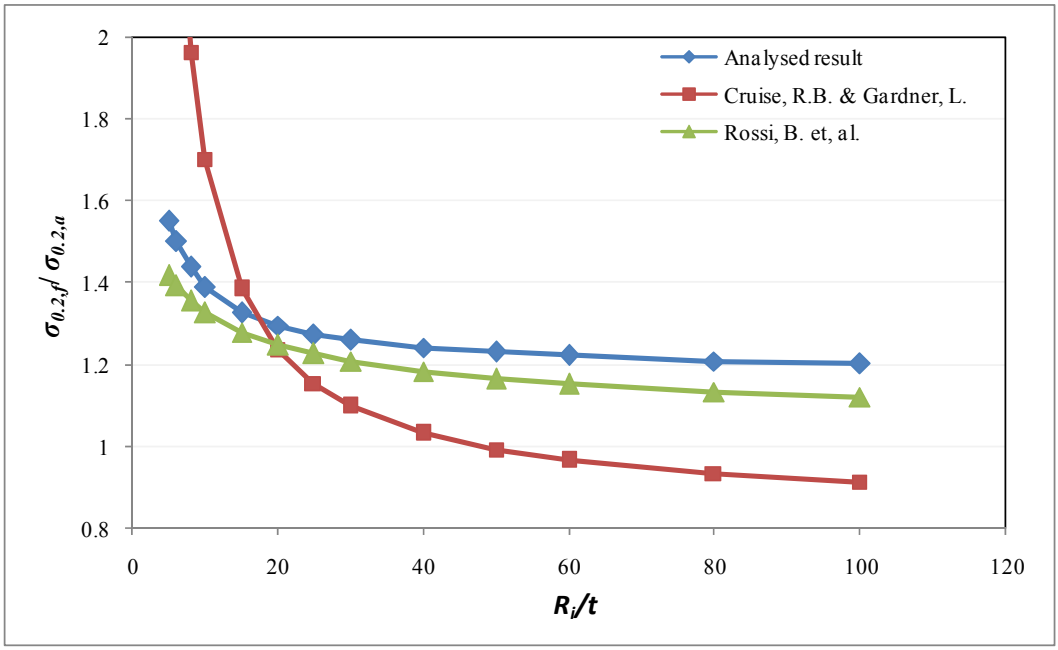

Figure 4.16: Variation of increased strength at flat faces against R_i/t ratio due to cold bending (ferritic steel).

4.2.3. Lean-duplex Steel

The material properties of the lean-duplex steel without plastic strain and the different % of induced plastic strain are shown in Tab. 4.5 and 4.6.

Table 4.5: Summary of tensile material properties for lean-duplex steel sheet.

Grade	Rolling direction	E_0 (GPa)	$\sigma_{0.2}$ (MPa)	$\sigma_{1.0}$ (MPa)	σ_u (MPa)	$\varepsilon_{pl,u}$ (%)	n	$n'_{0.2,1.0}$
1.4162	P	193.3	551.6	623.7	785.9	24.1	7.3	3.0
1.4162	T	195.5	556.5	624.8	765.6	21.1	7.5	3.1
Avg.		194.4	554.05	624.25	775.75	22.6	7.4	3.05

Table 4.6: 1.4162 grade tensile material properties for the coupons with induced plastic deformation.

RD	LPSI (%)	PSI	E (GPa)	$\sigma_{0.2}$ (MPa)	$\sigma_{1.0}$ (MPa)	σ_u (MPa)	$\varepsilon_{pl,u}$ (%)	n	$n'_{0.2,1.0}$
P	1	T	193.6	511.8	668.2	815.5	40.0	2.6	4.5
P	3	T	200.3	546.4	721.6	824.6	37.6	2.9	3.3
P	5	T	200.2	637.6	782.3	857.9	32.8	7.2	3.1
P	10	T	190.3	596.0	835.0	911.4	24.7	2.7	3.1
P	15	T	197.1	626.9	880.1	956.1	17.9	2.5	2.7
P	20	T	201.8	653.6	937.0	1002.5	12.3	2.4	3.0
T	1	T	209.9	556.5	674.4	816.2	38.0	3.4	3.6
T	3	T	208.6	574.1	728.0	834.9	34.8	2.9	3.5
T	5	T	201.1	583.6	768.9	850.0	32.4	2.8	3.6
T	10	T	202.8	646.4	859.5	925.6	22.3	2.7	3.0
T	15	T	198.7	690.6	912.2	971.2	13.9	2.7	3.8
T	20	T	202.3	673.6	917.9	1006.9	11.5	1.8	3.0

The ratio of 0.2% proof strength at corner and annealed material ($\sigma_{0.2,c}/\ \sigma_{0.2,a}$) is presented in graphical form against the ratio of internal corner radius and thickness ($r_i/\ t$) in Fig. 4.17 below.

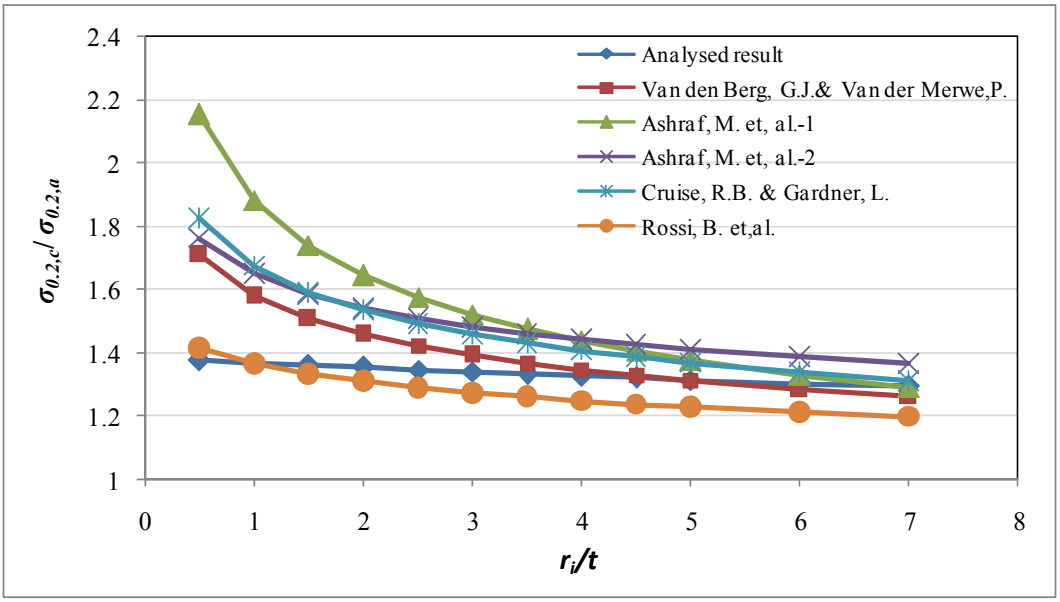

Figure 4.17: Variation of increased corner strength against r_i/t ratio due to cold bending (lean duplex).

The ratio of 0.2% proof strength at flat faces and annealed material ($\sigma_{0.2,f}/\sigma_{0.2,a}$) is plotted against the ratio of internal circle radius to thickness (R_i/t) in Fig. 4.18 below.

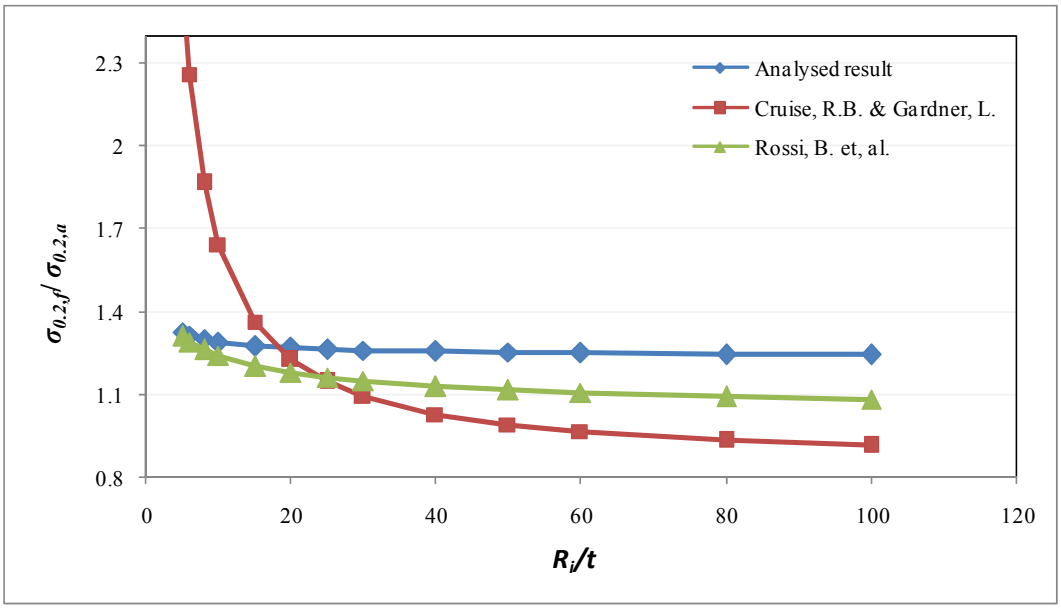

Figure 4.18: Variation of increased strength at flat faces against R_i/t ratio due to cold bending (lean-duplex steel).

4.2.4. Duplex Steel

The material properties of the duplex steel without plastic strain and the different % of induced plastic strain are shown in Tab. 4.7 and 4.8.

Table 4.7: Summary of tensile material properties for duplex steel sheet.

Grade	Rolling direction	E_0 (GPa)	$\sigma_{0.2}$ (MPa)	$\sigma_{1.0}$ (MPa)	σ_u (MPa)	$\varepsilon_{pl,u}$ (%)	n	$n'_{0.2,1.0}$
1.4462	P	195.8	600.1	676.6	843.0	22.6	6.9	2.9
1.4462	T	210.7	637.6	722.7	863.7	20.6	5.6	3.4
Avg.		203.25	618.85	699.65	853.35	21.59	6.25	3.15

Table 4.8: 1.4462 grade tensile material properties for the coupons with induced plastic deformation.

RD	LPSI (%)	PSI	E (GPa)	$\sigma_{0.2}$ (MPa)	$\sigma_{1.0}$ (MPa)	σ_u (MPa)	$\varepsilon_{pl,u}$ (%)	n	$n'_{0.2,1.0}$
P	1	T	191.1	608.2	665.8	882.4	33.5	3.2	3.0
P	3	T	194.5	647.5	756.6	890.3	30.3	3.8	3.4
P	5	T	195.0	720.2	873.6	940.4	22.3	3.2	3.8
P	10	T	196.2	747.7	933.9	994.1	16.3	3.0	4.2
P	15	T	188.2	844.5	1030.9	1072.2	10.2	2.9	4.3
P	20	T	188.8	897.3	1080.9	1116.0	7.0	3.0	4.2
T	1	T	211.0	648.4	757.2	900.9	38.4	3.7	3.6
T	3	T	208.9	691.6	836.8	927.6	32.0	2.7	4.0
T	5	T	208.4	732.3	860.3	939.3	24.3	3.3	4.0
T	10	T	209.2	827.2	933.9	994.1	19.9	3.5	4.3
T	15	T	203.1	865.9	1039.6	1117.4	16.2	3.2	4.4
T	20	T	213.5	887.3	1070.6	1115.4	15.1	3.1	4.8

The ratio of 0.2% proof strength at corner and annealed material ($\sigma_{0.2,c}/\ \sigma_{0.2,a}$) is presented in graphical form against the ratio of internal corner radius and thickness ($r_i/\ t$) in Fig. 4.19 below.

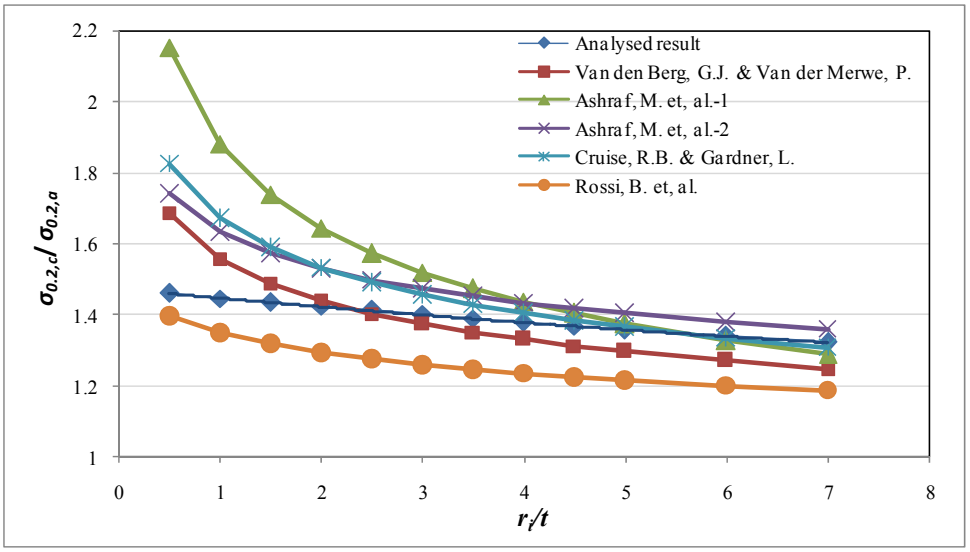

Figure 4.19: Variation of increased corner strength against r_i/t ratio due to cold bending (duplex steel).

The ratio of 0.2% proof strength at flat faces and annealed material ($\sigma_{0.2,f}/\sigma_{0.2,a}$) is plotted against the ratio of internal circle radius to thickness (R_i/t) in Fig. 4.20 below.

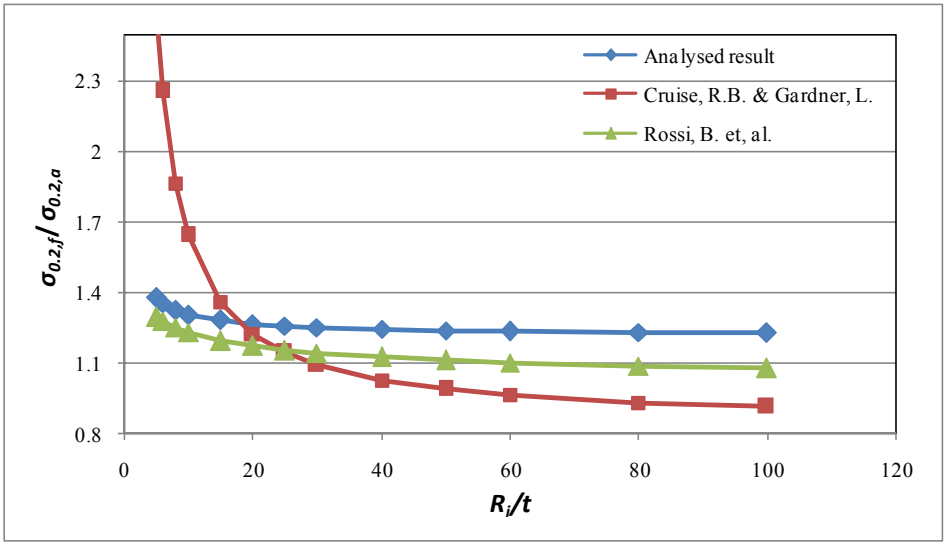

Figure 4.20: Variation of increased strength at flat faces against R_i/t ratio due to cold bending (duplex steel).

4.3. COMPILATION OF DATA

4.3.1. For Increased Corner Strength

The ratio of increased 0.2% proof strength at corner to the 0.2% proof strength of the annealed material is ($\sigma_{0.2,c}/\sigma_{0.2,a}$) from the analysis is compared to the previous model in Tab. 4.9- 4.12 for four steel types in separate tables. The comparison is done by dividing the analytical result with the previous model data and taking the mean variation and standard deviation of the compared values.

For austenitic steel it is seen that the Rossi, B. et, al. (2013) model gives the result with less mean value and the standard deviation (SD). The other models also satisfy the result but the mean value and the SD value is greater and the mean variation value is 17 to 23 percent except the Rossi, B. et, al. (2013) result of mean variation 7 percent.

In case of ferritic steel though the mean variation value is less in case of other model than the Rossi, B. et al. (2013) model, it is seen that the result for lower ratio of r_i/t, the

analytical result shows lower values compared to the previous model. Only the Rossi, B. et al. (2013) are conventional to the analysed result and the SD value is the less than the others. But one thing is said that most of the test result is taken from the ferritic steel, so the previous models data is close enough to the analytical result.

For the other two types of steel named lean-duplex and duplex, for the whole range of r_i/t value only the Rossi, B. et, al. (2013) give the satisfactory result with SD value for both steel is lower than other model. Also the mean variation values are 4% for lean-duplex and 10% for duplex steel.

So, it is said that the Rossi, B. et, al. (2013) model fits for all types of stainless steel to predict the 0.2 % proof strength at corner due to cold bending with a good factor of safety to the designers for all ranges of bending radius of corner.

Table4.9: Comparison of obtained analytical results with the previous proposed models for austenitic steel.

r_i/t	$\sigma_{0.2,c}/\ \sigma_{0.2,a}$						Analytical result/Van den Berg, G.J. and Van der Merwe, P.	Analytical result/Ashraf, M. et al.-1	Analytical result/Ashraf, M. et, al.-2	Analytical result/Cruise, R.B. and Gardner, L.	Analytical result/Rossi, B. et, al.
	Analytical result	Van den Berg, G.J. and Van der Merwe, P.	Ashraf, M. et al.-1	Ashraf, M. et, al.-2	Cruise, R.B. and Gardner, L.	Rossi, B. et, al .					
0.5	2.18	1.85	2.15	2.29	1.83	2.06	1.18	1.01	0.95	1.20	1.06
1.0	2.10	1.64	1.88	1.91	1.67	1.93	1.28	1.12	1.10	1.26	1.09
1.5	2.02	1.53	1.74	1.72	1.59	1.84	1.32	1.16	1.17	1.27	1.09
2.0	1.94	1.46	1.64	1.59	1.53	1.78	1.33	1.18	1.21	1.26	1.09
2.5	1.86	1.40	1.57	1.50	1.49	1.72	1.33	1.18	1.24	1.25	1.08
3.0	1.80	1.36	1.52	1.43	1.46	1.68	1.33	1.19	1.26	1.24	1.07
3.5	1.76	1.32	1.48	1.38	1.43	1.65	1.33	1.20	1.28	1.23	1.07
4.0	1.72	1.29	1.44	1.33	1.40	1.62	1.33	1.20	1.29	1.22	1.06
4.5	1.69	1.27	1.40	1.29	1.38	1.59	1.34	1.21	1.31	1.22	1.07
5.0	1.66	1.24	1.38	1.25	1.37	1.57	1.33	1.21	1.32	1.22	1.06
6.0	1.63	1.21	1.33	1.19	1.33	1.53	1.35	1.22	1.36	1.22	1.07
7.0	1.59	1.17	1.29	1.15	1.31	1.49	1.35	1.23	1.38	1.21	1.06
					Mean		**1.32**	**1.17**	**1.24**	**1.23**	**1.07**
SD = standard deviation					**SD**		**0.05**	**0.06**	**0.12**	**0.02**	**0.01**

Table 4.10: Comparison of obtained analytical results with the previous proposed models for ferritic steel.

r_i/t	$\sigma_{0.2,c}/\ \sigma_{0.2,a}$						Analytical result/Van den Berg, G.J. and Van der Merwe, P.	Analytical result/Ashraf, M. et al.-1	Analytical result/Ashraf, M. et, al.-2	Analytical result/Cruise, R.B. and Gardner, L.	Analytical result/Rossi, B. et, al.
	Analytical result	Van den Berg, G.J. and Van der Merwe, P.	Ashraf, M. et al.-1	Ashraf, M. et, al.-2	Cruise, R.B. and Gardner, L.	Rossi, B. et, al .					
0.5	1.78	1.80	2.15	1.85	1.83	1.55	0.99	0.82	0.96	0.97	1.14
1.0	1.74	1.66	1.88	1.71	1.67	1.49	1.05	0.93	1.02	1.04	1.17
1.5	1.72	1.58	1.74	1.63	1.59	1.45	1.09	0.99	1.06	1.08	1.19
2.0	1.69	1.52	1.64	1.58	1.53	1.41	1.11	1.03	1.07	1.10	1.19
2.5	1.66	1.48	1.57	1.54	1.49	1.39	1.12	1.06	1.08	1.12	1.20
3.0	1.63	1.45	1.52	1.51	1.46	1.37	1.13	1.07	1.08	1.12	1.19
3.5	1.61	1.42	1.48	1.48	1.43	1.35	1.13	1.09	1.09	1.13	1.19
4.0	1.58	1.40	1.44	1.46	1.40	1.34	1.13	1.10	1.08	1.12	1.18
4.5	1.55	1.38	1.40	1.44	1.38	1.32	1.13	1.11	1.08	1.12	1.18
5.0	1.54	1.36	1.38	1.42	1.37	1.31	1.13	1.12	1.08	1.12	1.17
6.0	1.49	1.33	1.33	1.39	1.33	1.29	1.12	1.12	1.07	1.12	1.16
7.0	1.46	1.31	1.29	1.37	1.31	1.27	1.11	1.13	1.07	1.11	1.14
					Mean		**1.10**	**1.05**	**1.06**	**1.10**	**1.18**
					SD		**0.04**	**0.09**	**0.04**	**0.05**	**0.02**

Table4.11: Comparison of obtained analytical results with the previous proposed models for lean-duplex steel.

r_i/t	$\sigma_{0.2,c}/\ \sigma_{0.2,a}$						Howlader,M. /Van den Berg, G.J. and Van der Merwe, P.	Howlader,M ./Ashraf, M. et al.-1	Howlader, M./Ashraf, M. et, al.-2	Howlader, M./Cruise, R.B. and Gardner, L.	Howlader, M./Rossi, B. et, al.
	Howlader, M	Van den Berg, G.J. and Van der Merwe, P.	Ashraf, M. et al.-1	Ashraf, M. et, al.-2	Cruise, R.B. and Gardner, L.	Rossi, B. et, al .					
0.5	1.37	1.71	2.15	1.76	1.83	1.41	0.80	0.64	0.78	0.75	0.97
1.0	1.36	1.58	1.88	1.65	1.67	1.36	0.87	0.73	0.83	0.82	1.00
1.5	1.36	1.51	1.74	1.58	1.59	1.33	0.90	0.78	0.86	0.85	1.02
2.0	1.35	1.46	1.64	1.54	1.53	1.31	0.93	0.82	0.88	0.88	1.03
2.5	1.34	1.42	1.57	1.51	1.49	1.29	0.95	0.85	0.89	0.90	1.04
3.0	1.34	1.39	1.52	1.48	1.46	1.27	0.96	0.88	0.90	0.92	1.05
3.5	1.33	1.37	1.48	1.46	1.43	1.26	0.98	0.90	0.91	0.93	1.06
4.0	1.32	1.34	1.44	1.44	1.40	1.25	0.99	0.92	0.92	0.94	1.06
4.5	1.32	1.33	1.40	1.42	1.38	1.24	0.99	0.94	0.93	0.95	1.07
5.0	1.31	1.31	1.38	1.41	1.37	1.23	1.00	0.95	0.93	0.96	1.07
6.0	1.30	1.28	1.33	1.38	1.33	1.21	1.01	0.98	0.94	0.97	1.08
7.0	1.29	1.26	1.29	1.36	1.31	1.20	1.03	1.00	0.95	0.99	1.08
					Mean COV		**0.95**	**0.87**	**0.89**	**0.91**	**1.04**
						SD	**0.07**	**0.11**	**0.05**	**0.07**	**0.03**

Table4.12: Comparison of obtained analytical results with the previous proposed models for duplex steel.

r_i/t	$\sigma_{0.2,c}/\sigma_{0.2,a}$						Analytical result/Van den Berg, G.J. and Van der Merwe, P.	Analytical result/Ashraf, M. et al.-1	Analytical result/Ashraf, M. et, al.-2	Analytical result/Cruise, R.B. and Gardner, L.	Analytical result/Rossi, B. et, al.
	Analytical result	Van den Berg, G.J. and Van der Merwe, P.	Ashraf, M. et al.-1	Ashraf, M. et, al.-2	Cruise, R.B. and Gardner, L.	Rossi, B. et, al .					
0.5	1.46	1.69	2.15	1.74	1.83	1.40	0.87	0.68	0.84	0.80	1.05
1.0	1.45	1.56	1.88	1.63	1.67	1.35	0.93	0.77	0.89	0.86	1.07
1.5	1.43	1.49	1.74	1.57	1.59	1.32	0.96	0.83	0.91	0.90	1.09
2.0	1.43	1.44	1.64	1.53	1.53	1.29	0.99	0.87	0.93	0.93	1.10
2.5	1.41	1.40	1.57	1.50	1.49	1.28	1.01	0.90	0.94	0.95	1.11
3.0	1.40	1.38	1.52	1.47	1.46	1.26	1.02	0.92	0.95	0.96	1.11
3.5	1.39	1.35	1.48	1.45	1.43	1.25	1.03	0.94	0.96	0.97	1.11
4.0	1.38	1.33	1.44	1.43	1.40	1.24	1.04	0.96	0.96	0.98	1.12
4.5	1.37	1.31	1.40	1.42	1.38	1.23	1.04	0.97	0.96	0.99	1.12
5.0	1.36	1.30	1.38	1.40	1.37	1.22	1.05	0.99	0.97	0.99	1.12
6.0	1.34	1.27	1.33	1.38	1.33	1.20	1.05	1.01	0.97	1.00	1.12
7.0	1.33	1.25	1.29	1.36	1.31	1.19	1.06	1.03	0.97	1.01	1.11
					Mean		**1.00**	**0.91**	**0.94**	**0.95**	**1.10**
					SD		**0.06**	**0.10**	**0.04**	**0.06**	**0.02**

4.3.2. For Increased Flat Faces Strength

From the analysis, it is shown that the Cruise, R. B. and Gardner, L. (2008) model for predicting the increased strength at the fat faces due to cold rolling for $R_i/t > 50$ represent unexpected result where the value of $\sigma_{0.2,f}/\sigma_{0.2,a}$ is less than 1.0. Also this value is larger for R_i/t <10. They have predicted the model by using the test result of certain dimension of square and rectangular sections (100×50×2, 100×100×2, 100×50×3, 100×100×3, 100×50×4, 100×100×4, 150×150×3), where the R_i/t ranges from 11.25 to 31.2. The Rossi, B. et, al. (2013) results are in good agreements with the analysed results with good mean variation value ≤ 9% for all types of stainless steel. The ratio of increased 0.2% proof strength at flat faces to the 0.2% proof strength of the annealed material is ($\sigma_{0.2,f}/\sigma_{0.2,a}$) from the analysis is compared to the previous models in Tab. 4.13- 4.16 for four steel types in separate tables.

Table 4.13: Comparison of obtained analytical results with the previous proposed models for austenitic steel.

R_i/t	$\sigma_{0.2,f}/\sigma_{0.2,a}$			Analytical result/Cruise, R.B. and Gardner, L.	Analytical result/Rossi, B. et, al.
	Analytical result	Cruise, R.B. and Gardner, L.	Rossi, B. et, al .		
5.0	1.92	2.59	1.78	0.74	1.08
6.0	1.85	2.26	1.73	0.82	1.07
8.0	1.73	1.87	1.66	0.93	1.04
10.0	1.66	1.64	1.60	1.01	1.04
15.0	1.57	1.36	1.51	1.15	1.04
20.0	1.51	1.22	1.45	1.24	1.05
25.0	1.49	1.14	1.41	1.30	1.06
30.0	1.47	1.09	1.37	1.35	1.07
40.0	1.43	1.03	1.33	1.39	1.08
50.0	1.42	0.99	1.29	1.44	1.10
60.0	1.41	0.96	1.27	1.46	1.11
80.0	1.40	0.93	1.23	1.50	1.13
100.0	1.40	0.91	1.21	1.53	1.15
			Mean	**1.22**	**1.08**
			SD	**0.27**	**0.04**

Table 4.14: Comparison of obtained analytical results with the previous proposed models for ferritic steel.

R_i/t	$\sigma_{0.2,f}/\sigma_{0.2,a}$			Analytical result/Cruise, R.B. and Gardner, L.	Analytical result/Rossi, B. et, al.
	Analytical result	Cruise, R.B. and Gardner, L.	Rossi, B. et, al .		
5.0	1.55	2.90	1.42	0.53	1.09
6.0	1.50	2.45	1.39	0.61	1.08
8.0	1.44	1.96	1.36	0.73	1.06
10.0	1.39	1.70	1.33	0.82	1.05
15.0	1.33	1.38	1.28	0.96	1.04
20.0	1.29	1.24	1.25	1.05	1.04
25.0	1.27	1.15	1.23	1.11	1.04
30.0	1.26	1.10	1.21	1.15	1.04
40.0	1.24	1.03	1.18	1.20	1.05
50.0	1.23	0.99	1.16	1.24	1.06
60.0	1.22	0.96	1.15	1.27	1.06
80.0	1.21	0.93	1.13	1.30	1.07
100.0	1.20	0.91	1.12	1.32	1.07
			Mean	**1.02**	**1.06**
			SD	**0.27**	**0.02**

Table 4.15: Comparison of obtained analytical results with the previous proposed methods for lean-duplex steel.

R_i/t	$\sigma_{0.2,f}/\sigma_{0.2,a}$			Analytical result/Cruise, R.B. and Gardner, L.	Analytical result/Rossi, B. et, al.
	Analytical result	Cruise, R.B. and Gardner, L.	Rossi, B. et, al .		
5.0	1.33	2.59	1.31	0.51	1.01
6.0	1.31	2.26	1.29	0.58	1.02
8.0	1.30	1.87	1.26	0.70	1.03
10.0	1.29	1.64	1.24	0.78	1.04
15.0	1.27	1.36	1.20	0.94	1.06
20.0	1.27	1.22	1.18	1.03	1.07
25.0	1.26	1.14	1.16	1.10	1.09
30.0	1.26	1.09	1.15	1.15	1.10
40.0	1.26	1.03	1.13	1.22	1.11
50.0	1.25	0.99	1.12	1.27	1.12
60.0	1.25	0.96	1.11	1.30	1.13
80.0	1.25	0.93	1.09	1.34	1.14
100.0	1.25	0.91	1.08	1.36	1.15
			Mean	**1.02**	**1.08**
			SD	**0.29**	**0.05**

Table 4.16: Comparison of obtained analytical results with the previous proposed models for duplex steel.

R_i/t	$\sigma_{0.2,f}/\sigma_{0.2,a}$			Analytical result/Cruise, R.B. and Gardner, L.	Analytical result/Rossi, B. et, al.
	Analytical result	Cruise, R.B. and Gardner, L.	Rossi, B. et, al .		
5.0	1.38	2.59	1.30	0.53	1.06
6.0	1.35	2.26	1.28	0.60	1.06
8.0	1.32	1.86	1.25	0.71	1.06
10.0	1.30	1.64	1.23	0.79	1.06
15.0	1.28	1.36	1.19	0.94	1.07
20.0	1.26	1.22	1.17	1.03	1.08
25.0	1.26	1.14	1.15	1.10	1.09
30.0	1.25	1.09	1.14	1.15	1.10
40.0	1.24	1.03	1.12	1.21	1.11
50.0	1.24	0.99	1.11	1.25	1.11
60.0	1.23	0.96	1.10	1.28	1.12
80.0	1.23	0.93	1.09	1.32	1.13
100.0	1.23	0.91	1.08	1.35	1.14
			Mean	**1.02**	**1.09**
			SD	**0.28**	**0.03**

4.3.3 Proposed Modification of Rossi, B. et, al. (2013) Model

The power law model of Rossi, B. et, al. (2013) is modified form the analysed result of four different stainless steel type to determine the increase of 0.2% proof strength at corner and flat face of the section. Here, the strain for 1% proof strength ($\varepsilon_{1.0}$) is considered also.

$$\sigma_{0.2,c/0.2,f}=p\varepsilon^{(q\text{-}\varepsilon_{0.2})}$$

$$p=\frac{\sigma_{0.2,a}}{(\varepsilon_{0.2})^{q}}$$

$$q=\frac{\ln(\sigma_{0.2,a}/\sigma_{u,a})}{\ln(\varepsilon_{0.2}/\varepsilon_{u})}+\varepsilon_{1.0}$$

in which,

$$\varepsilon=\varepsilon_{c,av/f,av}+\varepsilon_{0.2}$$

$$\varepsilon_{c,av}=0.5[(t/2)/R_c]$$

$$R_c=r_i+t/2$$

$$\varepsilon_{f,av}=[(t/2)/R_{coiling}]+[(t/2)/R_f]$$

$$R_f=(b+h-2t)/\pi$$

Where,

$\sigma_{0.2,c}$ /$\sigma_{0.2,f}$ is the increased 0.2% proof stress at corner or flat faces.

$\varepsilon_{c,av}$ /$_{f,av}$ is average plastic strain through thickness at the corner or flat faces of the section.

$\sigma_{0.2,a}$ is the 0.2% proof stress for annealed material.

$\sigma_{u,a}$ is the ultimate strength of the annealed material.

r_i is the internal bending radius at corner.

R_f is the internal circle radius before making the square or rectangular hollow section due to cold rolling.

b and *h* are the width and height of the section.

t is the thickness of the section.

The new proposed model by modifying the Rossi, B. et, al. (2013) is compared to the result for increased 0.2% proof strength in case of both corner and flat faces of the sections in Tab. 4.17 -4.24. The new proposed model reduces the variation with the analysed result and also safe with respect to the analysed result for all stainless steel grades.

Table 4.17: Comparison of obtained analytical results with the previous and new proposed models for austenitic steel.

r_i/t	$\sigma_{0.2,c}/\ \sigma_{0.2,a}$							Analytical result/Van den Berg, G.J. and Van der Merwe, P.	Analytical result/Ashraf, M. et al.-1	Analytical result/Ashraf, M. et, al.-2	Analytical result/Cruise, R.B. and Gardner, L.	Analytical result/Rossi, B. et, al.	Analytical result/ Modified Rossi, B. et, al.
	Analytical result	Van den Berg, G.J. and Van der Merwe, P.	Ashraf, M. et al.-1	Ashraf, M. et, al.-2	Cruise, R.B. and Gardner, L.	Rossi, B. et, al .	Modified Rossi, B. et,al.						
0.5	2.18	1.85	2.15	2.29	1.83	2.06	2.18	1.18	1.01	0.95	1.20	1.06	1.00
1.0	2.10	1.64	1.88	1.91	1.67	1.93	2.03	1.28	1.12	1.10	1.26	1.09	1.03
1.5	2.02	1.53	1.74	1.72	1.59	1.84	1.94	1.32	1.16	1.17	1.27	1.09	1.04
2.0	1.94	1.46	1.64	1.59	1.53	1.78	1.86	1.33	1.18	1.21	1.26	1.09	1.04
2.5	1.86	1.40	1.57	1.50	1.49	1.72	1.81	1.33	1.18	1.24	1.25	1.08	1.03
3.0	1.80	1.36	1.52	1.43	1.46	1.68	1.76	1.33	1.19	1.26	1.24	1.07	1.02
3.5	1.76	1.32	1.48	1.38	1.43	1.65	1.72	1.33	1.20	1.28	1.23	1.07	1.03
4.0	1.72	1.29	1.44	1.33	1.40	1.62	1.69	1.33	1.20	1.29	1.22	1.06	1.02
4.5	1.69	1.27	1.40	1.29	1.38	1.59	1.66	1.34	1.21	1.31	1.22	1.07	1.02
5.0	1.66	1.24	1.38	1.25	1.37	1.57	1.63	1.33	1.21	1.32	1.22	1.06	1.02
6.0	1.63	1.21	1.33	1.19	1.33	1.53	1.59	1.35	1.22	1.36	1.22	1.07	1.02
7.0	1.59	1.17	1.29	1.15	1.31	1.49	1.55	1.35	1.23	1.38	1.21	1.06	1.02
					Mean			**1.32**	**1.17**	**1.24**	**1.23**	**1.07**	**1.02**
					SD			**0.05**	**0.06**	**0.12**	**0.02**	**0.01**	**0.01**

Table 4.18: Comparison of obtained analytical results with the previous and new proposed models for ferritic steel.

r_i/t	$\sigma_{0.2,c}/\sigma_{0.2,a}$							Analytical result/Van den Berg, G.J. and Van der Merwe, P.	Analytical result/Ashraf, M. et al.-1	Analytical result/Ashraf, M. et, al.-2	Analytical result/Cruise, R.B. and Gardner, L.	Analytical result/Rossi, B. et, al.	Analytical result/ Modified Rossi, B. et, al.
	Analytical result	Van den Berg, G.J. and Van der Merwe, P.	Ashraf, M. et al.-1	Ashraf, M. et, al.-2	Cruise, R.B. and Gardner, L.	Rossi, B. et, al .	Modified Rossi, B. et,al.						
0.5	1.78	1.80	2.15	1.85	1.83	1.55	1.64	0.99	0.82	0.96	0.97	1.14	1.08
1.0	1.74	1.66	1.88	1.71	1.67	1.49	1.57	1.05	0.93	1.02	1.04	1.17	1.11
1.5	1.72	1.58	1.74	1.63	1.59	1.45	1.52	1.09	0.99	1.06	1.08	1.19	1.13
2.0	1.69	1.52	1.64	1.58	1.53	1.41	1.48	1.11	1.03	1.07	1.10	1.19	1.14
2.5	1.66	1.48	1.57	1.54	1.49	1.39	1.46	1.12	1.06	1.08	1.12	1.20	1.14
3.0	1.63	1.45	1.52	1.51	1.46	1.37	1.43	1.13	1.07	1.08	1.12	1.19	1.14
3.5	1.61	1.42	1.48	1.48	1.43	1.35	1.41	1.13	1.09	1.09	1.13	1.19	1.14
4.0	1.58	1.40	1.44	1.46	1.40	1.34	1.39	1.13	1.10	1.08	1.12	1.18	1.13
4.5	1.55	1.38	1.40	1.44	1.38	1.32	1.38	1.13	1.11	1.08	1.12	1.18	1.13
5.0	1.54	1.36	1.38	1.42	1.37	1.31	1.37	1.13	1.12	1.08	1.12	1.17	1.13
6.0	1.49	1.33	1.33	1.39	1.33	1.29	1.34	1.12	1.12	1.07	1.12	1.16	1.11
7.0	1.46	1.31	1.29	1.37	1.31	1.27	1.32	1.11	1.13	1.07	1.11	1.14	1.10
					Mean			**1.10**	**1.05**	**1.06**	**1.10**	**1.18**	**1.12**
					SD			**0.04**	**0.09**	**0.04**	**0.05**	**0.02**	**0.02**

Table 4.19: Comparison of obtained analytical results with the previous and new proposed models for lean-duplex steel.

r_i/t	$\sigma_{0.2,c}/\sigma_{0.2,a}$							Analytical result/Van den Berg, G.J. and Van der Merwe, P.	Analytical result/Ashraf, M. et al.-1	Analytical result/Ashraf, M. et, al.-2	Analytical result/Cruise, R.B. and Gardner, L.	Analytical result/Rossi, B. et, al.	Analytical result/ Modified Rossi, B. et, al.
	Analytical result	Van den Berg, G.J. and Van der Merwe, P.	Ashraf, M. et al.-1	Ashraf, M. et, al.-2	Cruise, R.B. and Gardner, L.	Rossi, B. et, al .	Modified Rossi, B. et,al.						
0.5	1.37	1.71	2.15	1.76	1.83	1.41	1.50	0.80	0.64	0.78	0.75	0.97	0.92
1.0	1.36	1.58	1.88	1.65	1.67	1.36	1.44	0.87	0.73	0.83	0.82	1.00	0.95
1.5	1.36	1.51	1.74	1.58	1.59	1.33	1.41	0.90	0.78	0.86	0.85	1.02	0.97
2.0	1.35	1.46	1.64	1.54	1.53	1.31	1.38	0.93	0.82	0.88	0.88	1.03	0.98
2.5	1.34	1.42	1.57	1.51	1.49	1.29	1.35	0.95	0.85	0.89	0.90	1.04	0.99
3.0	1.34	1.39	1.52	1.48	1.46	1.27	1.34	0.96	0.88	0.90	0.92	1.05	1.00
3.5	1.33	1.37	1.48	1.46	1.43	1.26	1.32	0.98	0.90	0.91	0.93	1.06	1.01
4.0	1.32	1.34	1.44	1.44	1.40	1.25	1.31	0.99	0.92	0.92	0.94	1.06	1.01
4.5	1.32	1.33	1.40	1.42	1.38	1.24	1.29	0.99	0.94	0.93	0.95	1.07	1.02
5.0	1.31	1.31	1.38	1.41	1.37	1.23	1.28	1.00	0.95	0.93	0.96	1.07	1.02
6.0	1.30	1.28	1.33	1.38	1.33	1.21	1.27	1.01	0.98	0.94	0.97	1.08	1.03
7.0	1.29	1.26	1.29	1.36	1.31	1.20	1.25	1.03	1.00	0.95	0.99	1.08	1.04
					Mean			**0.95**	**0.87**	**0.89**	**0.91**	**1.04**	**0.99**
					SD			**0.07**	**0.11**	**0.05**	**0.07**	**0.03**	**0.04**

Table 4.20: Comparison of obtained analytical results with the previous and new proposed models for duplex steel.

r_i/t	$\sigma_{0.2,c}/\ \sigma_{0.2,a}$							Analytical result/Van den Berg, G.J. and Van der Merwe, P.	Analytical result/Ashraf, M. et al.-1	Analytical result/Ashraf, M. et, al.-2	Analytical result/Cruise, R.B. and Gardner, L.	Analytical result/Rossi, B. et, al.	Analytical result/ Modified Rossi, B. et, al.
	Analytical result	Van den Berg, G.J. and Van der Merwe, P.	Ashraf, M. et al.-1	Ashraf, M. et, al.-2	Cruise, R.B. and Gardner, L.	Rossi, B. et, al.	Modified Rossi, B. et,al.						
0.5	1.46	1.69	2.15	1.74	1.83	1.40	1.49	0.87	0.68	0.84	0.80	1.05	0.98
1.0	1.45	1.56	1.88	1.63	1.67	1.35	1.44	0.93	0.77	0.89	0.86	1.07	1.01
1.5	1.43	1.49	1.74	1.57	1.59	1.32	1.40	0.96	0.83	0.91	0.90	1.09	1.03
2.0	1.43	1.44	1.64	1.53	1.53	1.29	1.37	0.99	0.87	0.93	0.93	1.10	1.04
2.5	1.41	1.40	1.57	1.50	1.49	1.28	1.35	1.01	0.90	0.94	0.95	1.11	1.05
3.0	1.40	1.38	1.52	1.47	1.46	1.26	1.33	1.02	0.92	0.95	0.96	1.11	1.05
3.5	1.39	1.35	1.48	1.45	1.43	1.25	1.31	1.03	0.94	0.96	0.97	1.11	1.06
4.0	1.38	1.33	1.44	1.43	1.40	1.24	1.30	1.04	0.96	0.96	0.98	1.12	1.06
4.5	1.37	1.31	1.40	1.42	1.38	1.23	1.29	1.04	0.97	0.96	0.99	1.12	1.06
5.0	1.36	1.30	1.38	1.40	1.37	1.22	1.28	1.05	0.99	0.97	0.99	1.12	1.06
6.0	1.34	1.27	1.33	1.38	1.33	1.20	1.26	1.05	1.01	0.97	1.00	1.12	1.06
7.0	1.33	1.25	1.29	1.36	1.31	1.19	1.25	1.06	1.03	0.97	1.01	1.11	1.06
					Mean			**1.00**	**0.91**	**0.94**	**0.95**	**1.10**	**1.04**
					SD			**0.06**	**0.10**	**0.04**	**0.06**	**0.02**	**0.03**

Table 4.21: Comparison of obtained analytical results with the previous and new proposed models for austenitic steel.

R_i/t	$\sigma_{0.2,f}/\sigma_{0.2,a}$				Analytical result/Cruise, R.B. and Gardner, L.	Analytical result/Rossi, B. et, al.	Analytical result/ Modified Rossi, B. et, al.
	Analytical result	Cruise, R.B. and Gardner, L.	Rossi, B. et, al .	Modified Rossi, B. et, al.			
5.0	1.92	2.59	1.78	1.87	0.74	1.08	1.03
6.0	1.85	2.26	1.73	1.81	0.82	1.07	1.02
8.0	1.73	1.87	1.66	1.73	0.93	1.04	1.00
10.0	1.66	1.64	1.60	1.67	1.01	1.04	1.00
15.0	1.57	1.36	1.51	1.57	1.15	1.04	1.00
20.0	1.51	1.22	1.45	1.50	1.24	1.05	1.01
25.0	1.49	1.14	1.41	1.46	1.30	1.06	1.02
30.0	1.47	1.09	1.37	1.42	1.35	1.07	1.03
40.0	1.43	1.03	1.33	1.37	1.39	1.08	1.04
50.0	1.42	0.99	1.29	1.34	1.44	1.10	1.06
60.0	1.41	0.96	1.27	1.31	1.46	1.11	1.08
80.0	1.40	0.93	1.23	1.27	1.50	1.13	1.10
100.0	1.40	0.91	1.21	1.25	1.53	1.15	1.12
			Mean		**1.22**	**1.08**	**1.04**
			SD		**0.27**	**0.04**	**0.04**

Table 4.22: Comparison of obtained analytical results with the previous and new proposed models for ferritic steel.

R_i/t	$\sigma_{0.2,f}/\sigma_{0.2,a}$				Analytical result/Cruise, R.B. and Gardner, L.	Analytical result/Rossi, B. et, al.	Analytical result/ Modified Rossi, B. et, al.
	Analytical result	Cruise, R.B. and Gardner, L.	Rossi, B. et, al .	Modified Rossi, B. et, al.			
5.0	1.55	2.90	1.42	1.49	0.53	1.09	1.04
6.0	1.50	2.45	1.39	1.46	0.61	1.08	1.03
8.0	1.44	1.96	1.36	1.42	0.73	1.06	1.01
10.0	1.39	1.70	1.33	1.39	0.82	1.05	1.00
15.0	1.33	1.38	1.28	1.33	0.96	1.04	1.00
20.0	1.29	1.24	1.25	1.30	1.05	1.04	1.00
25.0	1.27	1.15	1.23	1.27	1.11	1.04	1.00
30.0	1.26	1.10	1.21	1.25	1.15	1.04	1.01
40.0	1.24	1.03	1.18	1.22	1.20	1.05	1.01
50.0	1.23	0.99	1.16	1.20	1.24	1.06	1.02
60.0	1.22	0.96	1.15	1.19	1.27	1.06	1.03
80.0	1.21	0.93	1.13	1.17	1.30	1.07	1.03
100.0	1.20	0.91	1.12	1.15	1.32	1.07	1.04
			Mean		**1.02**	**1.06**	**1.02**
			SD		**0.27**	**0.02**	**0.02**

Table4.23: Comparison of obtained analytical results with the previous and new proposed models for lean-duplex steel.

R_i/t	$\sigma_{0.2,f}/\sigma_{0.2,a}$				Analytical result/Cruise, R.B. and Gardner, L.	Analytical result/Rossi, B. et, al.	Analytical result/ Modified Rossi, B. et, al.
	Analytical result	Cruise, R.B. and Gardner, L.	Rossi, B. et, al .	Modified Rossi, B. et, al.			
5.0	1.33	2.59	1.31	1.38	0.51	1.01	0.96
6.0	1.31	2.26	1.29	1.36	0.58	1.02	0.97
8.0	1.30	1.87	1.26	1.32	0.70	1.03	0.98
10.0	1.29	1.64	1.24	1.30	0.78	1.04	0.99
15.0	1.27	1.36	1.20	1.26	0.94	1.06	1.01
20.0	1.27	1.22	1.18	1.23	1.03	1.07	1.03
25.0	1.26	1.14	1.16	1.21	1.10	1.09	1.04
30.0	1.26	1.09	1.15	1.19	1.15	1.10	1.05
40.0	1.26	1.03	1.13	1.17	1.22	1.11	1.07
50.0	1.25	0.99	1.12	1.16	1.27	1.12	1.08
60.0	1.25	0.96	1.11	1.15	1.30	1.13	1.09
80.0	1.25	0.93	1.09	1.13	1.34	1.14	1.10
100.0	1.25	0.91	1.08	1.12	1.36	1.15	1.11
			Mean		**1.02**	**1.08**	**1.04**
			SD		**0.29**	**0.05**	**0.05**

Table 4.24: Comparison of obtained analytical results with the previous and new proposed models for duplex steel.

R_i/t	$\sigma_{0.2,f}/\sigma_{0.2,a}$				Analytical result/Cruise, R.B. and Gardner, L.	Analytical result/Rossi, B. et, al.	Analytical result/ Modified Rossi, B. et, al.
	Analytical result	Cruise, R.B. and Gardner, L.	Rossi, B. et, al .	Modified Rossi, B. et, al.			
5.0	1.38	2.59	1.30	1.37	0.53	1.06	1.00
6.0	1.35	2.26	1.28	1.35	0.60	1.06	1.00
8.0	1.32	1.86	1.25	1.32	0.71	1.06	1.00
10.0	1.30	1.64	1.23	1.29	0.79	1.06	1.01
15.0	1.28	1.36	1.19	1.25	0.94	1.07	1.02
20.0	1.26	1.22	1.17	1.23	1.03	1.08	1.03
25.0	1.26	1.14	1.15	1.21	1.10	1.09	1.04
30.0	1.25	1.09	1.14	1.19	1.15	1.10	1.05
40.0	1.24	1.03	1.12	1.17	1.21	1.11	1.06
50.0	1.24	0.99	1.11	1.15	1.25	1.11	1.07
60.0	1.23	0.96	1.10	1.14	1.28	1.12	1.08
80.0	1.23	0.93	1.09	1.13	1.32	1.13	1.09
100.0	1.23	0.91	1.08	1.12	1.35	1.14	1.10
			Mean		**1.02**	**1.09**	**1.04**
			SD		**0.28**	**0.03**	**0.04**

4.3.4 Comparison of Corner Strength with the Ultimate Strength of Annealed Material

Rasmussen, K. J. R. and Hancock, G. J. (1993), Ashraf, M. et al. (2005) and Cruise, R.B. and Gardner, L. (2008) have given linear relationship 0.2% proof strength $\sigma_{0.2,c}$ of the formed corners and the ultimate strength $\sigma_{u,f}$ of the flat faces only is case of cold rolled section. As there is not so much changes of the ultimate strength at lower induced plastic strain from the ultimate strength of the annealed material, the increased corner strength, $\sigma_{0.2,c}$ is compared with the ultimate strength of the annealed material, $\sigma_{u,a}$ for all type of steel grades. For graphical representation, the bending radius to thickness ratio (r_i/t) is taken 1.5 as most of the test which is previously done with this ratio.

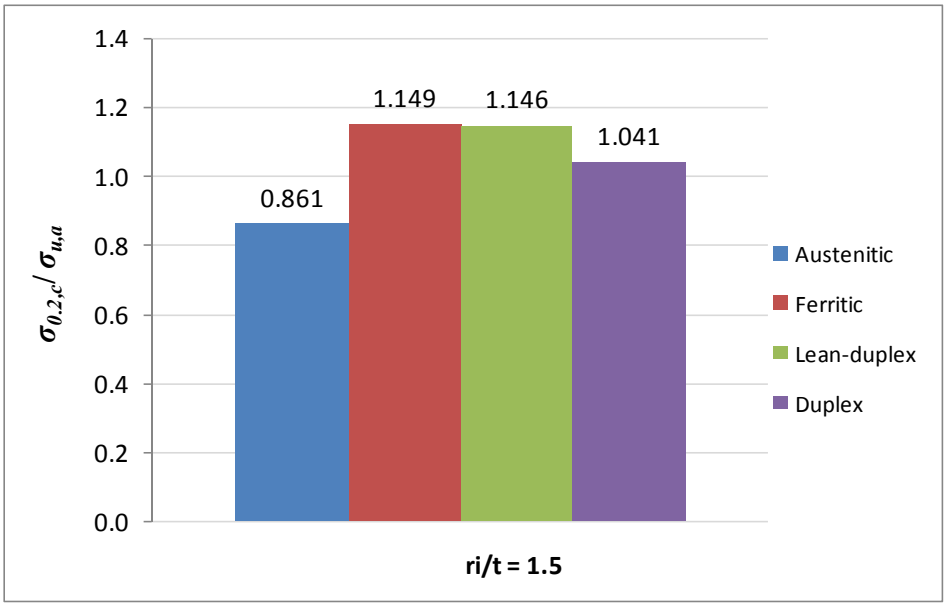

Figure 4.21: Relationship between the $\sigma_{u,a}$ and $\sigma_{0.2,c}$ for commonly used r_i/t ratio 1.5.

The value of $\sigma_{0.2,c}/\ \sigma_{u,a}$ is grater than 1.0 because $\sigma_{u,a}$ value is taken as engineering ultimate strength from the tensile coupon test which differs from the true ultimate strength.

The latest relationship of Cruise, R. B. and Gardner, L. (2008) from the modification of previous model is that the increased corner strength is 0.83 times the ultimate strength of the flat faces. The analytical result presented in the fig. 4.21 shows the conservative result with the latest model though the exact value of the ultimate strength of the flat faces is

unknown here. So it is said that the analytical result is valid for this simple relationship between 0.2% proof strength $\sigma_{0.2,c}$ of the formed corners and the ultimate strength $\sigma_{u,f}$ of the flat faces for cold rolled sections.

4.4. INCREASED YIELD STRENGTH FOR THE WHOLE SECTION

For determining the strength enhancement of the whole section ($\sigma_{0.2,section}$) a cold rolled square box hollow section of SHS 80×80×4 is taken. Here, the mostly used bending radius to thickness ratio (r_i/t) equal to 1.5 is used for calculation.

Rossi, B. et, al's (2013) expression for the increase of 0.2% proof strength of the cross-section according to the Cruise, R.B. and Gardner, L. (2008) confined zone of enhanced corner strength for cold-rolled section is used. For cold rolled box section the enhanced corner strength is extended by 2t into the flat faces. Hence by multiplying the increased strength with the confined zone for corner and flat faces and averaging those with respect to the cross -section the average increase of the strength is calculated which is expressed in Eq. 1.40 in the literature review.

The area of the corner zone,

$$A_{c,rolled} = A_c + 4n_c t^2$$
$$= (n_c \pi t/4)(2r_i + t) + 4n_c t^2$$
$$= (4*3.14*4/4)(2*1.5+4)+4*4*4^2$$
$$= 343.92 \text{ mm}^2$$

The area of the flat faces,

$$A_{f,rolled} = A - A_{c,rolled}$$
$$= \{2(80+72)*4\}-343.92$$
$$= 872.08 \text{ mm}^2$$

The internal circle radius $R_i = (b+h-2t)/\pi = 48.4$,

Hence, $R_i/t = 48.4/4 = 12.1$, taking the increase strength value $R_i/t = 15$ for safety.

Hence, the yield strength increase for the whole section is calculated by using eq. 1.40 for four types of steel grades from the value of $\sigma_{0.2,c}$ and $\sigma_{0.2,f}$ which are presented in the new proposed modified power model of Rossi, B. et, al. (2013).

For Austenitic steel

$$\sigma_{0.2,section} = \{(519*343.92)+(358*872.08)\}/(343.92+872.08)$$
$$= 403.54 \text{ MPa.}$$

Similarly the strength enhancement for the cross-section is calculated for all type of steel and presented in a tabular form in Tab. 4.25 below.

Table 4.25: Calculation of strength increase for whole section due to cold rolling.

Steel Type	Grade	A	$A_{c,\text{ rolled}}$	$A_{f,\text{ rolled}}$	$\sigma_{0.2,a}$	$\sigma_{0.2,c}$	$\sigma_{0.2,f}$	$\sigma_{0.2,section}$	$\sigma_{0.2,section}/\sigma_{0.2,a}$
		mm^2	mm^2	mm^2	MPa	MPa	MPa	MPa	--
Austenitic	1.4404	1216	343.92	872.08	268.1	519	420	448.0	1.67
Ferritic	1.4003				335.2	510	446	464.1	1.38
Lean-duplex	1.4162				554.0	753	696	712.1	1.29
Duplex	1.4462				618.8	866	775	800.7	1.29

CEN1996, EN 1993-1-3 accounts the increased of strength of cross section for carbon steel by using the eq. 1.17 which is expressed in the literature review. By using this relationship the increased strength for the whole section of each type of steel is represented in Tab. 4.26 below.

Table 4.26: Calculation of strength increase for whole section due to cold rolling using expression used for carbon steel.

Steel Type	Grade	A	$\sigma_{0.2,a}$	$\sigma_{u,a}$	$\sigma_{0.2,section}$	$\sigma_{0.2,section}/\sigma_{0.2,a}$	$(\sigma_{u,a}+\sigma_{0.2,a})/2$
		mm^2	MPa	MPa	MPa	--	MPa
Austenitic	1.4404	1216	268.1	627.85	400.6	1.49	448.0
Ferritic	1.4003		335.2	502.29	396.8	1.18	418.7
Lean-duplex	1.4162		554.0	775.75	635.7	1.15	664.9
Duplex	1.4462		618.8	853.35	705.2	1.14	736.1

The value of $\sigma_{0.2,section}$ should be less than $(\sigma_{u,a}+\sigma_{0.2,a})/2$, according to the formula which satisfies for all steel types.

5. SUMMARY AND CONCLUSIONS

This thesis work concerned with the development of analytical modelling by using the Maple for simulation of the manufacturing process of cold worked sections for both press-braked and cold rolled process. This model is developed to predict the resulting residual stresses and equivalent plastic strain due to cold bending by using the Quach, W.M. (2005) analytical formula. The stainless steel material is considered as the isotropic non-linear strain hardening materials in this analysis. Also the stress-strain relationship is expressed in three stages which is suitable for describing the full range of stress-strain diagram and for both tension and compression coupon test result.

The analysis is done considering the plain stain pure bending of sheet. From the analysis it is shown that the variation of residual stresses in two perpendicular directions and the equivalent plastic strain through thickness follows nonlinear pattern for both coiling and uncoiling including flattening process. The values are depends mainly on the coiling curvature of the sheet which is in most case is unknown to the designers, and the values after uncoiling including flattening are considered the residual stress and plastic strain values at the flat faces of press-braked section.

The cold bending is the main part for the introduction of residual stresses and plastic strain. As the radius of curvature is so small at bending, there is the shifting of neutral axis from the mid plane surface towards the inner surface. The shifting of neutral axis is considered in this analysis following the theory of cold bending of sheet given by Hill, R. (1950). Then the in plane stresses and strains are calculated as the same manner used in coiling and uncoiling process.

For the calculation of cold bending effect for stainless steel it is important to use the true stress-strain relationship because at large strain level, the nominal stress-strain relationship deviates from the real stress-strain response. This effect in the value of residual stresses and strain is compared and it is observed that the comparison is significant. Also, the cold bending of sheet with or without considering the elastic springback effect is analysed. It is seen that when considering the springback, the residual stresses changes from compression to tension for inner surface and tension to compression for outer surface at the bending

direction and the maximum stresses are at the middle 1/4th thickness region. But without considering springback the maximum stresses are at the surface of the sheet.

The analysis is also done for the corner and flat faces of the cold rolled box section, where the coiling-uncoiling of sheet, making it circle then to final shape of the section considering the elastic springback and the model is validated with the test result of Grander, L. (2002).

For determining the cold bending effect on the mechanical properties of the stainless steel sheet, the test result of Marik, J. and Jandera, M. (2014) of austenitic (1.4404), ferritic (1.4003), duplex (1.4462) and relatively new grade lean-duplex (1.4162) are taken where the basic material properties are calculated introducing different magnitude of plastic strain. The new material properties with respect to plastic strain are included in the analysis after the formation of section for both corner and flat faces. The stress is calculated from the small increment of strain and from the stress-strain diagram 0.2% proof stress is calculated by varying the internal bending radius to thickness ratio (r_i/t) for corner and the internal circle radius to thickness ratio (R_i/t) for flat faces.

From the result, it is seen that the 0.2% proof strength increase 100% for austenitic steel, 70% for ferritic steel, 35% for lean-duplex steel and 40% for duplex steel with mostly used r_i/t value 1.5 at corner. The analysed result is compared with the previous model for predicting the strength increase. Of them the latest power model of Rossi, B. et, al. (2013) shows the more conservative results which satisfy for all ranges of r_i/t value and all type of steel grades.

Hence, a formula is proposed based on the analytical result by modifying the Rossi, B. et, al. (2013) formula and strength increase is observed 90% for austenitic steel, 50% for freeitic steel and 40% for duplex steel with r_i/t value 1.5 at corner and are safe for design engineers because the coiling radius of the sheet is unknown to them. Only the exception is for lean-duplex steel where the Rossi, B. et, al. (2013) model (strength increase 33%) is more safe than the proposed modified model with the analytical result.

Other thing is that the previous model is developed considering the annealed material properties got from the mill certificates. It is believed that the mill certificate tests are

carried out at higher strain rates as the standards for material testing allow some variation in the rate. As stainless steels are very sensitive to the strain rate, this is probably the reason that the 0.2% proof strength in the mill certificate can be bigger than the tested result in the laboratory for zero strain condition which is used here as the annealed material properties. In case of strength increase at the flat faces, also the proposed modified formula agrees with the analytical result.

The calculation of strength increment for the whole section is done by considering the area in which the corner and flat faces strength confined and it is shown that for austenitic steel the strength increase of the whole section is 65%, for ferritic steel 35% and for other two types it is 25% of the annealed material. So, it is said that for economic design of cold worked stainless steel sections, designer can use this benefit of increased strength.

For designing the slender member, it should be careful to use the increased strength, as for slender member the load carrying capacity not only depends on the section resistance, buckling resistance of member is also taken into account which has no effect of the increased strength and depends on modulus of elasticity *(E)* mostly which remain almost constant due to the induced plastic strain (at least the initial one).

6. FUTURE WORKS

Here the results of residual stresses, equivalent plastic strain and the increased strength in got from the analytical analysis. Finite element analysis can be done for the material behaviour due to cold working and full member strength can be observed with or without considering the increased strength of the material.

More steel grade can be tested and analysed for all steel type to get more precise model to predict the strength increment of the sections.

Geometric imperfection due to cold working should be considered, taking into account the formation process.

REFERENCES

Abdel-Rahman, N. and Sivakumaran, K. S. (1997). Material properties models for analysis of cold-formed steel members. *Journal of Structural Engineering*, ASCE, 123:9, 1135-1143.

Afshan, S., Rossi, B. and Gardner, L. (2013). Strength enhancements in cold-formed structural sections-Part I: Material testing. *Journal of Constructional Steel Research*, 83,177–188.

AISI (1996). *Cold-Formed Steel Design Manual*, American Iron and Steel Institute, Washington, D.C.

AS/NZS (2001). *Cold-Formed Stainless Steel Structures*, AS/NZS 4673, Australian/New Zealand Standard, Standards Australia, Sydney.

Ashraf, M., Gardner, L., and Nethercot, D. A. (2005). Strength enhancement of the corner regions of stainless steel cross-sections. *Journal of Constructional Steel Research,* 61(1):37–52.

Avci, O. (2002). Web-crippling strength of multi-web cold-formed steel deck sections subjected to end one flange (EOF) loading. *MSc thesis*. Virginia Tech, USA.

Batista, E. M. and Rodrigues, F. C. (1992). Residual stresses measurements on cold-formed profiles. *Experimental Techniques*, 25-29.

BSI (1998). Structural use of steelwork in building – Part 5. *Code of Practice for Design of Cold Formed Thin Gauge Sections*, BS5950-5, British Standards Institution, London.

Coetsee, J. S., Van den Berg, G. J. and Van der Merwe, P. (1990). The effect of work hardening and residual stresses due to cold work of forming on the strength of cold-formed stainless steel lipped channel sections. *Proceedings of the Tenth International Specialty Conference on Cold-Formed Steel Structures* , St. Louis, Missouri, United States, 505-523.

CEN (1996). Eurocode 3: Design of steel structures–Part 1.3: *General Rules-Supplementary Rules for Cold-Formed Thin Gauge Members and Sheeting*, EN 1993-1-3, European Committee for Standardisation.

CEN (1996). Eurocode 3: Design of steel structures–Part 1.4: *General Rules-Supplementary Rules for Stainless Steels*, EN 1993-1-4, European Committee for Standardisation.

EN ISO 6892-1, CEN (2009). Metallic materials – *Tensile testing – part 1: Method of test at room temperature*, Brussels, European Committee for Standardization.

Cruise, R.B., Gardner, L. (2008). Strength enhancements induced during cold forming of stainless steel sections. *Journal of Constructional Steel Research*, 64(11), 1310 –1316.

Gardner, L. (2002). A new approach to structural stainless steel design*, PhD Thesis, Department of Civil and Environmental Engineering,* Imperial College*,* London, U.K.

Gardner, L. and Nethercot, D. A. (2004). Experiments on stainless steel hollow sections – Part 1: Material and cross-sectional behaviour. *Journal of Constructional Steel Research*, 60, 1291-1318.

Hill, R. (1950). *The Mathematical Theory of Plasticity*, Oxford University Press, United States.

Ingvarsson, L. (1975). Cold-forming residual stresses–effect on buckling. *Proceedings of the 3rd International Specialty Conference on Cold-Formed Steel Structures*, University of Missouri-Rolla, United States, 85-119.

Jandera, M., Gardner, L. and Machaceka, J. (2008). Residual stresses in cold-rolled stainless steel hollow sections. *Journal of Constructional Steel Research,* 64:1255–1263.

Karren, K. W. (1967). Material properties models for analysis of cold-formed steel members. *Journal of the Structural Division, ASCE*, 93, 401-432.

Karren, K. W. and Winter, G. (1967). Effect of cold-forming on light-gage steel members. *Journal of the Structural Division, ASCE,* 93, 433-469.

Kato, B. and Aoki, H. (1978). Residual stresses in cold-formed tubes. *Journal of Strain analysis*, 13:4, 193-204.

Key, P. W. and Hancock, G. J. (1993). A theoretical investigation of the column behaviour of cold- formed square hollow sections. *Thin-Walled Structures*, 16, 31-64.

Macdonald, M., Rhodes, J. and Taylor, G. T. (2000). Mechanical properties of stainless steel lipped channels. *Proceedings of the 15th International Specialty Conference on Cold-Formed Steel Structures*, St. Louis, Missouri, United States, 673-686.

Marik, J. and Jandera, M. (2014). Cold-forming effect on material properties of stainless steel. *EUROSTEEL*, Naples, Italy.

Mirambell, E. and Real, E. (2000). On the calculation of deflections in structural stainless steel beams: An experimental and numerical investigation. *Journal of Constructional Steel Research*, 54, 109-133.

Moen, C. D., Igusa T. and Schafer, B. (2008). Prediction of residual stresses and strains in cold-formed steel members. *Thin Walled Structures*, 46(11), 1274 -1289.

Olsson, A. (2001). Stainless steel plasticity–Material modelling and structural applications. *Doctoral Thesis, Division of Steel Structures, Department of Civil and Mining Engineering,* Luleå University of Technology, Sweden.

Quach, W. M. (2005). Residual stress in cold-formed steel sections and their effect on column behaviour. *Doctoral Thesis, Department of Civil and Structural Engineering,* The Hong Kong Polytechnic University, Hong Kong.

Rasmussen, K. J. R. (2003). Full-range stress-strain curves for stainless steel alloys. *Journal of Constructional Steel Research*, 59, 47-61.

Rasmussen, K. J. R., Burns, T., Bezkorovainy, P. and Bambach, M. R. (2003). Numerical modelling of stainless steel plates in compression. *Journal of Constructional Steel Research*, 59, 1345-1362.

Rasmussen, K. J. R. and Hancock, G. J. (1993). Design of cold-formed stainless steel tubular members. I: Columns. *Journal of the Structural Engineering*, ASCE, 119 (8), 2349–2367.

Rondal, J. (1987). Residual stresses in cold-rolled profiles. *Construction & Building Materials*, 1:3, 150-164.

Rossi, B., Habraken, A. M. and Pascon, F. (2007). *10th International ESAFORM Conference on Material Forming: ESAFORM*, Zaragoza, Spain, 570- 577.

Rossi, B. (2008). Mechanical properties, residual stresses and structural behaviour of thin-walled stainless steel profiles. *PhD thesis*, University of Liège, Belgium.

Rossi, B., Afshan, S. and Gardner, L. (2013). Strength enhancements in cold-formed structural sections - Part II: Predictive models. *Journal of Constructional Steel Research*, 83,189–196.

SCI (2003). Design manual for structural stainless steel. Commentary, Second Edition, Euro Inox and the Steel Construction Institute.

SCI (2006). Design manual for structural stainless steel. Third Edition, Euro Inox and the Steel Construction Institute.

Schafer, B. W. and Peköz, T. (1998). Computational modelling of cold-Formed steel: Characterizing geometric imperfections and residual stresses. *Journal of Constructional Steel Research*, 47, 193-210.

Van den Berg, G. J. and Van der Merwe, P. (1992). Prediction of corner mechanical properties for stainless steels due to cold forming. *Proceedings of the 11th international specialty conference on cold-formed steel structures,* 571–586.

Weng, C. C. and Pekoz, T. (1990). Residual stresses in cold-formed steel members. *Journal of Structural Engineering*, ASCE, 116:6, 1611-1625.

Weng, C. C. and White, R. N. (1990). Residual stresses in cold-bent thick steel plates. *Journal of Structural Engineering*, ASCE, 116:1, 24-39.

Yu, T. X. and Zhang, L. C. (1996). Plastic Bending: Theory and applications, *World Scientific Publishing Co*., New Jersey.

Annex A:

Material Properties at Corner due to Cold Bending (Austenitic Steel)

units [N, mm, MPa]

Material and geometrical characteristics

---

material

```
> E[0]:=195.4e3:
nu:= 0.3:
sigma[y0]:= 0.001:
sigma[0.2]:=268.1:
sigma[1.0]:=314.85:
sigma[ult]:=627.85:
epl[f]:=0.533:
epsilon[ult]:=epl[f]+sigma[ult]/E[0];
n[0]:=6.35;
E[0.2]:= E[0]/(1+0.002*n[0]*E[0]/sigma[0.2]);
m[0.2,1.0]:=2.25;
e[0.2]:=sigma[0.2]/E[0];
B[0]:=0.018+e[0.2]*((E[0]/E[0.2])-1);
A[0]:=B[0]/(0.008+e[0.2]*(sigma[1.0]/sigma[0.2]-1)*(1-
E[0]/E[0.2]));
sigma[2.0]:=sigma[0.2]+(sigma[1.0]-
sigma[0.2])*(A[0]^(1/m[0.2,1.0]))*(1-((1/E[0.2]-
1/E[0])*sigma[0.2])/B[0])^(1/m[0.2,1.0]);
epsilon[2.0]:=(sigma[2.0]/E[0])+0.02;
b[0]:=(sigma[ult]*(1+epsilon[ult])-
sigma[2.0]*(1+epsilon[2.0]))/(epsilon[ult]-epsilon[2.0]);
a[0]:=sigma[2.0]*(1+epsilon[2.0])-b[0]*epsilon[2.0];
```

$$\varepsilon_{ult} := 0.5362131525$$

$$n_0 := 6.35$$

$$E_{0.2} := 19051.94059$$

$$m_{0.2,\ 1.0} := 2.25$$

$$e_{0.2} := 0.001372057318$$

$$B_0 := 0.03070000000$$

$$A_0 := 5.306429409$$

$$\sigma_{2.0} := 345.5220227$$

$$\varepsilon_{2.0} := 0.02176828057$$

$$b_0 := 1188.597686$$

$$a_0 := 327.1697153$$

coiling curvature

```
> Kappa[c]:=1/(450);
```

$$K_c := \frac{1}{450}$$

corner radius

```
> t:=2:
w1:=0:
w2:=0:
ri:=1.5*t:
radius:=ri+t/2;
Kappa[cs]:= 1/radius;
```

$$radius := 4.0$$

$$K_{cs} := 0.2500000000$$

Forming Process

Loop for coiling and uncoiling (small strain condition)

```
> i:=-1:
for y from (t/2) by (-t/10) while y > 0 do
i:=i+1:
axy[i]:=y:
####coiling
epsilon[z,cy]:= sigma[y0]*(1-nu^2)/(E[0]*sqrt(1-nu+nu^2)):
epsilon[z,c]:= Kappa[c]*y:
if epsilon[z,cy] < epsilon[z,c] then
e:= 0:
sigma[c]:= sigma[y0]:
omega[c]:= nu:
omega[last]:=omega[c]:
for s from sigma[y0] by 0.5 to sigma[ult] while abs(e) <
abs(epsilon[z,c]-epsilon[z,cy])do
ds:= s - sigma[c]:
if s <= sigma[0.2] then
eps:= X/(E[0])+0.002*(X/(sigma[0.2]))^n[0]:
else if s <= sigma[2.0] then
eps:=(X-sigma[0.2])/(E[0.2])+(0.008+(sigma[1.0]-
sigma[0.2])*((1/E[0])-(1/E[0.2])))*((X-
sigma[0.2])/(sigma[1.0]-
sigma[0.2]))^m[0.2,1.0]+(sigma[0.2])/(E[0])+0.002:
else
eps:=(X-a[0])/(b[0]-X):
end if:
end if:
dH:=((diff(eps,X))-(1/E[0]))^(-1):
Omega[c]:=(4*nu*(subs(X=s,dH))*(1-omega[c]+omega[c]^2)-
E[0]*(2-omega[c])*(2*omega[c]-1))/(E[0]*(2*omega[c]-
1)^2+4*(subs(X=s,dH))*(1-omega[c]+omega[c]^2)):
dom[c]:= (2*(1-omega[c]+omega[c]^2)*(Omega[c]-
omega[c]))/(s*((2-omega[c])+Omega[c]*(2*omega[c]-1)))*ds:
```

```
omega[c] := omega[c] + dom[c]:
de:=  subs(X=omega[c],(((1-2*X)^2-2*nu*(1-2*X)*(2-X)+(2-
X)^2)*s)/(2*E[0]*(1-2*X)*(1-X+X^2)^(3/2)))*dom[c] +
subs(X=s,((1-omega[c]^2)*(1-2*nu))/(E[0]*(1-
2*omega[c])*sqrt(1-omega[c]+omega[c]^2)))*ds;
e:= de + e:
sigma[c]:= s:
end do:
sigma[z,c]:= sigma[c]/sqrt(1-omega[c]+omega[c]^2):
sigma[x,c]:= omega[c]*sigma[c]/sqrt(1-omega[c]+omega[c]^2):
else
sigma[z,c]:= E[0]*epsilon[z,c]/(1-nu^2):
sigma[x,c]:= nu*E[0]*epsilon[z,c]/(1-nu^2):
omega[c]:= nu:
end if:
epsilon[c,pl,i]:=e-s/E[0]:
#####uncoiling including flatening
Kappa[u]:=-Kappa[c]:
Kappa[uy]:=-(sigma[c]*(1-nu^2)*(2-nu+(2*nu-
1)*omega[c]))/(E[0]*y*(1-nu+nu^2)*sqrt((1-
omega[c]+omega[c]^2))):
epsilon[z,uy]:= (Kappa[c]+Kappa[uy])*y:
epsilon[z,r]:= 0:
if abs(Kappa[uy]) < abs(Kappa[u]) then
omega[uy]:=((1-nu^2)*omega[c]-nu*(2-nu))/((1-2*nu)*omega[c]-
(1-nu^2)):
omega[last]:=omega[uy]:
sigma[u]:= sigma[c]:
omega[u]:= omega[uy]:
e:=0:
for s from sigma[u] by 0.5 to sigma[ult] while abs(e) <
abs(epsilon[z,uy] + epsilon[z,r]) do
ds:= s - sigma[u]:
if s <= sigma[0.2] then
eps:= X/(E[0])+0.002*(X/(sigma[0.2]))^n[0]:
else if s <= sigma[2.0] then
eps:=(X-sigma[0.2])/(E[0.2])+(0.008+(sigma[1.0]-
sigma[0.2])*((1/E[0])-(1/E[0.2])))*((X-
sigma[0.2])/(sigma[1.0]-
sigma[0.2]))^m[0.2,1.0]+(sigma[0.2])/(E[0])+0.002:
else
eps:=(X-a[0])/(b[0]-X):
end if:
end if:
dH:=((diff(eps,X))-(1/E[0]))^(-1):
Omega[u]:=(4*nu*(subs(X=s,dH))*(1-omega[u]+omega[u]^2)-
E[0]*(2-omega[u])*(2*omega[u]-1))/(E[0]*(2*omega[u]-
1)^2+4*(subs(X=s,dH))*(1-omega[u]+omega[u]^2)):
dom[u]:= (2*(1-omega[u]+omega[u]^2)*(Omega[u]-
omega[u]))/(s*((2-omega[u])+Omega[u]*(2*omega[u]-1)))*ds:
```

```
omega[u]:= omega[u] + dom[u]:
de:= subs(X=omega[u],(((1-2*X)^2-2*nu*(1-2*X)*(2-X)+(2-
X)^2)*s)/(2*E[0]*(1-2*X)*(1-X+X^2)^(3/2)))*dom[u] +
subs(X=s,((1-omega[u]^2)*(1-2*nu))/(E[0]*(1-
2*omega[u])*sqrt(1-omega[u]+omega[u]^2)))*ds;
e:= de + e:
sigma[u]:=s:
end do:
sigma[u,i]:= sigma[u]:
sigma[z,r,i]:=-sigma[u]/sqrt(1-omega[u]+omega[u]^2):
sigma[x,r,i]:=-omega[u]*sigma[u]/sqrt(1-
omega[u]+omega[u]^2):
epsilon[i]:=e:
epsilon[u,pl,i]:=e-(s-sigma[c])/E[0]:
epsilon[r,pl,i]:=epsilon[u,pl,i]+epsilon[c,pl,i]:
else
sigma[z,u] := E[0]*Kappa[u]*y/(1-nu^2):
sigma[x,u] := nu*E[0]*Kappa[u]*y/(1-nu^2):
sigma[z,r,i] := sigma[z,c]+sigma[z,u]:
sigma[x,r,i] := sigma[x,c]+sigma[x,u]:
omega[u,i]:= sigma[x,r,i]/sigma[z,r,i]:
sigma[u,i]:= sigma[c]:
s:=sigma[c]:
epsilon[i]:=Kappa[u]*y:
epsilon[u,pl,i]:=0:
epsilon[r,pl,i]:=epsilon[u,pl,i]+epsilon[c,pl,i]:
end if:
end do:
```

Using simmetry for whole thickness data

```
> axy[5]:=0:
sigma[us,5]:=sigma[y0]:
sigma[z,r,5]:=sigma[y0]*(1-nu^2)/(E[0]):
sigma[x,r,5]:=sigma[y0]*(1-nu^2)/(E[0]*nu):
epsilon[r,pl,5]:=0:
sigma[u,5]:=sigma[y0]:
> for i from 0 by 1 to 4 do
axy[10-i]:=-axy[i]:
sigma[u,10-i]:= sigma[u,i]:
sigma[z,r,10-i]:=-sigma[z,r,i]:
sigma[x,r,10-i]:=-sigma[x,r,i]:
epsilon[r,pl,10-i]:= epsilon[r,pl,i]:
end do:
```

Bending to the corner radius (x-axis bending)

```
> q[x]:=1:
for shift from 0.001 by 0.001 while q[x] > 0.25 do
for i from 0 by 1 to 10 do
y:= axy[i]:
epsilon[x,cs,i]:= ln(1+(shift-y)/(1/Kappa[cs]-shift)):
epsilon[x,csy,i]:= sigma[u,i]*(1-nu^2)/(E[0]*sqrt(1-
```

```
nu+nu^2)):
if abs(epsilon[x,csy,i])<abs(epsilon[x,cs,i])then
e:= 0:
sigma[z,cs,i]:= sigma[z,r,i]+ nu*E[0]*epsilon[x,csy,i]/(1-
nu^2):
sigma[x,cs,i]:= sigma[x,r,i] + E[0]*epsilon[x,csy,i]/(1-
nu^2):
omega[cs]:= sigma[z,cs,i]/sigma[x,cs,i]:
sigma[cs]:=sigma[u,i]:
for s from sigma[u,i] by 1 to sigma[ult] while abs(e)
<(abs(epsilon[x,cs,i]-epsilon[x,csy,i])) do
ds:= s-sigma[cs]:
if s <= sigma[0.2] then
eps:= X/(E[0])+0.002*(X/(sigma[0.2]))^n[0]:
dt:=ds+ds*((2*X/E[0])+0.002*(n[0]+1)*(X/sigma[0.2])^n[0]):
else if s <= sigma[2.0] then
eps:=(X-sigma[0.2])/(E[0.2])+(0.008+(sigma[1.0]-
sigma[0.2])*((1/E[0])-(1/E[0.2])))*((X-
sigma[0.2])/(sigma[1.0]-
sigma[0.2]))^m[0.2,1.0]+(sigma[0.2])/(E[0])+0.002:
dt:=ds+ds*(((sigma[0.2])/(E[0]))+0.002+(((2*X-
sigma[0.2])/E[0.2])+(((m[0.2,1.0]+1)*X)-
sigma[0.2]))*(0.008+(sigma[1.0]-sigma[0.2])*((1/E[0])-
(1/E[0.2])))*((X-sigma[0.2])^(m[0.2,1.0]-1)/(sigma[1.0]-
sigma[0.2])^m[0.2,1.0])):
else
eps:=(X-a[0])/(b[0]-X):
dt:=ds+ds*(((2*X-a[0])*(b[0]-X)+X*(X-a[0]))/(b[0]-X)^2):
end if:
end if:
dH:=(((diff(eps,X))/((1+eps)*((1+eps)+X*((diff(eps,X))))))-
(1/E[0]))^(-1):
Omega[cs]:=(4*nu*(subs(X=s,dH))*(1-omega[cs]+omega[cs]^2)-
E[0]*(2-omega[cs])*(2*omega[cs]-1))/(E[0]*(2*omega[cs]-
1)^2+4*(subs(X=s,dH))*(1-omega[cs]+omega[cs]^2)):
dom[cs]:=((2*(1-omega[cs]+omega[cs]^2)*(Omega[cs]-
omega[cs]))/(s*((2-omega[cs])+Omega[cs]*(2*omega[cs]-
1))))*(subs(X=s,dt)):
omega[cs]:= omega[cs] + dom[cs]:
de:= subs(X=omega[cs],(((1-2*X)^2-2*nu*(1-2*X)*(2-X)+(2-
X)^2)*s)/(2*E[0]*(1-2*X)*(1-X+X^2)^(3/2)))*dom[cs] +
subs(X=s,((1-omega[cs]^2)*(1-2*nu))/(E[0]*(1-
2*omega[cs])*sqrt(1-omega[cs]+omega[cs]^2)))*ds:
e:= de + e:
sigma[cs]:=s:
end do:
if y>= shift then
sigma[z,cs,i]:= -omega[cs]*sigma[cs]/sqrt(1-
omega[cs]+omega[cs]^2):
sigma[x,cs,i]:= -sigma[cs]/sqrt(1-omega[cs]+omega[cs]^2):
```

```
else
sigma[z,cs,i]:=omega[cs]*sigma[cs]/sqrt(1-
omega[cs]+omega[cs]^2):
sigma[x,cs,i]:=sigma[cs]/sqrt(1-omega[cs]+omega[cs]^2):
end if:
sigma[cs,i]:=s:
omega[cs,i]:=omega[cs]:
epsilon[cs,pl,i]:=ln(1+e)-(s*(1+e)/E[0]):
else
sigma[z,cs,i]:=sigma[z,r,i]+ nu*E[0]*epsilon[x,cs,i]/(1-
nu^2):
sigma[x,cs,i]:=sigma[x,r,i] + E[0]*epsilon[x,cs]/(1-nu^2):
sigma[cs,i]:=sigma[u,i]:
omega[cs,i]:=sigma[z,cs,i]/sigma[x,cs,i]:
epsilon[cs,pl,i]:= 0:
end if:
end do:
#### membrane residual stress
q[x]:= 0:
for i from 0 by 1 to 9 do
q[x]:= q[x]-(sigma[x,cs,i+1]+sigma[x,cs,i])/2*(axy[i]-
axy[i+1]):
end do:
q[x]:=q[x]/t;
end do:
q[x];
shift;
####Spring back
M[t]:=0:
for i from 0 by 1 to 10 do
if i=0 then
M[i]:=(sigma[x,cs,i]*axy[i]*t/10)/2:
elif i=10 then
M[i]:=(sigma[x,cs,i]*axy[i]*t/10)/2:
else
M[i]:=sigma[x,cs,i]*axy[i]*t/10:
end if:
M[t]:=M[t]+M[i]:
end do:
Iy:=1*t^3/12:
###Final stress(including spring back)
for i from 0 by 1 to 10 do
epsilon[x,sb,i]:= M[t]*axy[i]/(Iy*E[0]):
sigma[x,sb,i]:=epsilon[x,sb,i]*E[0]:
sigma[z,sb,i]:=nu*epsilon[x,sb,i]*E[0]:
sigma[z,pb,i]:=sigma[z,cs,i]-sigma[z,sb,i]:
sigma[x,pb,i]:=sigma[x,cs,i]-sigma[x,sb,i]:
end do:
```

0.003

ploting of the results

```
> with(plots):
pointplot({seq([axy[i],sigma[x,cs,i]],i=0..10)}),
symbol=cross);
pointplot({seq([axy[i],sigma[z,cs,i]],i=0..10)}),
symbol=cross);
pointplot({seq([axy[i],epsilon[cs,pl,i]],i=0..10)}),
symbol=cross);
```

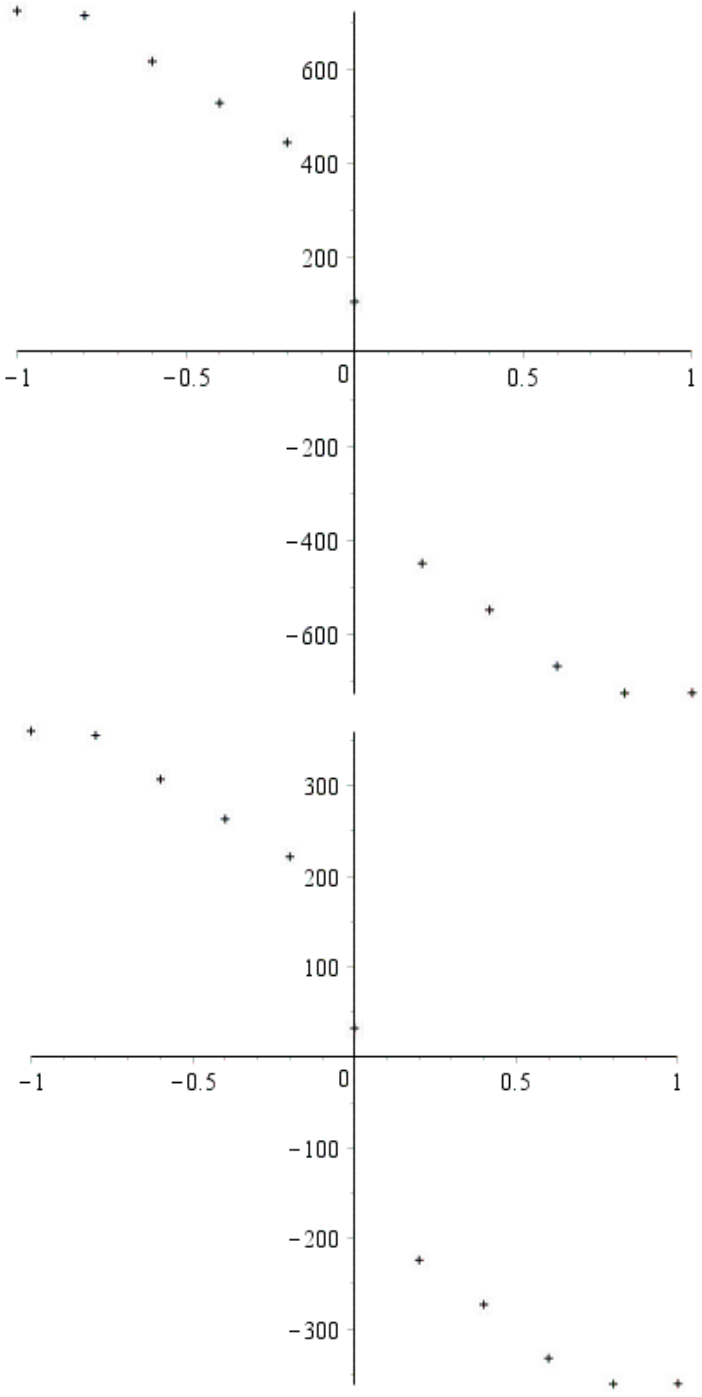

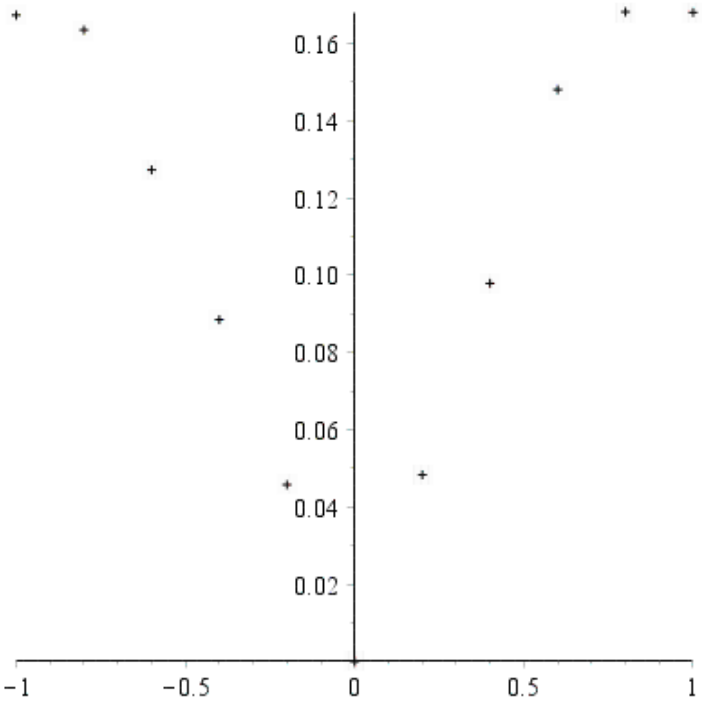

Stress strain diagram after cold bending at corner in the bending direction

```
> for i from 0 by 1 to 10 do
sigma[x,i]:=0.0001;
sigma[z,i]:=0.0001;
sigma[i]:= 0.0001;
omega[i]:=sigma[z,i]/sigma[x,i];
sigma[cs,i]:=0.0001;
end do:
> precise:= 0.0001;
beginning:= 0;
de:= 1e-5;
e:=0:
ss[z] := 0:
ss[x] := 0:
ss[av] := 0:
for i from 0 by 1 to 10 do
E[0,pl,i] :=(0.014*epsilon[cs,pl,i]+1.020)*E[0]:
nu :=0.3:
sigma[0.2,pl,i]:=(-6.472*epsilon[cs,pl,i]^2 +
5.829*epsilon[cs,pl,i] + 1.119)*sigma[0.2]:
sigma[1.0,pl,i]:=(-6.360*epsilon[cs,pl,i]^2 +
6.33*epsilon[cs,pl,i] + 1.162)*sigma[1.0]:
sigma[ult,pl,i]:=(0.156*epsilon[cs,pl,i]+1.707)*sigma[ult]:
epsilon[ult,pl,i]:=(1.359*epsilon[cs,pl,i]^2 -
1.672*epsilon[cs,pl,i] + 0.938)*epsilon[ult]:
n[0,pl,i]:=(-0.172*epsilon[cs,pl,i]+0.538)*n[0]:
E[0.2,pl,i]:=
```

```
E[0,pl,i]/(1+0.002*n[0,pl,i]*E[0,pl,i]/sigma[0.2,pl,i]):
m[0.2,1.0,pl,i]:=(1.241*(epsilon[cs,pl,i])+1.555)*m[0.2,1.0]
:
e[0.2,pl,i]:=sigma[0.2,pl,i]/E[0,pl,i]:
B[0,pl,i]:=0.018+e[0.2,pl,i]*((E[0,pl,i]/E[0.2,pl,i])-1):
A[0,pl,i]:=B[0,pl,i]/(0.008+e[0.2,pl,i]*(sigma[1.0,pl,i]/sig
ma[0.2,pl,i]-1)*(1-E[0,pl,i]/E[0.2,pl,i])):
sigma[2.0,pl,i]:=sigma[0.2,pl,i]+(sigma[1.0,pl,i]-
sigma[0.2,pl,i])*(A[0,pl,i]^(1/m[0.2,1.0,pl,i]))*(1-
((1/E[0.2,pl,i]-
1/E[0,pl,i])*sigma[0.2,pl,i])/B[0,pl,i])^(1/m[0.2,1.0,pl,i])
:
epsilon[2.0,pl,i]:= (sigma[2.0,pl,i]/E[0,pl,i])+0.02:
b[0,pl,i]:=(sigma[ult,pl,i]*(1+epsilon[ult,pl,i])-
sigma[2.0,pl,i]*(1+epsilon[2.0,pl,i]))/(epsilon[ult,pl,i]-
epsilon[2.0,pl,i]):
a[0,pl,i]:=sigma[2.0,pl,i]*(1+epsilon[2.0,pl,i])-
b[0,pl,i]*epsilon[2.0,pl,i]:
end do:
for e from de by de while e <0.3 do
for i from 0 by 1 to 10 do
if sigma[i] < sigma[cs,i] then
dsigma[x] :=  E[0,pl,i] / (1-nu^2)*de:
dsigma[z] := nu *E[0,pl,i]/(1-nu^2)* de:
else
if sigma[i] <= sigma[0.2,pl,i] then
eps:= X/(E[0,pl,i])+0.002*(X/(sigma[0.2,pl,i]))^n[0,pl,i]:
else if sigma[i] <= sigma[2.0,pl,i] then
eps:=(X-
sigma[0.2,pl,i])/(E[0.2,pl,i])+(0.008+(sigma[1.0,pl,i]-
sigma[0.2,pl,i])*((1/E[0,pl,i])-(1/E[0.2,pl,i])))*((X-
sigma[0.2,pl,i])/(sigma[1.0,pl,i]-
sigma[0.2,pl,i]))^m[0.2,1.0,pl,i]+(sigma[0.2,pl,i])/(E[0,pl,
i])+0.002:
else
eps:=(X-a[0,pl,i])/(b[0,pl,i]-X):
end if:
end if:
dH:=subs(X=sigma[i],((diff(eps,X))-(1/E[0,pl,i]))^(-1));
depsilon[x]:= de;
dsigma[z]:= E[0,pl,i]*(4/9*nu*sigma[i]^2*dH/E[0,pl,i]-
(2/3*sigma[z,i]-1/3*sigma[x,i])*(2/3*sigma[x,i]-
1/3*sigma[z,i]))*depsilon[x]/(4/9*sigma[i]^2*dH*(1-
nu^2)/E[0,pl,i]+(2/3*sigma[z,i]-
1/3*sigma[x,i])^2+(2/3*sigma[x,i]-
1/3*sigma[z,i])^2+2*nu*(2/3*sigma[z,i]-
1/3*sigma[x,i])*(2/3*sigma[x,i]-1/3*sigma[z,i]));
dsigma[x]:= E[0,pl,i]*((2/3*sigma[z,i]-
1/3*sigma[x,i])^2+4/9*sigma[i]^2*dH/E[0,pl,i])*depsilon[x]/(
4/9*sigma[i]^2*dH*(1-nu^2)/E[0,pl,i]+(2/3*sigma[z,i]-
```

```
1/3*sigma[x,i])^2+(2/3*sigma[x,i]-
1/3*sigma[z,i])^2+2*nu*(2/3*sigma[z,i]-
1/3*sigma[x,i])*(2/3*sigma[x,i]-1/3*sigma[z,i]));
end if;
if i = 0 then
ss[x]:= ss[x] + 0.5 * dsigma[x];
ss[z]:= ss[z] + 0.5 * dsigma[z];
ss[av]:= ss[av] + 0.5 * dsig[i]:
elif i = 10 then
ss[x]:= ss[x] + 0.5 * dsigma[x];
ss[z]:= ss[z] + 0.5 * dsigma[z];
ss[av]:= ss[av] + 0.5 * dsig[i]:
else
ss[x]:= ss[x] + dsigma[x];
ss[z]:= ss[z] + dsigma[z];
ss[av]:= ss[av] + dsig[i]:
end if:
sigma[x,i]:= sigma[x,i] + dsigma[x];
sigma[z,i]:= sigma[z,i] + dsigma[z];
omega[i]:=sigma[z,i]/sigma[x,i];
dsig[i]:= abs(sqrt(sigma[x,i]^2+sigma[z,i]^2-
sigma[z,i]*sigma[x,i]) - sigma[i]);
sigma[i]:= max(sqrt(sigma[x,i]^2+sigma[z,i]^2-
sigma[z,i]*sigma[x,i]),sigma[i]);
end do:
sigma[yield]:= sqrt((ss[z]/10)^2+(ss[x]/10)^2-
(ss[x]/10)*(ss[z]/10)):
for ep from 1 to 3000 by 1 do
if (e-beginning)=ep*precise then
sigma[ep,plot]:=(ss[x]/10):
epsilon[ep,plot]:=e:
end if:
end do:
end do:
sigma[x,yield]:=sigma[yield]:
epsilon[yield,pl]:= e-sigma[yield]/E[0,pl,i];
ss[x]:= ss[x]/10;
ss[z]:= ss[z]/10;
sqrt(ss[z]^2+ss[x]^2-ss[z]*ss[x]);
sigma[ep,plot];
epsilon[ep,plot];
sigma[100,plot];
epsilon[100,plot];
```

$$precise := 0.0001$$

$$beginning := 0$$

$$de := 0.00001$$

$$ss_x := 1162.448278$$

$$ss_z := 580.0416880$$

1006.710434

$\sigma_{3001,\,plot}$

$\varepsilon_{3001,\,plot}$

621.8408180

0.01000

Plot the curve

```
> with(plots):
pointplot({seq([epsilon[ep,plot],sigma[ep,plot]],ep=1..2999
)}), symbol=cross);
```

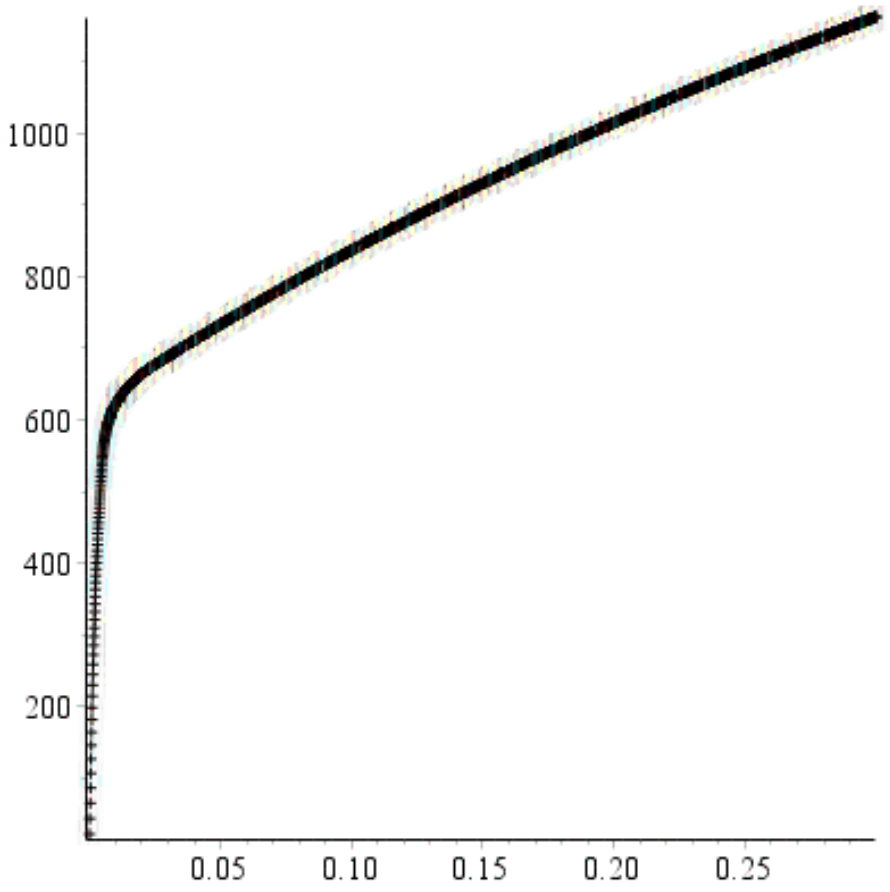

Printing of results

```
> S := array([[Kappa[c],w1],
[E[0], sigma[0.2]],
seq([epsilon[ep,plot], sigma[ep,plot]], ep=1..2999)]);
> writedata(output,S):
```

Annex B:

Variation of Material Properties with Respect to Induced Plastic Strain

B. 1 Ferritic Steel

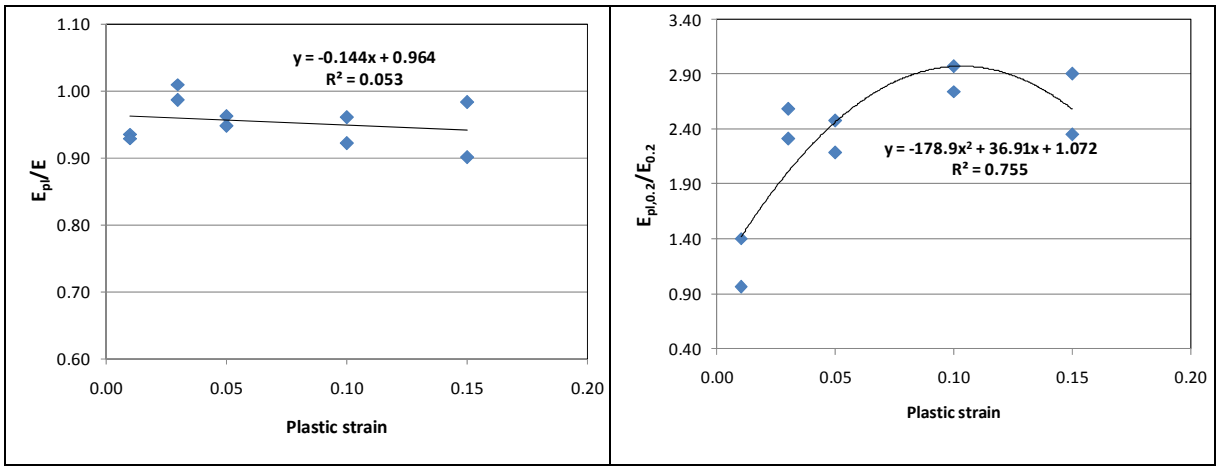

(a) Modulus of elasticity (E) *(b) Tangent modulus at the 0.2% proof stress ($E_{0.2}$)*

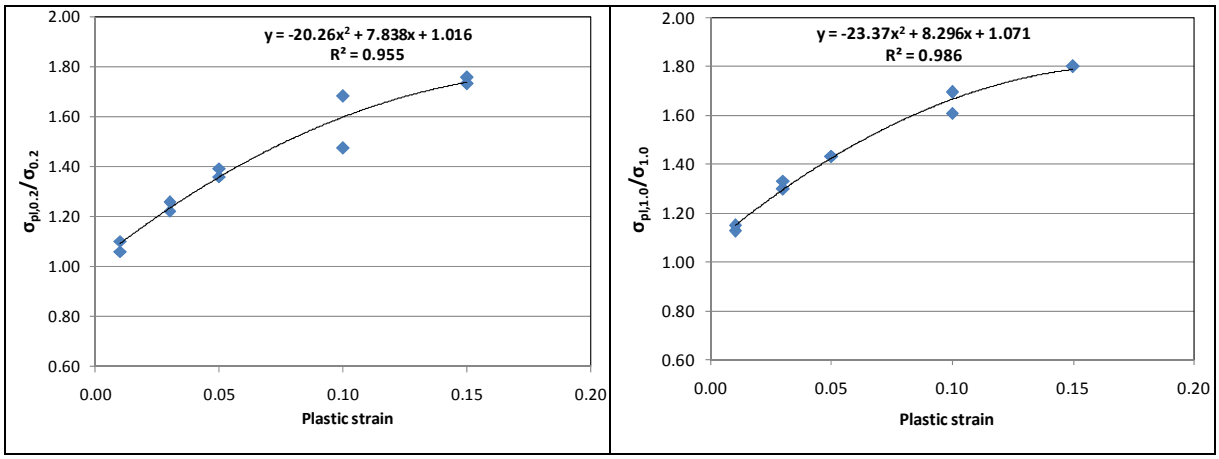

(c) 0.2% proof stress ($\sigma_{0.2}$) *(d) 1.0 % proof stress ($\sigma_{1.0}$)*

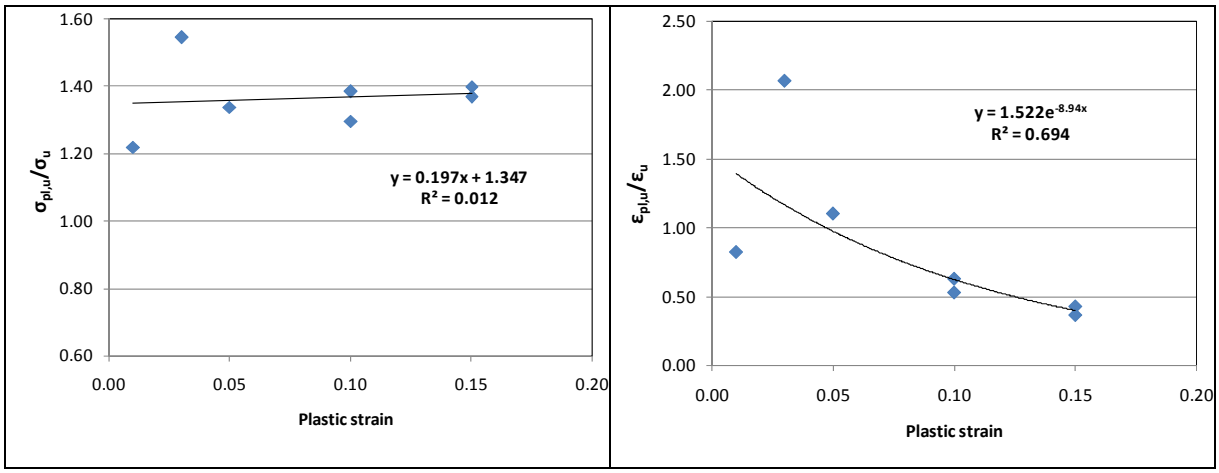

(e) Ultimate strength (σ_u) *(f) Ultimate strain (ε_u)*

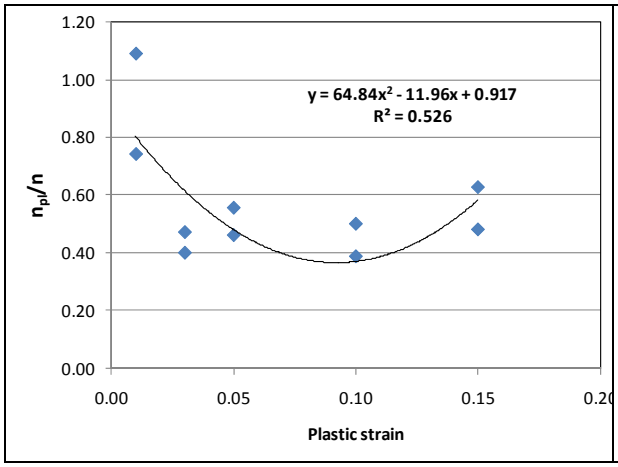

(g) Ramberg-Osgood hardening exponent (n)

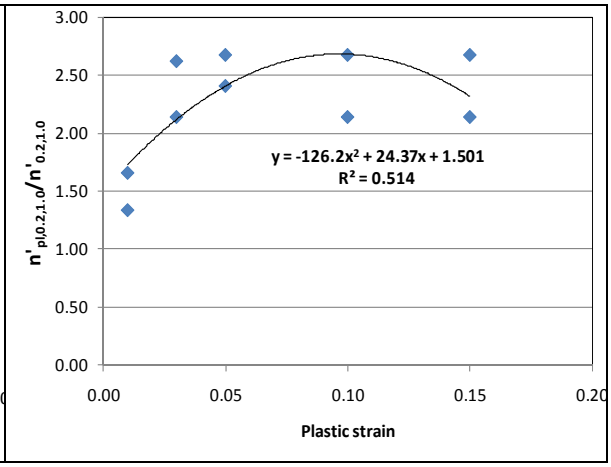

(h) Compound Ramberg-Osgood hardening exponent ($n'_{0.2,1.0}$)

B. 2 Lean-duplex Steel

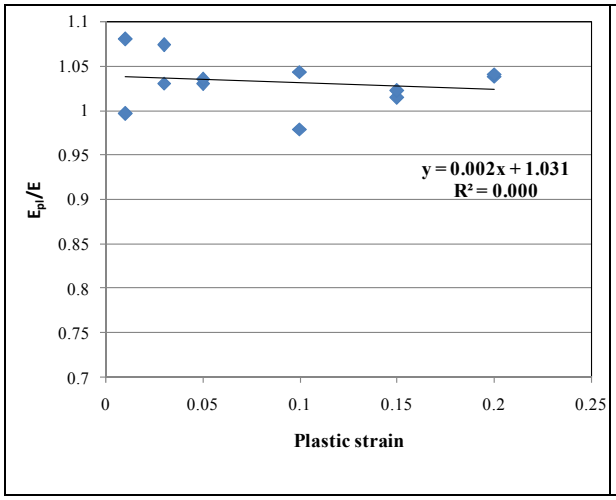

(a) Modulus of elasticity (E)

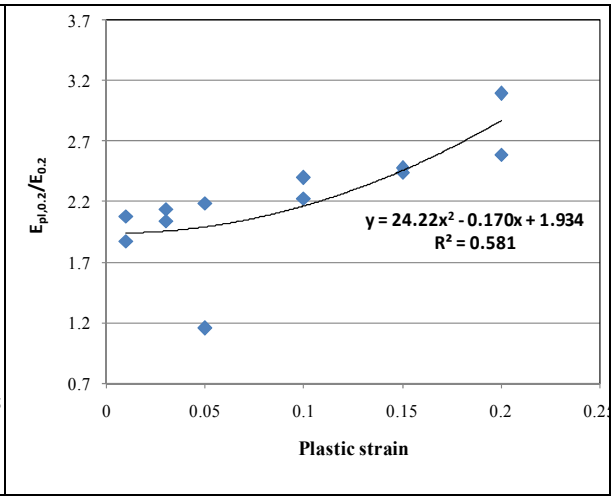

(b) Tangent modulus at the 0.2% proof stress ($E_{0.2}$)

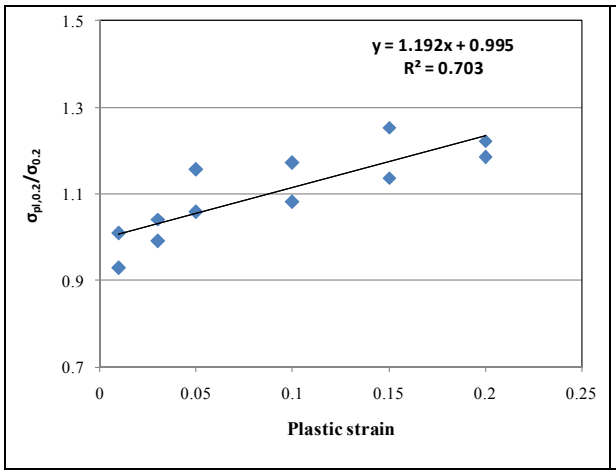

(c) 0.2% proof stress ($\sigma_{0.2}$)

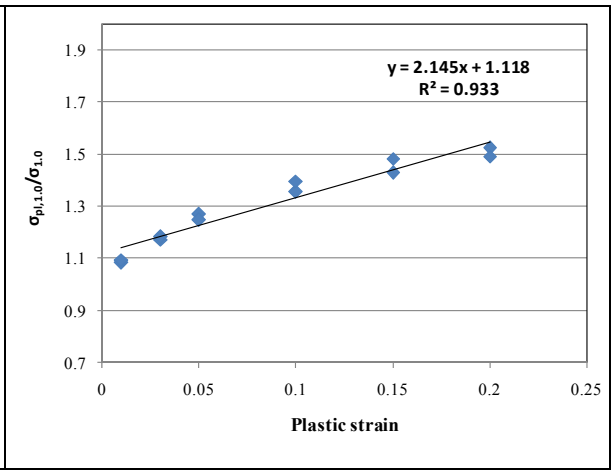

(d) 1.0 % proof stress ($\sigma_{1.0}$)

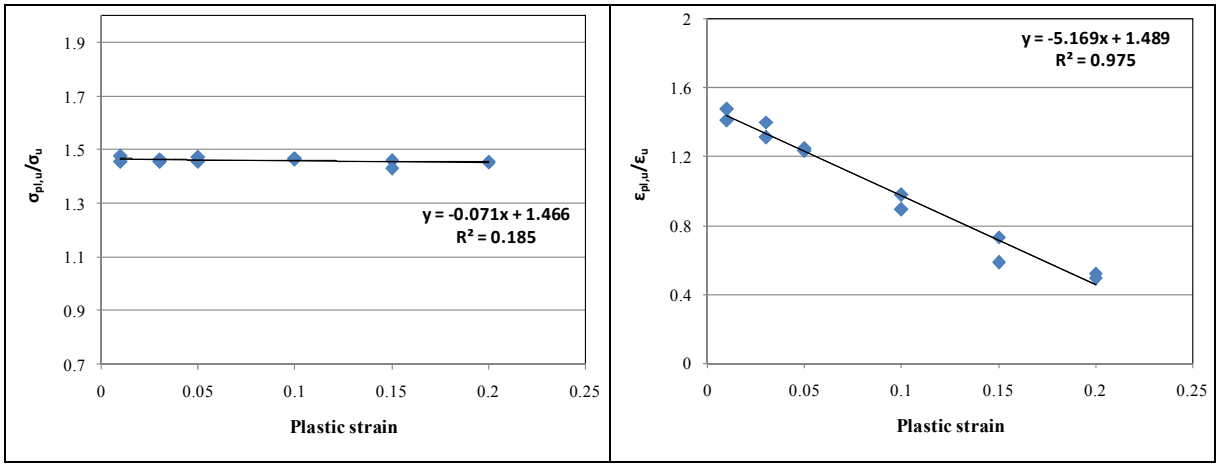

(e) Ultimate strength (σ_u) *(f) Ultimate strain (ε_u)*

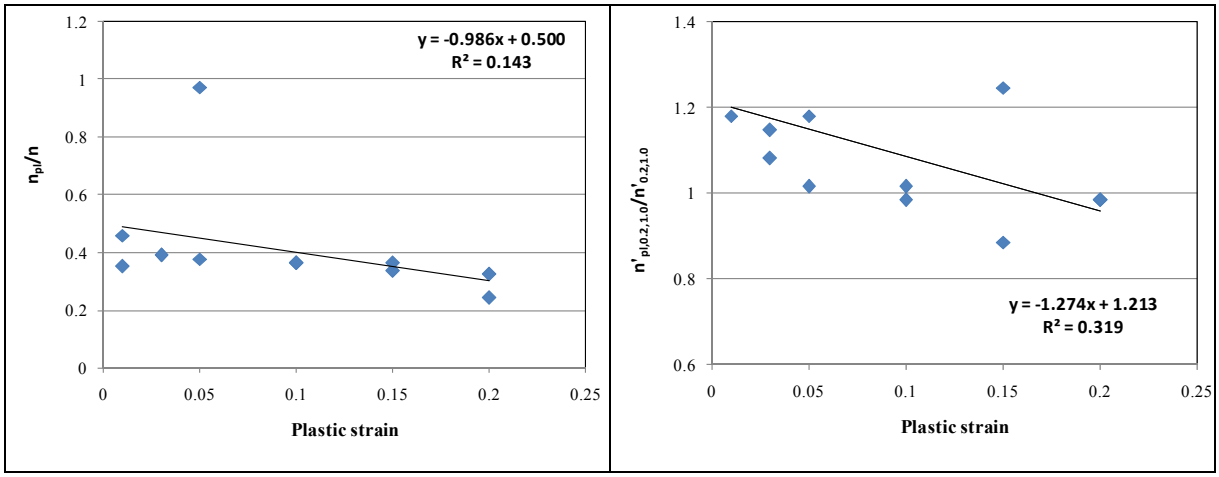

(g) Ramberg-Osgood hardening exponent (n) *(h) Compound Ramberg-Osgood hardening exponent ($n'_{0.2,1.0}$)*

B. 3 Duplex Steel

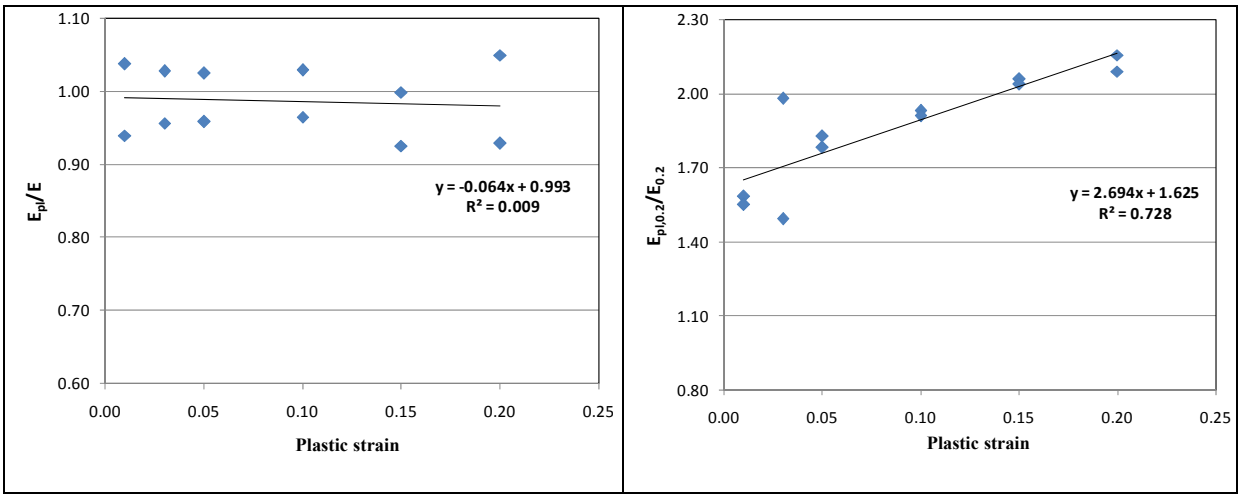

(a) Modulus of elasticity (E) *(b) Tangent modulus at the 0.2% proof stress ($E_{0.2}$)*

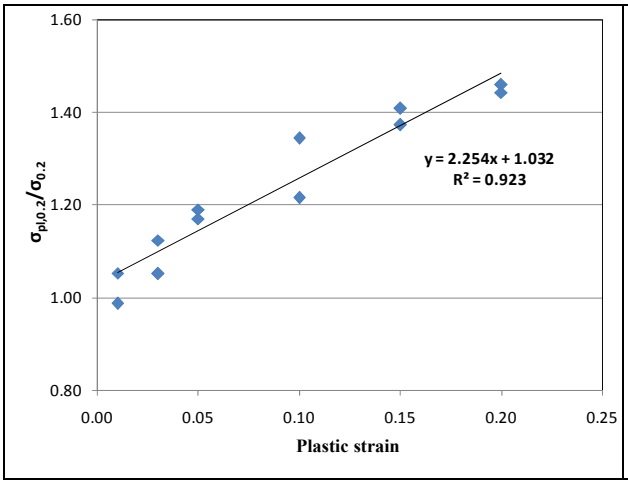

(c) 0.2% proof stress ($\sigma_{0.2}$)

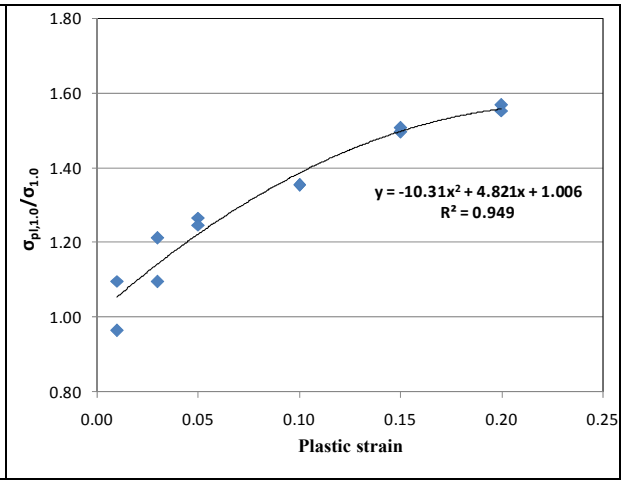

(d) 1.0 % proof stress ($\sigma_{1.0}$)

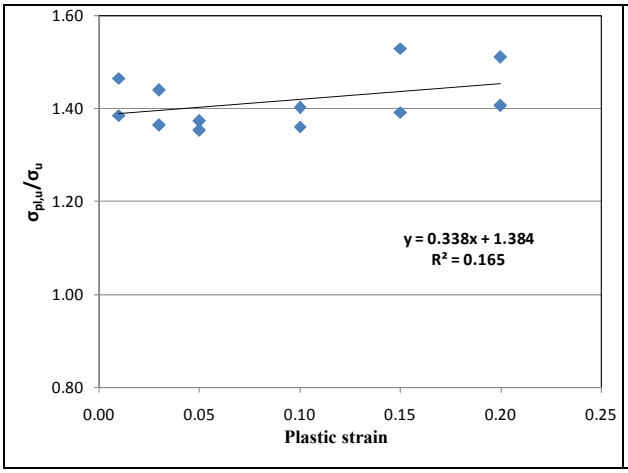

(e) Ultimate strength (σ_u)

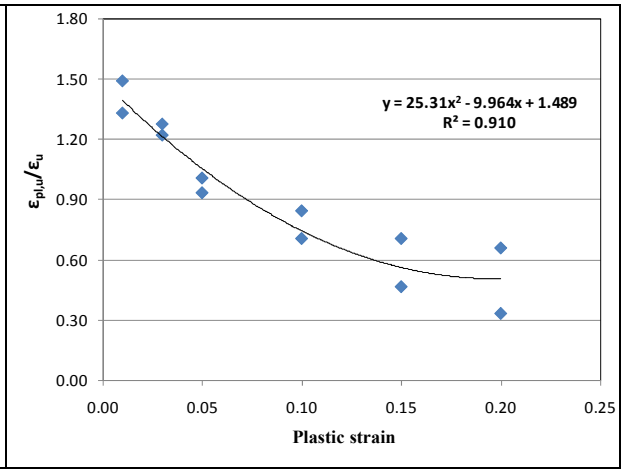

(f) Ultimate strain (ε_u)

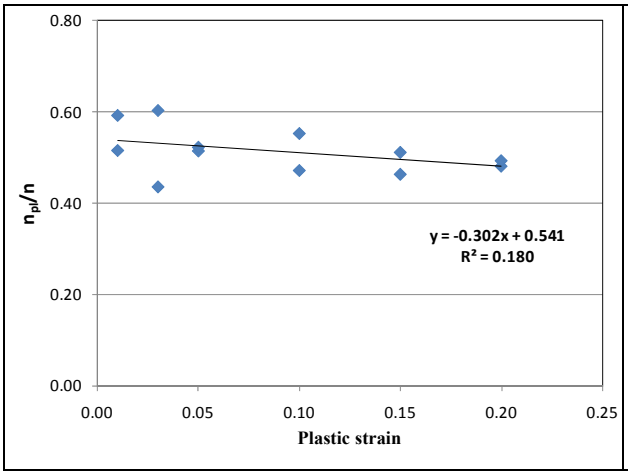

(g) Ramberg-Osgood hardening exponent (n)

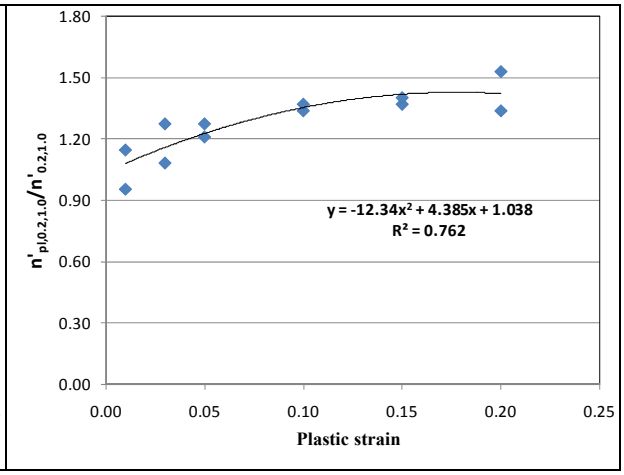

(h) Compound Ramberg-Osgood hardening exponent ($n'_{0.2,1.0}$)